INTEGRIN $\alpha_5\beta_1$ AND FIBRONECTIN INTERACTION UNDER FORCE

A Thesis
Presented to
The Academic Faculty

by

Fang Kong

In Partial Fulfillment
of the Requirements for the Degree
Ph.D. in the
Woodruff School of Mechanical Engineering

Georgia Institute of Technology
Dec. 2008

INTEGRIN $\alpha_5\beta_1$ AND FIBRONECTIN INTERACTION UNDER FORCE

Approved by:

Dr. Cheng Zhu, Advisor
Department of Biomedical Engineering
Georgia Institute of Technology

Dr. Andres Garcia
School of Mechanical Engineering
Georgia Institute of Technology

Dr. Levent Degertekin
School of Mechanical Engineering
Georgia Institute of Technology

Dr. Larry McIntire
Department of Biomedical Engineering
Georgia Institute of Technology

Dr. Ronald Fox
School of Physics
Georgia Institute of Technology

Date Approved: Nov.17th, 2008

To my family

ACKNOWLEDGEMENTS

Both of my parents were teachers and they put great amount of effort in educating me through all my life. Here I express my gratitude to them. My sister stayed with them and took care of them as I am away. She contributed much more than I did to the family.

As a human being, I am always lazy and try my best to settle with as little work as I can. Fortunately, my advisor, Dr. Cheng Zhu never felt tired in pushing me to extra miles. During the six and a half years in this lab, I have been introduced to the wonderful world of biology and moved my first step to think independently. I also thank Dr. Zhu for the financial support that keeps me alive. Dr. Andres Garcia, Dr. Martin Humphries and Dr. Paul Mould provided reagents and valuable advices. Dr. Levent Degertekin helped on my construction of the atomic force microscopy.

I also need to thank all my colleagues, especially two former members of our lab, Ning Jiang and Fang Zhang. Not only are they pretty, but also provided me with great advices and encouragement for my research.

To my wife, you make my life a lot more meaningful.

Thank God for my life and everything!

TABLE OF CONTENTS

LIST OF FIGURES

LIST OF SYMBOLS AND ABBREVIATIONS

FN	Fibronectin
$FNIII_{7-10}$	Fibronectin module III number 7 to 10 fragment
MIDAS	Metal ion dependent adhesion site
AFM	Atomic force microscopy
EM	Electron microscopy
mAb	Monoclonal antibody
$m\alpha_5\beta_1$	Membrane integrin $\alpha_5\beta_1$
s.e.m	Standard error of the mean
PZT	Piezoelectric translator

SUMMARY

Integrins are heterodimers (e.g., $\alpha_5\beta_1$) that mediate cell adhesion in many physiological processes. Binding of integrins to ligands (e.g., fibronectin, FN) provides anchorage and signals for the cell, making them prime candidates for mechanosensing molecules. However, how force regulates integrin/ligand dissociation is unclear. Atomic force microscopy was used to measure the force dependence of lifetimes of single bonds between a FN fragment ($FNIII_{7\text{-}10}$) on the cantilever tip and an integrin $\alpha_5\beta_1$-Fc fusion protein captured by an anti-Fc monoclonal antibody (mAb) on a Petri dish or membrane $\alpha_5\beta_1$ reconstituted in a lipid bilayer.

First, lifetime-force relationships demonstrated that force prolonged bond lifetimes in the 10-30 pN range, a counterintuitive behavior called catch bonds. Changing divalent cations from Ca^{2+}/Mg^{2+} to Mg^{2+}/EGTA and to Mn^{2+} caused more pronounced catch bonds by further prolonging lifetimes. In addition, flow cytometric analysis showed that Mg^{2+}/EGTA and Mn^{2+} favored extended conformation of $\alpha_5\beta_1$ and Mn^{2+} promoted hybrid domain swing-out. Therefore, extension and hybrid domain swing out did not change the catch bond behavior. A truncated $\alpha_5\beta_1$ construct containing the headpiece but not the legs (tr$\alpha_5\beta_1$-Fc) formed much longer-lived catch bonds in the same force range that were not affected by cation changes. Bindings of two activating mAbs, 12G10 and TS2/16, left shift the catch bond and converted catch bonds to slip bonds, respectively. Both mAbs, 12G10 and TS2/16, bind to α2 helix of A (I-like) domain in the β1

subunit, which is close to the α1 helix that directed connects to the binding pocket. This suggests that the catch bonds may result from force stabilization of an active conformation of the headpiece that involves position changing of α1 helix. Catch bonds may provide a mechanical mechanism for the cell to regulate adhesion by applying different forces.

Second, $FNIII_{7-10}/\alpha_5\beta_1$-Fc/GG-7 bond was stretched to ~ 30 pN and then relaxed to ~ 7 pN at which the bond's lifetime was measured. The strong bond state induced by the 30 pN stretching stayed stable even after the force was reduced to 7 pN. In other words, lower the force would not weaken $FNIII_{7-10}/\alpha_5\beta_1$-Fc bond once it had been stretched. Similar behaviors were observed for $FNIII_{7-10}$/tr$\alpha_5\beta_1$-Fc and $FNIII_{7-10}$/m$\alpha_5\beta_1$ interactions. In addition, the efficiency of the force to induce such a strong bond state for $FNIII_{7-10}/\alpha_5\beta_1$-Fc interaction in 2 mM Mg^{2+}/EGTA condition was characterized. The probability of force to induce the strong bond state increased as force increased and when the force reached 26 pN, all bonds were transit to the strong state.

Moreover, reversible unbending of $\alpha_5\beta_1$ binding with $FNIII_{7-10}$ under mechanical force were observed, which proved that integrin bending and unbending was dynamic. Importantly, integrin could restore bent conformation even when engaged with its ligand, providing a mechanism for mechanotransduction.

Third, structural changes of $\alpha_5\beta_1$ under force were observed. The structural changes did not change the trend of lifetime-force relationships of

$FNIII_{7\text{-}10}/\alpha_5\beta_1$/GG-7 bond. Moreover, the lifetime for the structural changes to occur and molecular length changes caused by them were characterized.

CHAPTER 1

OBJECTIVES

The following objectives were proposed to study force regulation of $FNIII_{7-10}/\alpha_5\beta_1$ interaction.

1. Characterize bond lifetime-force relationships of integrin $\alpha_5\beta_1$ and fibronectin interaction

Integrin $\alpha_5\beta_1$ binds to fibronectin (FN) in the extracellular matrix, which helps cells attach, spread, and migrate, etc. During these processes, the $\alpha_5\beta_1$/FN bond is constantly under stress. Therefore, it is important to characterize the dissociation of the bond under the influence of force. In order to do that, we measured the bond's lifetime at constant forces, namely, the time for the bond to dissociate being pulled by a constant force.

Moreover, integrin $\alpha_5\beta_1$ can bind FN with different affinities that correlate to different conformations. It is suggested that integrins with a bent conformation has low affinity whereas an extended integrin gives higher affinity (1). In addition to the extension of integrin, hybrid domain swing out is another important process for integrin activation (2). These conformational states coexist in equilibrium that can be shifted by signals within the cell, or exogenous influences such as divalent cations and antibodies.

Together, the bond lifetime-force relationships were characterized as integrin $\alpha_5\beta_1$ in different affinity states manipulated by three divalent cation conditions and two activating antibodies.

The result demonstrated that force at range between 10 and 30 pN enhanced lifetime of $FNIII_{7-10}/\alpha_5\beta_1$ bond in all three metal ion conditions that correlate with different integrin conformations and affinity states. In addition, lifetime-force relationships of $\alpha_5\beta_1$ headpiece vs. $FNIII_{7-10}$ are indistinguishable in the same three metal ion conditions.

2. Investigate the bond state in relationship with difference force levels for $FNIII_{7-10}/\alpha_5\beta_1$ interaction

The lifetimes of $FNIII_{7-10}/\alpha_5\beta_1$ interaction were greatly prolonged by a pulling force at range of 10 to 30 pN. It is thus proposed that force induces a strong state of the bond. Does the bond remain at the strong state if the force is released? How does the bond state relate to different magnitude of pulling force? To answer the two questions, the $FNIII_{7-10}/\alpha_5\beta_1$ bond was pulled to different levels of force and then released to a lower force range between 5 to 10 pN, the lifetime of which is then measured. we compared this lifetime with the one at similar force (5~10 pN) without the pre-stress. At an average pulling force about 7pN, as the pre-stress increased, the average lifetime is gradually enhanced compared to the case without the pre-stress. At the lowest pre-stress (< 10pN), the lifetime distributions revealed as single exponential decay. As the pre-stress increased, a second population of much longer lifetimes emerged. As the pre-stress increased to 26 pN and beyond, the two populations again reduced to one. Correspondingly, the average lifetime increased and reached a plateau.

The molecular extensions of FNIII7-10/$\alpha_5\beta_1$-Fc/GG-7 were compared before and after the stretching-relaxation cycle to reveal the molecules' conformational changes.

3. Investigate integrin structural changes induced by force

When integrin $\alpha_5\beta_1$/FN or $\alpha_5\beta_1$/antibody complexes were pulled by a constant force with forceclamp technique, for more than 60% of the events, more than one steps in the force curves were observed even though the overall adhesion frequency is less than 25%. Several evidences demonstrated that this was caused by structural changes of integrin $\alpha_5\beta_1$. This aim not only provides evidences mentioned above, but analyzes some features of the structural changes of integrin $\alpha_5\beta_1$.

CHAPTER 2

INTRODUCTION

INTEGRIN FAMILY AND THEIR FUNCTIONS

Integrins are the principal receptors on animal cells that bind extracellular matrix proteins and also play important roles in certain cell-cell adhesions (3). They integrate the cytoskeleton with points of attachment in the extracellular environment to mediate force-resistant adhesion and signals for a wide variety of cellular functions (Fig 2-1A). Integrin-dependent physiological processes include tissue morphogenesis, inflammation, wound healing, and regulation of cell growth and differentiation.

Integrin are heterodimers, consisting of an α subunit and a β subunit. Each subunit has a large (> 700 residue) NH_2-terminal extracellular domain, a single membrane-spanning domain, and a generally short (13-70 residue) cytoplasmic domain. So far, 18 α subunits and 8 β subunits have been identified and they assemble into 24 distinct integrins (Fig. 2-1A, B) (3, 4). A sub-family of the integrins also include an I domain in their α subunits; where present, this domain is the major site of ligand binding.

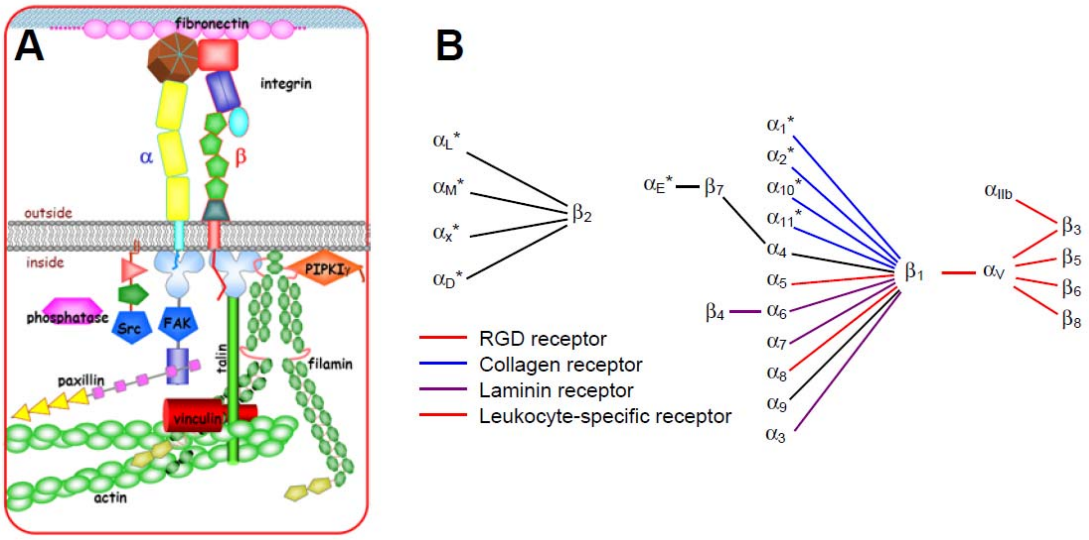

Fig. 2-1 Integrins as mechanical linker and signal transducer and the integrin receptor family. (A) Integrin, an αβ heterodimer, links cytoskeleton of the cell with extracellular matrix (5). (B) 18 α subunits and 8 β subunits assemble into 24 distinct integrins. The α subunits with asterisks have an I domain. Integrins can be classified into several subfamilies based on their ligands (3, 4).

STRUCTURAL BASIS OF INTEGRIN'S FUNCTION REGULATION

Integrins' functions are tightly regulated. In many cases, integrins are expressed on the cell with very low affinity to their ligands, an inactive state. They can be activated by inside-out signaling which enhance integrins' affinity thousands of times (3). Besides inside-out signaling, exogenous influences such as divalent cations and "activating" monoclonal antibodies (mAb) can mimic inside-out signaling and regulate integrins' binding to their ligands (3). What is the structural basis of integrins' function regulation? What kind of signaling can trigger integrin's function? Because this thesis studies soluble forms of integrin in vitro, the first question will be mainly discussed while the studies on the second one will be shortly reviewed.

The studies on the integrins' function regulation were greatly advanced by the publication of crystal structure of the whole extracellular segment of integrin $\alpha_V\beta_3$ in 2001 (Fig. 2-2) (6), which was then followed by the structure of $\alpha_V\beta_3$ in complex with a RGD peptide in 2002 (7).

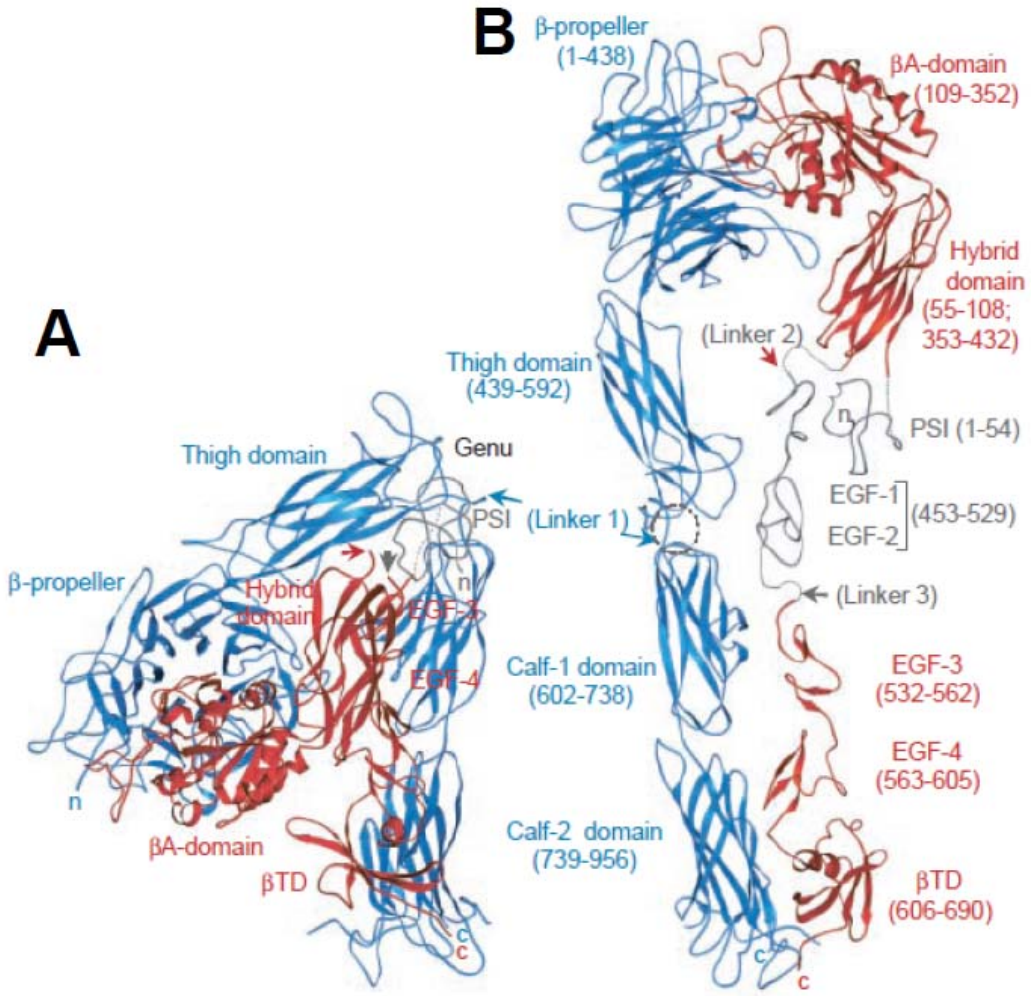

Fig. 2-2 Crystal structure of extracellular segment of integrin $\alpha_V\beta_3$ (6). (A) Structure of $\alpha_V\beta_3$ demonstrates a severely bent shape. (B) An extended view of the structure.

Earlier electron microscopy (EM) studies about $\alpha_{IIb}\beta_3$ revealed the shape of the integrin as an oblong head of ~8 X 10 nm with two rodlike tails extending ~14-17 nm from one side of the head (Fig. 2-3) (8-10). Albeit from earlier (EM) studies, the crystal structure of $\alpha_V\beta_3$ showed a severely bent structure (Fig. 2-2).

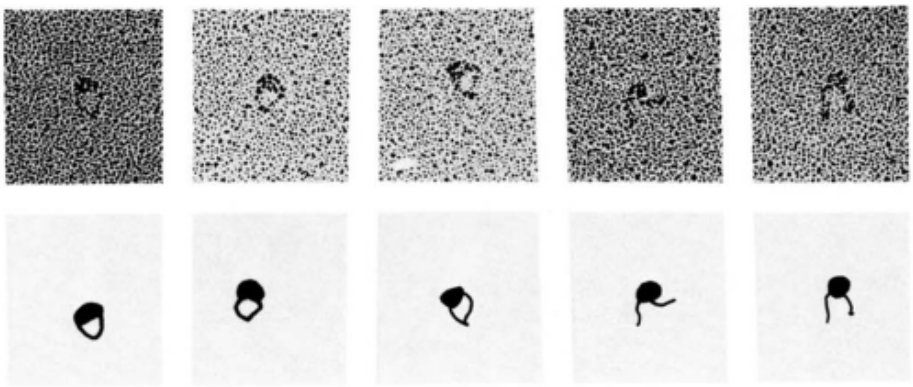

Fig. 2-3. Electron microscopy images of integrin $\alpha_{IIb}\beta_3$ (8). A headpiece with two extending tails were shown, which is significantly different from the crystal structure of $\alpha_V\beta_3$ solved in 2001.

The differences between the crystal structure and the EM images aroused a question that if the severely bent structure observed in the crystal structure was physiological. In 2002, Springer group published EM images of integrin $\alpha_V\beta_3$ under two metal ion conditions (2 mM Ca^{2+} and 1 mM Mn^{2+}) with or without the presence of a ligand mimic peptide (11). In this study, however, both bent and extended conformations of integrin $\alpha_V\beta_3$ were evident. In 5 mM Ca^{2+} condition that keeps the integrin in low affinity toward ligands, majority of the integrin $\alpha_V\beta_3$ displayed a bent conformation (Fig. 2-4 A, B). In 1 mM Mn^{2+} condition that keeps the integrin in high affinity, majority of $\alpha_V\beta_3$ adopt an extended conformation (Fig. 2-4 C, D). Moreover, with a ligand peptide binding to the integrin in both metal ion conditions, $\alpha_V\beta_3$ showed extended conformation (Fig. 2-4 E-H).

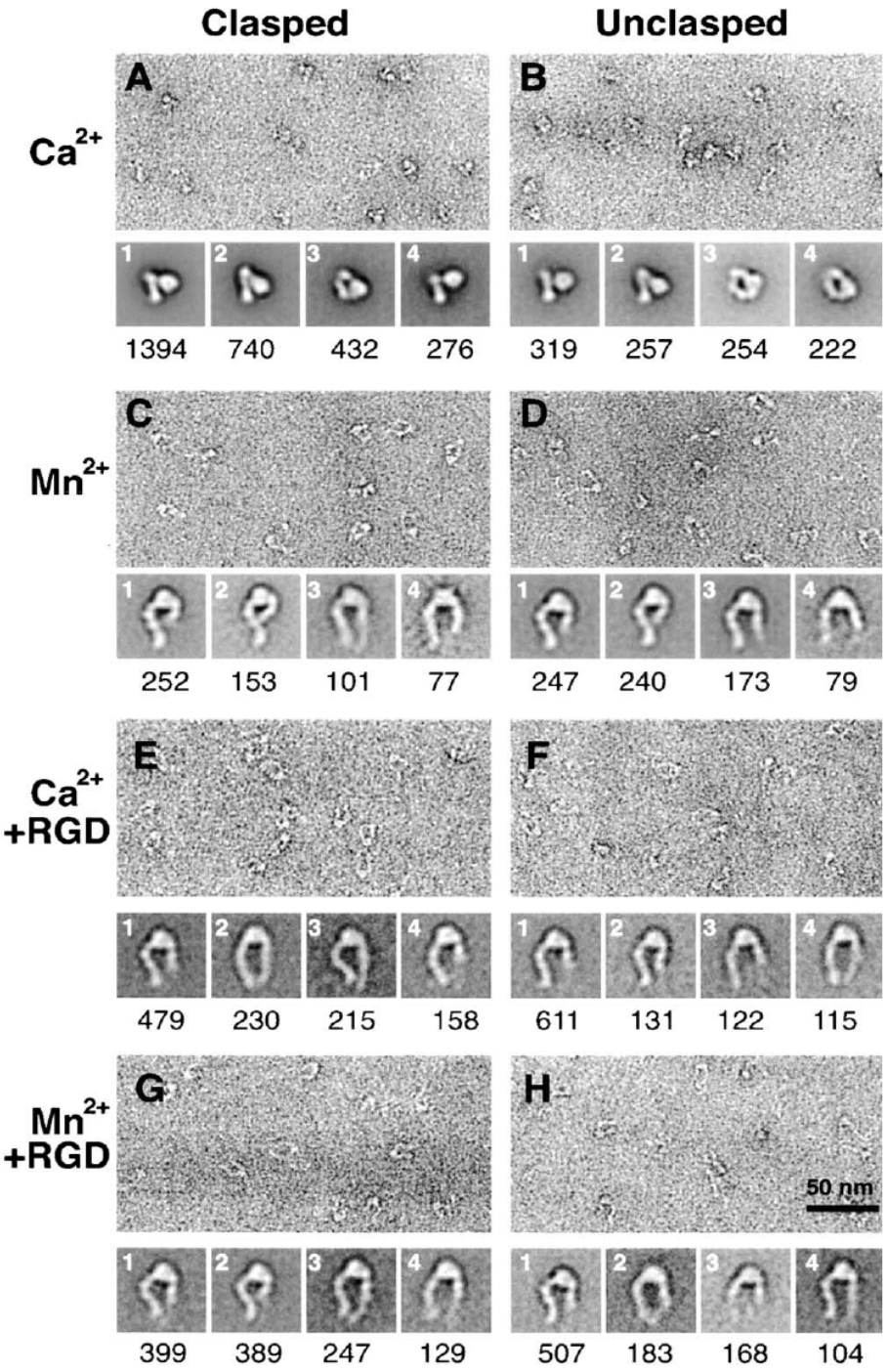

Fig. 2-4 Electron microscopic images of $\alpha_v\beta_3$ in 5 mM Ca^{2+} or 1 mM Mn^{2+} conditions with or without presence of a RGD peptide. The left lane (A, C, E, F) shows $\alpha_v\beta_3$, clasped at the end of legs, in four conditions. The integrins with the clasp cleaved were imaged in the same conditions and shown in the right lane (B, D, F, H). In Ca^{2+}, $\alpha_v\beta_3$ adopts a bent conformation whereas Mn^{2+} and the RGD peptide extended the integrin.

In addition to the EM data, large bodies of biochemical study have also revealed conformational change upon integrin activation and ligand binding. Treatment of $\alpha_{IIb}\beta_3$ with RGDS and LGGAKQAGDV peptides was reported to increase its Stokes radius from 7.4 nm to 8.2 or 8.5 nm, respectively, indicating a peptide-induced conformational change of the integrin (12). More extensive evidences come from identification of anti-integrin monoclonal antibodies, the epitopes for which are exposed when integrin is activated or bound with ligand. Many epitopes of these antibodies were identified at “genu” region of the integrin β subunit (Fig 2-2 A). In 2002, Springer group published the structure of EGF2 and modeled the EGF2 plus EGF3 complex of β_2 subunit. These domains are missing in the $\alpha_v\beta_3$ crystal structure. Two activating antibodies, i.e., CBR LFA-1/2 and MEM48, bind to epitopes on EGF3 domain. Another antibody, KIM127, which only binds to β_2 subunit when integrin is activated, binds to EGF2 domain. The author superimposed the two domains to the original $\alpha_v\beta_3$ crystal structure and demonstrated that the epitopes of the three mAbs were buried and not accessible when integrin is in a bent conformation (Fig. 2-5).

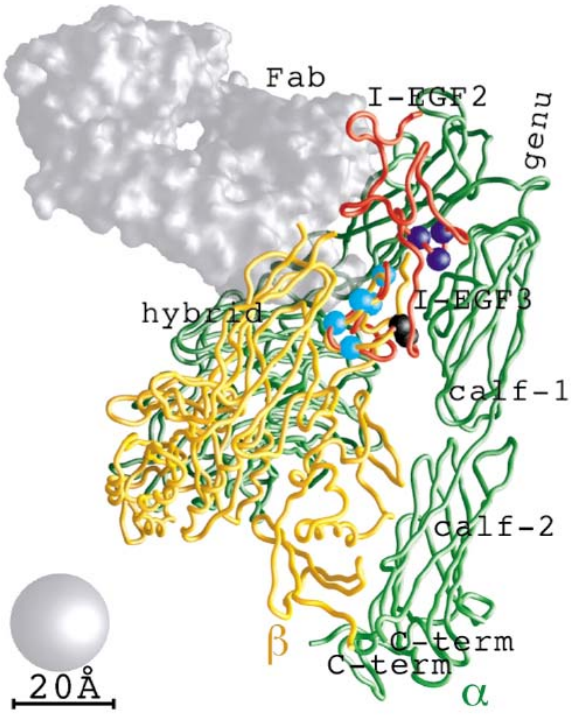

Fig. 2-5 Superposition of EGF2+3 from β_2 upon $\alpha_v\beta_3$. A backbone ribbon display of β_2 EGF2+3 and $\alpha_v\beta_3$ is shown. Polypeptide backbones are red for β_2 EGF2+3, green for α_v and yellow for β_3. Cα atoms of residues in the KIM127 epitope are purple, and cyan in the CBR LFA-1/2 and MEM48 epitopes. The surface of a representative Fab antibody fragment (gray), with its antigen-binding site oriented toward and at the closest approach to the KIM127 and CBR LFA1/2 epitopes, is also shown to illustrate that the KIM127 and CBR LFA-1/2 epitopes are inaccessible to its antigen-binding site (13).

Based on the EM and the biochemical data, the authors proposed a model for integrin's activation, that is: integrins in an inactive state adopt a bent conformation; activation of integrins triggers a switchblade-like opening of the interface between the headpiece and the stalk, which extends the ligand-binding headpiece of the integrin heterodimer away from the stalk region (13).

In addition to extension, the EM images of $\alpha_v\beta_3$ also revealed an outward swing of hybrid domain at its junction with the I-like domain that is linked to ligand binding (11). This is also observed with EM images of $\alpha_5\beta_1$ headpiece binding to a fibronectin fragment (FNIII6-10), which clearly showed hybrid domain swing out

upon ligand binding (Fig. 2-6) (2). The authors termed the headpiece with hybrid domain swung out as an “open” headpiece whereas the one without as the “close” headpiece. They proposed that the integrin with bent and closed headpiece is in low affinity whereas the extended and open headpiece is in high affinity. Integrins that are extended with closed headpiece are in intermediate affinity. Different activating conditions and ligand binding can shift the equilibrium of the three states.

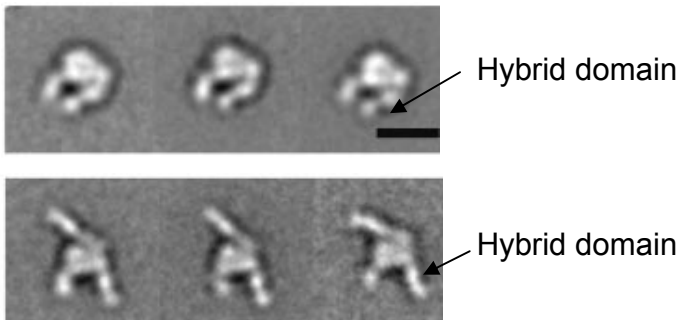

Fig. 2-6 Electron microscopy images of $\alpha_5\beta_1$ headpiece without (top) or with (bottom) ligand binding. The ligand (the extended strip shape protein on the top of the protein complex in the bottom figure) binding induced swung out of the hybrid domain.

The structural detail of an “open” headpiece of $\alpha_{IIb}\beta_3$ was resolved in 2004 (14). Xiao etc. solved two crystal structures of $\alpha_{IIb}\beta_3$ headpiece, one bound to 10E5 Fab, and ligand-mimetic antagonist or cacodylate ion bound to the β_3 I domain metal-ion-dependent adhesion site (MIDAS), and the other contains no Fab. Both structure shows similar conformations, with minor differences in the angle between the β I and hybrid domains. The crystal structures revealed an open, high-affinity conformation of $\alpha_{IIb}\beta_3$ headpiece similar to that in electron microscopy averages of the $\alpha_v\beta_3$ ectodomain with the open headpiece (11) and the $\alpha_5\beta_1$ headpiece bound with FNIII6-10 (2) (Fig. 2-7).

Compared to the $\alpha_v\beta_3$ structure, the $\alpha_{IIb}\beta_3$ open headpiece crystal structure demonstrated the hybrid domain swing out as the consequence of conformational changes of the β I domain. As shown in fig. 2-7 B, compared to the $\alpha_v\beta_3$ close headpiece, the phenomenal changes in the β I domain are β1-α1 loop, the α1-helix, the β6-α7 loop, the α7 helix. The straightening and upward shift of α1 helix in concert with a downward movement of α7 helix resulted the 62° hybrid domain swing-out.

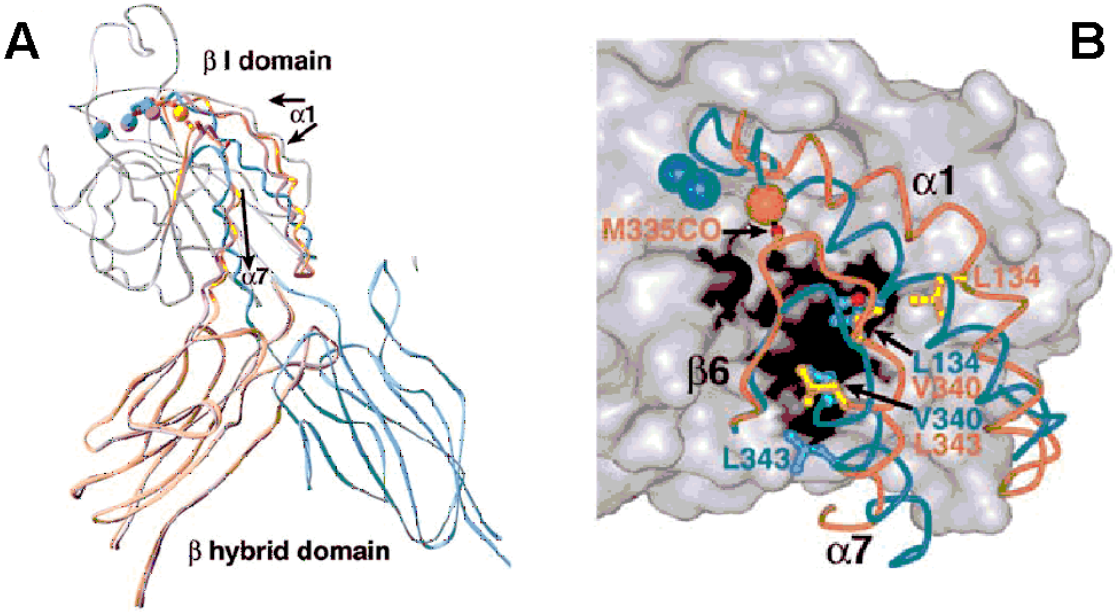

Fig. 2-7 Crystal structure of $\alpha_{IIb}\beta_3$ headpiece in comparison with $\alpha_v\beta_3$ headpiece (14). An overall comparison (A) demonstrates a 62° swing out of hybrid domain and a zoom-in figure (B) elucidates conformational change of the α1 and α7 helices of the I-like domain in comparison with the $\alpha_v\beta_3$ structure. The α1 and α7 helices of $\alpha_{IIb}\beta_3$ I domain are cyan whereas the ones of $\alpha_v\beta_3$ are orange. The rest of the domain is shown as a gray surface. A straighten and upward shift movements of α1 helix are evident, in accommodating the movements near its beginning at the MIDAS and ADMIDAS. In concert of the α1 helix movement, a downward movement of α7 helix is also clear.

The structure differences between the inactivated and activated integrin has so far been revealed in great detail. The inactivated integrins adopt a bent conformation with extensive interactions between the headpiece and the stalk

region that also keep the headpiece “closed”. The activated integrins bound to their ligands adopt an extended global conformation and an “open” headpiece.

However, how inside-out signaling changed integrins from an inactive form to an activated form? Based on the above integrin structures in different activation states and the fact that inside-out signaling has to initiate from the cytoplasmic domain and transit to the extracellular domain, it is reasonable to assume that integrin activation starts from the cytoplasmic portion. Studies have revealed that talin, a cytoskeleton protein, binds to cytoplasmic domain of integrin, which activate integrin $\alpha_{IIb}\beta_3$ (15, 16). Based on crystal and NMR structure of talin F3 domain interacting with β_3 tail domain, Wegener et al. proposed a model of how talin activates integrin (Fig. 2-8) (16). Basically, talin binds to the β_3 tail domain, through electrostatic interactions with the acidic lipid head groups, disengages β_3 cytoplasmic tail from the one of α_{IIb}, which in turn separate the tails and then activate integrin.

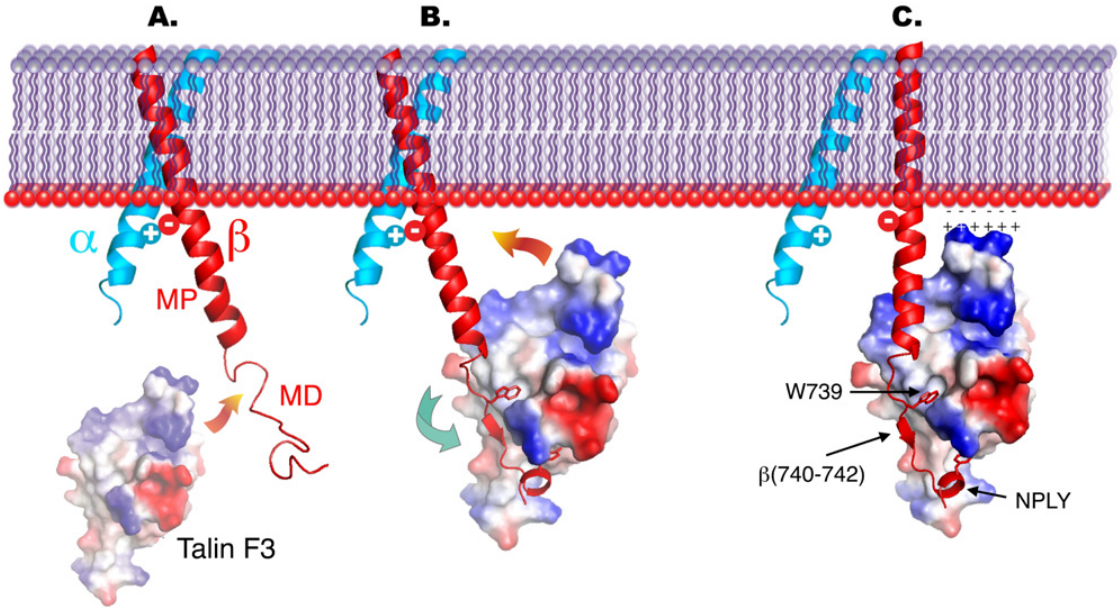

Fig. 2-8 Model of Talin-Induced Integrin Activation. (A) The ready-to-bind talin F3 domain (surface representation; colored by charge). (B) F3 binds the membrane distal (MD) part of the β3-integrin tail (in red), with the α-β integrin interactions that hold the integrin in the low-affinity conformation remain intact. (C) In a subsequent step, F3 engages the membrane proximal (MP) portion of the β3 tail while maintaining its membrane distal interactions. Consequences of this additional interaction are (1) destabilization of the putative integrin salt bridge; (2) stabilization of the helical structure of the MP region; and (3) electrostatic interactions between F3 and the acidic lipid head groups. The net result is a change in the position of the transmembrane helix, which is continuous with the MP-b-tail helix. This position change causes a packing mismatch with the αIIb-transmembrane helix, separation or reorientation of the integrin tails, and activation.

On the extracellular portion, Springer group proposed how the separation of cytoplasmic domains activates the extracellular domains (Fig. 2-9) (14). The separation of cytoplasmic domains breaks the interactions between α and β stalk regions and destabilizes their interface with the headpiece, after which the integrin is able to extend and the hybrid domain could swing out (Fig. 2-9 d-i-j-h) (14). This is partly supported by FRET experiments of integrin $\alpha_4\beta_1$ on living cells demonstrating a displacement of the integrin headpiece away from the cell membrane upon inside-out signaling (17).

Moreover, the authors also proposed how ligand binding could induce conformational change of integrin, i.e., outside-in signaling, as evident in fig. 2-

4C where a ligand peptide induce extension of integrin (Fig. 2-9). Ligand binding induces conformational changes in the metal ion dependent adhesion site (MIDAS), which causes the hybrid domain swing-out that disturbs interactions between the headpiece and the stalk region, which extends integrin and separate the legs (Fig. 2-9 d-f-g-h).

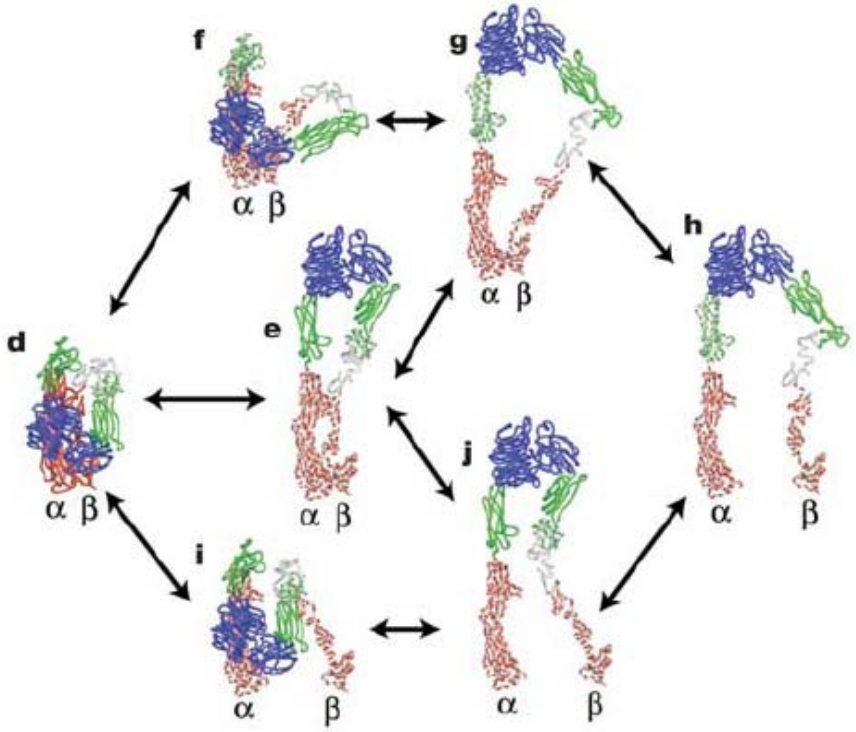

Fig. 2-9 Proposed intermediates in the equilibration between known conformational states. The upper pathways may be stimulated by ligand binding outside the cell, and the lower pathways by signals within the cell that separate the α and β subunit transmembrane domains.

All together, structural basis of integrins' function regulation through conformational change has been revealed in great detail. However, many questions remained to be answered. The proposed transition process between active and inactive integrins needs to be confirmed by experiments. Is this function regulation mechanism universal for all integrins? How does the

interaction between legs break or form? What is the nature of the interaction between headpiece and legs? How would interactions between headpiece and legs stable bent or extended integrin? How fast do bent and extended conformation switch, or do they? How does the switch between bent and extended conformation vary in different conditions? Even though the structural changes in I domain and I-like domain are similar, do they function the same way? Why are there I domains anyway?

FORCE AS A REGULATION FACTOR FOR INTEGRIN-LIGAND INTERACTION

Mechanical forces play an important role in the organization, growth, maturation, and function of living tissues (18). At the cellular level, focal adhesions and adherens junctions responses to external forces and transmit signals into the cell, which control the maturation or disassembly of these adhesions and initiates intracellular signaling cascades that ultimately alter many cellular behaviors. Integrins are core component of focal adhesions and involved in adherens junctions as well. Their role of withholding forces has been well known (18). In fact, local forces have been shown to be correlated with the orientation, size of the focal adhesions (19) (Fig. 2-10), and probably the number of the integrins. However, the evidence that force regulate integrin binding to their ligand has just been reported last year. Stable integrin adhesiveness promoted by lymph node chemokines was only observed under shear forces but not in shear-free environments (20). Therefore, it will of interest to study how force regulates integrins binding with their ligands. Based on integrins' structural and the switchblade model, it seems reasonable to speculate that tensile force applied via a bound ligand may induce unbending of the knees, thereby converting the integrin from a low affinity state with short bond lifetimes to a high affinity state with long bond lifetimes (4, 17, 21-23). Indeed, recent studies have provided experimental support for force-enhanced integrin function (20, 24). Also, steered molecular dynamics simulations have suggested how force-activation of integrin might occur (25, 26). In this study, we will demonstrate how force

regulates integrin $\alpha_5\beta_1$ binding with FN at single molecular level using atomic force microscopy.

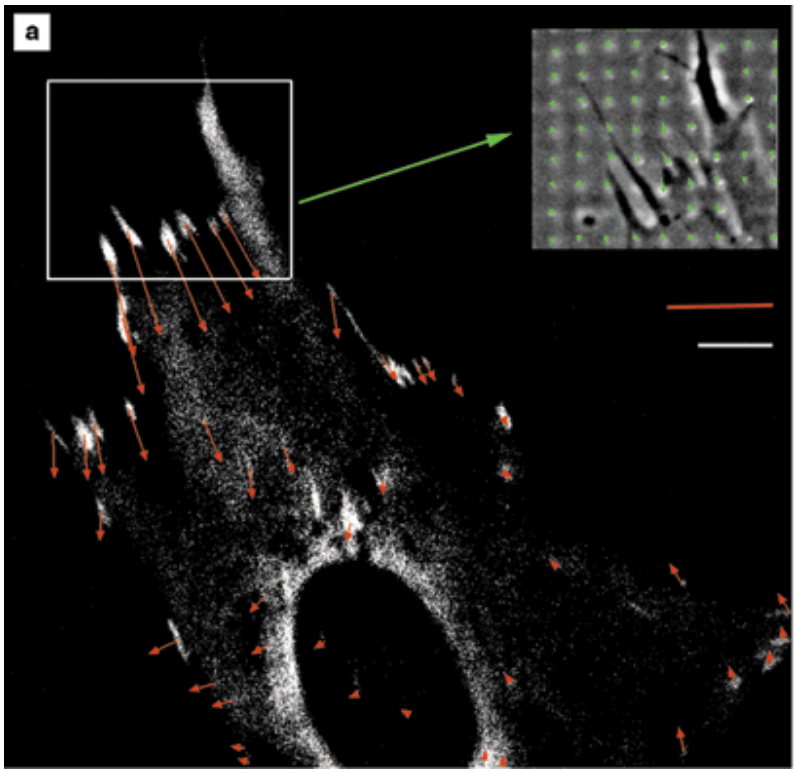

Fig. 2-10 Fluorescence image of a human foreskin fibroblast expressing GFP−vinculin, which localizes to focal adhesions. Red arrows correspond to forces extracted from the displacements of the patterned elastomer. Note the alignment of force with the direction of elongation of large focal adhesions. Inset, phase-contrast image of the upper part of the cell (white rectangle), showing displacements of the dots (green arrows); the pattern consists of small square pits.

CHAPTER 3

MATERIAL AND METHODS

REAGENTS

Recombinant $\alpha_5\beta_1$-Fc and tr$\alpha_5\beta_1$-Fc chimeras were generated and purified as previously described (27). Purified m$\alpha_5\beta_1$ was purchased from Millipore (Billerica, MA). $FNIII_{7\text{-}10}$ with a biotin tag at the N-terminus was generated and purified as described (28). Anti-$\alpha_5\beta_1$ blocking (P1D6) and activating (TS2/16) mAbs were from Millipore and reporting (9EG7) mAb was from BD Biosience (San Diego, CA). Reporting or activating mAb (HUTS-4) was purchased from Millipore. The anti-FN mAb (HFN7.1) was from Developmental Studies Hybridoma Bank (Iowa City, IA). The anti-human Fc capturing mAb (GG-7) was from Sigma (St. Louis, MO).

AFM SYSTEM

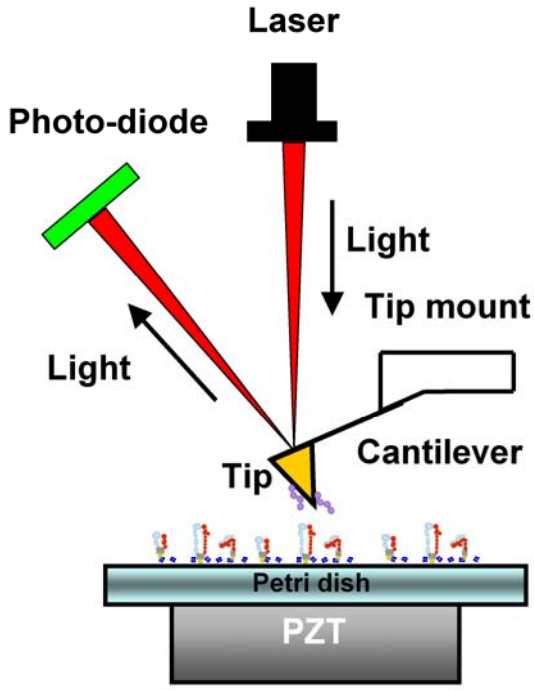

Fig. 3-1 Atomic force microscopy schematic. A laser shoot on the cantilever tip and reflected to a photo-diode which was split into two parts, A and B. The signal difference of A and B was used to monitor cantilever deflection. The Petri dish was mounted on a PZT that controls the movement of the Petri dish in subnanometer resolution.

The AFM is a modification of a previously described system (29, 30) built and calibrated in-house. It consists of a piezoelectric translator (PZT) on which a Peri-dish is directly mounted (Fig. 3-1A). The PZT has a capacitive feedback control that gives sub-nanometer position resolution. A laser (Oz Optics, Ontario, Canada) focused on the end of the cantilever (TM microscopes, Sunnyvale, CA) is deflected onto a photodiode (Hamamatsu, Bridgewater, NJ) to measure cantilever deflection, which is converted to force using the cantilever spring constant. Spring constant (3-12 pN/nm) for each cantilever was calibrated in situ using thermal fluctuation analysis (31). A personal computer with a data acquisition board (National Instruments, Austin, TX) was used to control

movements of the PZT and to collect signals from the photodiode. Labview (National Instruments) was used as the interface between the user and the data acquisition board.

FUNCTIONALIZATION OF AFM CANTILEVERS, PETRI DISHES, AND COVER GLASSES

To measure interaction of $\alpha_5\beta_1$-Fc or tr$\alpha_5\beta_1$-Fc with $FNIII_{7\text{-}10}$ (see Fig. 3-3E or Fig. 3-5E) or $\alpha_5\beta_1$-Fc with P1D6 (see cartoon below Fig. 3-4A), cantilever tips were incubated with 10-20 μg/ml $FNIII_{7\text{-}10}$ or P1D6 overnight at 4 ^{o}C (Fig. 3-1B). After rinsing with Tris buffered saline (TBS, 25 mM Tris-HCl, 150 mM NaCl, pH 7.4), the cantilevers were incubated for 15 min at room temperature in TBS containing 1% BSA to block nonspecific adhesion. GG-7 was cleaved into Fab and Fc fragments by using the Fab preparation kit following the manufacturer's instruction (Thermal Scientific, Rockford, IL). The fragmented GG-7 (at coating concentration indicated in Fig. 3-2 legend) was adsorbed on a small spot on a Petri dish by overnight incubation at 4 ^{o}C. To capture (tr)$\alpha_5\beta_1$-Fc, the GG-7-precoated Petri dish was rinsed three times with TBS and incubated with 10 μg/ml (tr)$\alpha_5\beta_1$-Fc in the desired cation condition (Ca^{2+}/Mg^{2+}, Mg^{2+}/EGTA, or Mn^{2+}) for 30 min. The Petri dish was rinsed three times with TBS again and then filled with 5 ml TBS plus 1% BSA and the indicated cations. In some experiments, 10 μg/ml HFN7.1, 1 mg/ml cyclo(-GRGDSP) (AnaSpec, Inc., San Jose, CA), or 10 μg/ml TS2/16 (see Fig. 3-5F) were added to the buffer.

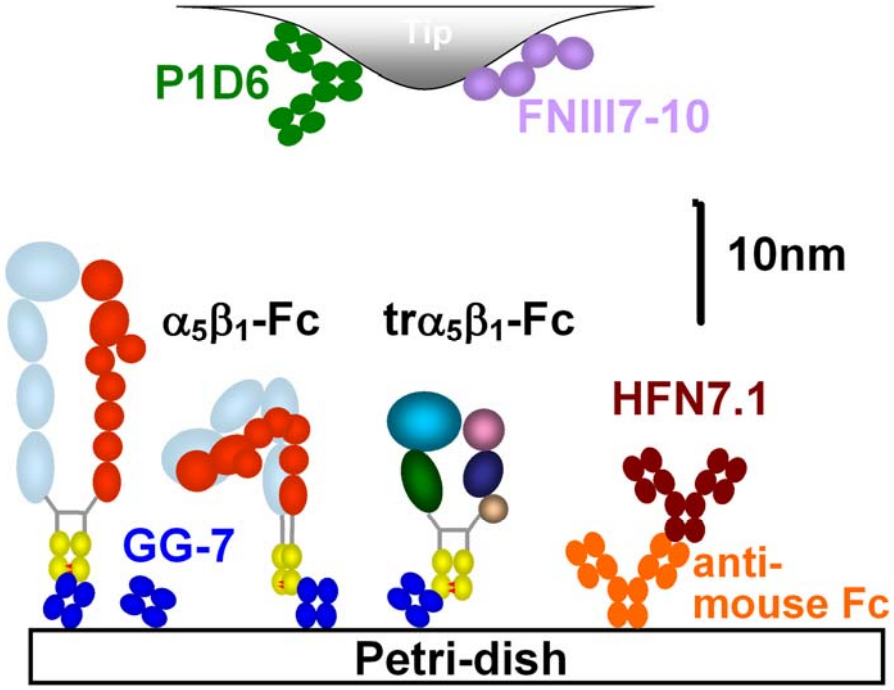

Fig. 3-2 Functionalization of AFM cantilevers, Petri dishes. Integrin (tr)$\alpha_5\beta_1$-Fc was captured by GG-7 that is preadsorbed on the Petri dish. The anti-FN (HFN7.1) was captured by anti-mouse Fc that is preadsorbed on the Petri dish. The $FNIII_{7-10}$ and anti- $\alpha_5\beta_1$ (P1D6) were adsorbed directly on the cantilever tip.

To measure interaction of $FNIII_{7-10}$ with HFN7.1 (see cartoon below 3-4B) or $\alpha_5\beta_1$-Fc with GG-7 Fab (see Fig. 3-3F), $FNIII_{7-10}$ or $\alpha_5\beta_1$-Fc was adsorbed on cantilevers and treated as described above. Goat anti-mouse Fc polyclonal Ab (10 μg/ml) or fragmented GG-7 (20 μg/ml) was adsorbed on a labeled spot on a Petri dish overnight at 4 ^{o}C. To capture HFN7.1, the Petri dish was rinsed three times with TBS and incubated with 10 μg/ml HFN7.1 for 30 min. The Petri dish was rinsed three times again with TBS and then filled with 5 ml TBS plus 1% BSA and indicated cations.

To measure interaction of $FNIII_{7-10}$ with m$\alpha_5\beta_1$, cantilevers were coated with streptavidin at 50 μg/ml overnight at 4 ^{o}C and further functionalized by

incubation with 10 μl of 1 μg/ml $FNIII_{7-10}$ for 15 min at room temperature. Membrane $\alpha_5\beta_1$-incoporated lipid vesicle solution was prepared according to a published method (32). Briefly, vesicles were formed by hydrating a dried lipid film of 1,2-Dimyristoyl-*sn*-Glycero-3-Phosphocholine and 1,2-Dimyristoyl-*sn* -Glycero-3-[Phospho-*rac*-(1-glycerol)] (Avanti Polar Lipids, Alabaster, AL) in 50:50 ratio with 0.1% Triton X-100 (Thermo Fisher Scientific Inc., Pittsburgh, PA) in TBS and mixed with $m\alpha_5\beta_1$, resulting in a final concentration of 0.27 mg/ml (0.4 mM) of lipid and 0.1 mg/ml of integrin. Triton X-100 was then removed by adsorption to BioBeads SM-2 (Bio-Rad Laboratories Inc., Richmond, CA) at 37 ^oC for 4 h. The resulting lipid vesicle solution was stored under argon at 4 ^oC and used within several months. Coverslips of 40 mm in diameter (Bioptechs, Butler, PA) were cleaned with a mixture of 70% 12 N sulfuric acid and 30% hydrogen peroxide by volume at 100 ^oC for 45 min, rinsed extensively with deionized water, and dried completely under an argon stream. The cleaned coverslip, which was used immediately, was placed in a Petri dish and a 4μl drop of $m\alpha_5\beta_1$-incorporated lipid vesicle solution was placed on the coverslip surface. After 20 min of incubation under a damp paper towel, the Petri dish was filled with 5 ml of TBS with 2 mM Mg^{2+}, 2 mM EGTA and 1% BSA. The $m\alpha_5\beta_1$ bilayers so formed had low molecular densities to ensure their infrequent binding to the $FNIII_{7-10}$ coated cantilever tips, as required for measuring single bonds. Bilayers were immediately used in AFM experiments.

LIFETIME MEASUREMENT WITH FORCECLAMP TECHNIQUE

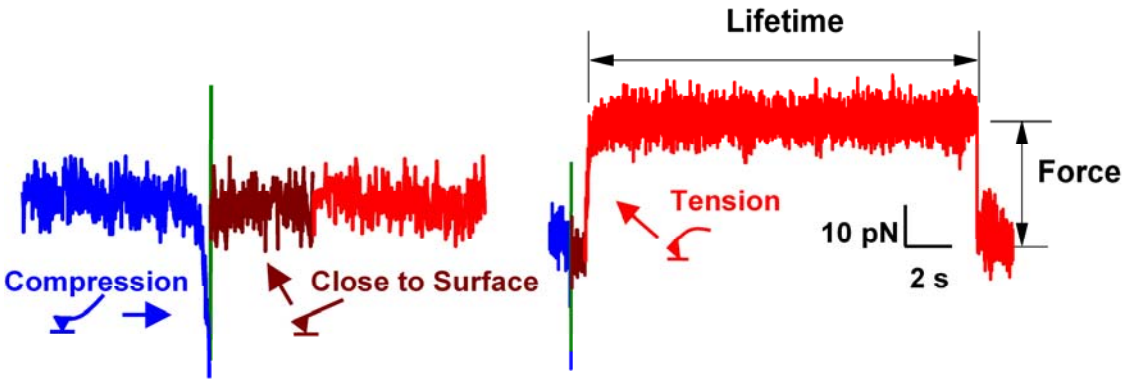

Fig. 3-3 Force-scan trace with (right panel) or without (left panel) adhesion. The Petri dish was moved up by the PZT to contact the cantilever tip (blue trace), immediately retracted to a small distance (green trace) from the tip to reduce nonspecific adhesion, held at this distance for 0.5 s to allow for bond formation (brown trace), retracted away from the tip to detect adhesion (red trace). The left trace illustrates a contact cycle without binding where the retraction curve returned to zero force upon Petri dish retraction. The right trace demonstrate force-scan trace with adhesion. The color-codes are the same as those in left panel, which illustrates a contact cycle with binding and lifetime measurement. Petri dish retraction resulted in a tensile force indicating binding. Once the pulling force reached a preset value, a feedback loop was triggered to keep the cantilever deflection at the set point. The lifetime at that force (indicated) was measured until bond failure, signified by the springing back of the cantilever tip to the level of zero mean force.

The AFM force-clamp experiments were performed by repeatedly bringing the Petri dish in contact with the cantilever tip, then immediately retracting a small distance (0-5 nm), holding at that distance for 0.5 s to allow bond formation, and retracting again at a speed of 200 nm/s. By preventing the cantilever from pushing the Petri dish during the time for molecular association, the nonspecific binding was greatly suppressed (Fig. 4-1). The presence of adhesion was detected from the force-scan curves (Fig. 1 C and D). A feedback system was used to clamp the force at a desired level to enable measurement of bond lifetime at constant force.

CHAPTER 4

DEMONSTRATION OF FN/$\alpha_5\beta_1$ SPECIFICITY

NONSPECIFIC ADHESIONS CONTROL

When the Petri dish is pushed against the cantilever tip, often times nonspecific adhesions occur and can be observed from the force curve when the Petri dish is retracted away. As specific adhesions of receptor/ligand interaction are measured, they are difficult to differentiate from the nonspecific adhesion. Therefore, it is critical to reduce the nonspecific adhesion so that majority of adhesions measured are specific interaction between the receptor and the ligand.

The nonspecific adhesion between the Petri dish and the cantilever tip could come from electrostatic and van der Waals interaction, et al. The harder pushed against each other, the higher probability and strength is the nonspecific adhesion. In a typical cycle of experiment, the Petri dish is brought in contact with the cantilever tip for a period of time (contact time) to allow receptor/ligand bonds to form and then retracted away to measure the interaction. In such a process, an initial pushing force between the Petri dish and the cantilever tip is necessary to locate them close to each other so that receptor/ligand interaction can form. Thus, a way to reduce nonspecific adhesions is to reduce the amount of pushing force of the Petri dish against the cantilever at initial contact and create a space between the cantilever tip and the Petri dish during the contact time so that nonspecific adhesions can be reduced whereas specific adhesions are still able to form. Therefore, the new process brings the Petri dish in contact with the

cantilever tip with a small pushing force (~ 30 pN) and then immediately retract the Petri dish away from the cantilever tip to create a small distance at where the Petri dish is held for a period of time (still named contact time) for the receptor/ligand interaction to form and then retract further away to measure the interaction. To determine a good distance between the Petri dish and the cantilever tip during the contact time, the adhesion frequencies were measured against such distances for both nonspecific and specific adhesion (Fig. 4-1). With a small pushing force (< 30 pN) and separating distance (0 ~ 4 nm), the nonspecific adhesion was less than 5% whereas reasonable amount of specific adhesions were still measured (~ 10%) (Fig. 4-1). All measurements using $\alpha_5\beta_1$-Fc functionalized Petri dishes were carried out this way. For membrane $\alpha_5\beta_1$ reconstituted in a glass supported bilayer, because the nonspecific adhesion was abolished by the bilayer (Fig. 4-4), the Petri dish was pushed against the cantilever tip during the contact time without a separation distance.

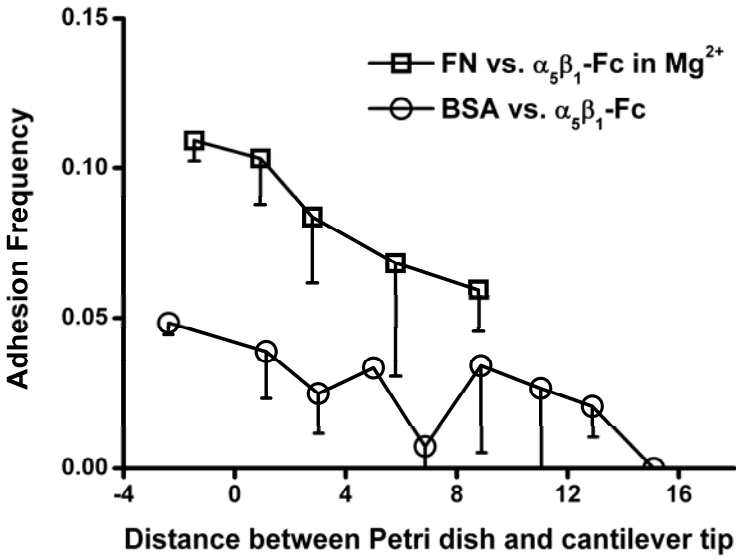

Fig. 4-1 Distance-adhesion frequency relationship of $FNIII_{7-10}$ or BSA coated cantilever tips interacting with $\alpha_5\beta_1$-Fc functionalized Petri dish.

SPECIFICITY OF $FNIII_{7-10}$ INTERACTING WITH $\alpha_5\beta_1$-Fc CHIMERA

Binding specificity of $FNIII_{7-10}/\alpha_5\beta_1$-Fc interaction was demonstrated by the ability of metal ion to regulate the binding frequency (a key feature of integrin/ligand interaction) (Fig. 4-2 A), the abolishment of adhesions by a blocking antibody or RGD peptide (Fig. 4-2 A), and the dramatic differences of adhesion frequencies compared to nonspecific adhesions (Fig 4-2 B).

Adhesions were measured at 1 mM Ca^{2+} plus 1 mM Mg^{2+} (1mM Ca^{2+}/Mg^{2+}), 2 mM Mg^{2+} plus 2 mM EGTA (2 mM Mg^{2+}/EGTA), and 2 mM Mn^{2+} conditions. As demonstrated in chapter 3, integrin $\alpha_5\beta_1$-Fc was captured by GG-7 preadsorbed on the Petri dish. When GG-7 at concentration of 15 μg/ml was used to coat the Petri dish and 10 μg/ml of $FNIII_{7-10}$ was used to coat the cantilever tip, the adhesion frequencies of $FNIII_{7-10}/\alpha_5\beta_1$-Fc interaction increases sequentially from Ca^{2+}/Mg^{2+}, to Mg^{2+}/EGTA and Mn^{2+} conditions (Fig. 4-2 A),

which is consistent with previous results that show higher and higher affinities as the same metal ion conditions were exchanged (33). Moreover, the adhesions were abolished by adding a blocking antibody (anti-FN, HFN7.1), and cyclo(-GRGDSP) which competes with the RGD sequence on the $FNIII_{7-10}$ binding with $\alpha_5\beta_1$.

The specificity of $FNIII_{7-10}/\alpha_5\beta_1$-Fc interaction was further demonstrated by the dramatic decrease of adhesion frequencies when the $FNIII_{7-10}$ coated cantilever was switched to a BSA coated cantilever, or when the Petri dish functionalized with $\alpha_5\beta_1$-Fc was switched to a Petri dish without $\alpha_5\beta_1$-Fc functionalization (Fig. 4-2 B).

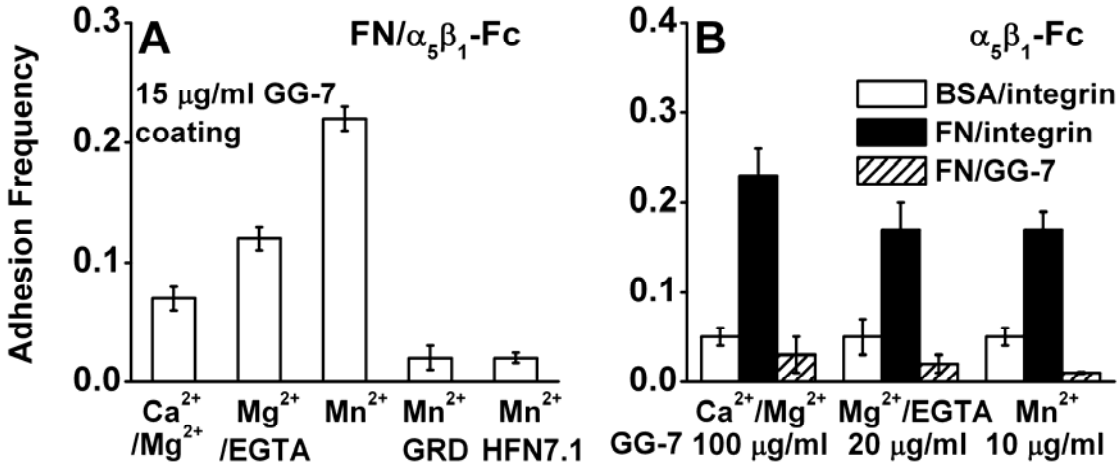

Fig. 4-2 Binding specificity of $FNIII_{7-10}/\alpha_5\beta_1$-Fc interaction. (A) Switching metal ion conditions or adding a blocking antibody and RGD peptide were able to regulate the binding frequencies. (B) Dramatic decreases of binding frequencies were shown by switching FN coated cantilever to BSA coated one or $\alpha_5\beta_1$-Fc functionalized Petri dish to the one without $\alpha_5\beta_1$-Fc functionalization. To obtain reasonable adhesion frequencies (~ 20%), different coating densities of GG-7 were used in Ca^{2+}/Mg^{2+} (100 μg/ml), Mg^{2+}/EGTA (20 μg/ml) and Mn^{2+} (10 μg/ml) conditions.

SPECIFIICTY OF $FNIII_{7-10}$ INTERACTING WITH $tr\alpha_5\beta_1$-Fc CHIMERA

The specificity of $FNIII_{7-10}/tr\alpha_5\beta_1$-Fc interaction was demonstrated similarly to $FNIII_{7-10}/\alpha_5\beta_1$-Fc interaction (Fig. 4-3). However, the binding frequencies of

$FNIII_{7-10}$/tr$\alpha_5\beta_1$-Fc interaction were lower in the same metal ion conditions given the same GG-7 coating density. This could be caused by shorter integrin length and more constraint on the headpiece. The same binding pocket with shorter molecular length was demonstrated to give lower association rate (34). In the experiment setup, α and β chain of $\alpha_5\beta_1$ were fused in the human Fc. For tr$\alpha_5\beta_1$, the β propeller and thigh domain of α subunit and A, hybrid and PSI domains of β subunit were fused to the Fc. Because of a closer position of the hybrid domain to Fc, the hybrid domain could be restrained more compared to the whole integrin structure and difficult to swing out, therefore contributed to a lower association rate (see introduction and Fig 3-1).

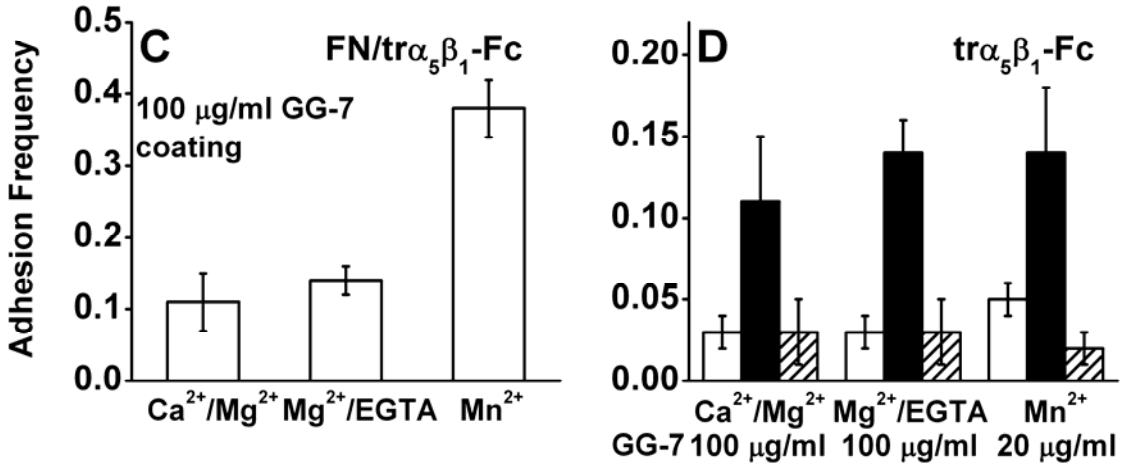

Fig. 4-3 Binding specificity of $FNIII_{7-10}$/ tr$\alpha_5\beta_1$-Fc interaction. (A) Switching metal ion conditions changed the binding frequencies. (B) Dramatic decreases of binding frequencies were shown by switching FN coated cantilever to BSA coated one or tr$\alpha_5\beta_1$-Fc functionalized Petri dish to the one without tr$\alpha_5\beta_1$-Fc functionalization. To obtain reasonable adhesion frequencies (~ 15%), different coating densities of GG-7 were used in Ca^{2+}/Mg^{2+} (100 μg/ml), Mg^{2+}/EGTA (100 μg/ml) and Mn^{2+} (20 μg/ml) conditions.

SPECIFICITY OF $FNIII_{7-10}$ INTERACTING WITH MEMBRANE $\alpha_5\beta_1$

Membrane $\alpha_5\beta_1$ was reconstituted into lipid bilayer as described in chapter 3. The $FNIII_{7-10}$ (with a biotin at N terminal) was captured by streptavidin

preadsorbed on the cantilever tip. The nonspecific adhesion was measured by using streptavidin coated cantilever tip against the m $\alpha_5\beta_1$ reconstituted in the bilayer. Then, the same cantilever was functionalized with $FNIII_{7\text{-}10}$ and than tested against the m$\alpha_5\beta_1$. The specific adhesion frequency is 4 times higher than the nonspecific adhesion, which justified that majority of the adhesions were specific.

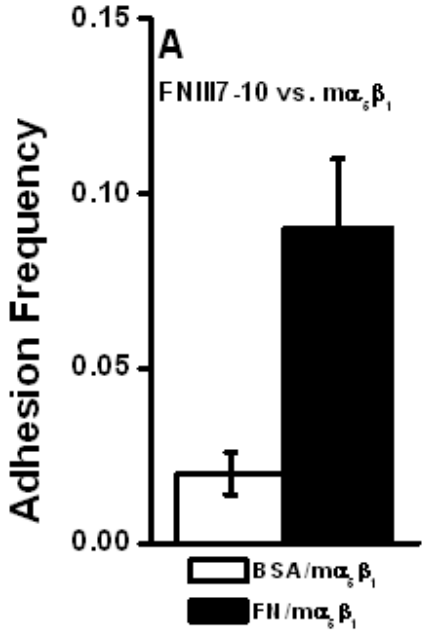

Fig. 4-4 Frequency of adhesion between m$\alpha_5\beta_1$ reconstituted into bilayers and streptavidin coated cantilever tips functionalized with (solid bar) or without (open bar) $FNIII_{7\text{-}10}$ in Mg^{2+}/EGTA.

SPECFICITY OF ANTIBODIES INTERACTING WITH $\alpha_5\beta_1$-Fc AND FN

The adhesions of $\alpha_5\beta_1$ and FN against their antibodies were also tested as comparisons to the receptor/ligand interaction. Their specificities were demonstrated similar to the receptor/ligand interaction (Fig. 4-5).

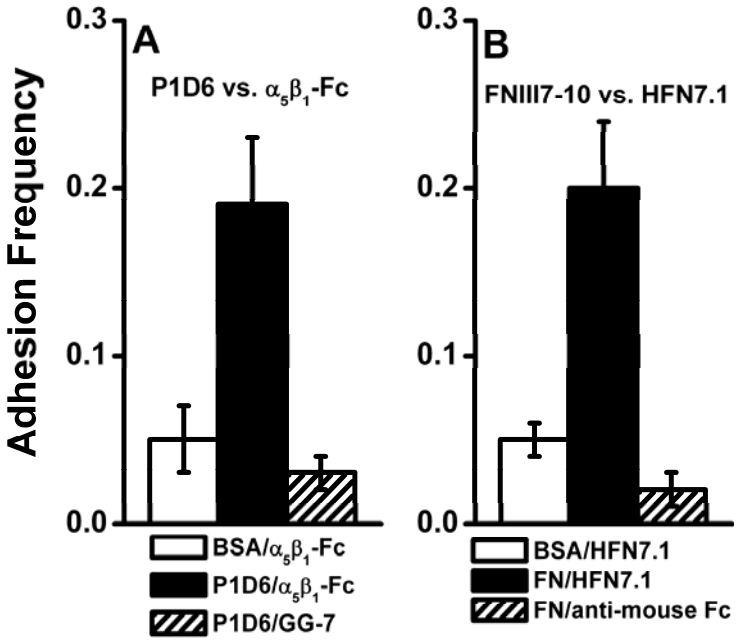

Fig. 4-5 Specificity of mAbs against $\alpha_5\beta_1$-Fc and FN. (A) Frequency of adhesion between $\alpha_5\beta_1$-Fc captured by GG-7 precoated on Petri dishes and P1D6 coated on cantilever tips (solid bar) is compared with that between $\alpha_5\beta_1$-Fc functionalized Petri dishes and BSA coated cantilever tips (open bar) and with that between P1D6 coated tips and GG-7 coated Petri dishes without incubation with $\alpha_5\beta_1$-Fc (hatched bar). (B) Frequency of adhesion between anti-FN mAb (HFN7.1) captured by goat anti-mouse Fc Ab preadsorbed on Petri dishes and $FNIII_{7\text{-}10}$ coated on cantilever tips (solid bar) is compared with that between HFN7.1 functionalized Petri dishes and BSA coated cantilever tips (open bar) and with that between goat anti-mouse Fc Ab coated Petri dishes without HFN7.1 incubation and $FNIII_{7\text{-}10}$ coated cantilever tips (hatched bar).

CHAPTER 5

LIFETIME-FORCE RELATIONSHIP OF FN/$\alpha_5\beta_1$ INTERACTION

LIFETIME-FORCE RELATIONSHIP OF FN/$\alpha_5\beta_1$ INTERACTION

Lifetime-force relationships of $FNIII_{7\text{-}10}$//$\alpha_5\beta1$ interaction were characterized to demonstrate mechanical regulation of the bond. The characterization was done in three metal ion conditions that manipulate conformational and affinity states of integrin $\alpha_5\beta_1$-Fc. As illustrated in chapter 2, $\alpha_5\beta_1$ are in low, intermediate and high affinities in Ca^{2+}/Mg^{2+}, Mg^{2+}/EGTA, and Mn^{2+} conditions, respectively, which correlates with bent, extended with close headpiece, extended with open headpiece conformations (11). To confirm this with $\alpha_5\beta_1$-Fc, flow cytometry was used to analyze staining of two anti- $\alpha_5\beta_1$ mAbs, 9EG7 and HUTS-4, that recognize extension and hybrid domain swing-out conformations of $\alpha_5\beta_1$, respectively (Fig 5-1, 5-2) (35, 36). 9EG7 staining data indeed showed that more integrin exist in extended conformation in Mg^{2+}/EGTA and Mn^{2+} than in Ca^{2+}/Mg^{2+} condition (Fig. 5-1). Moreover, staining of HUTS-4 demonstrated that only in Mn^{2+} did hybrid domain swing-out that gave an open headpiece.

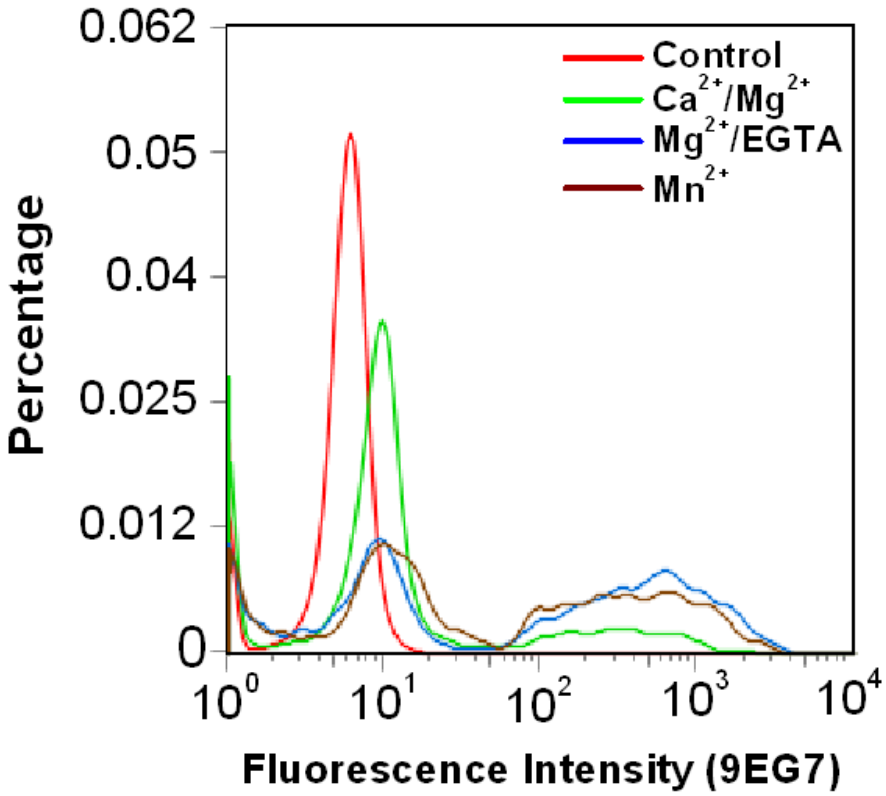

Fig. 5-1 Expression of 9EG7 epitope by $\alpha_5\beta_1$-Fc in three cation conditions. Binding of APC-conjugated anti-β_1 mAb 9EG7 to $\alpha_5\beta_1$-Fc was analyzed by flow cytometry. $\alpha_5\beta_1$-Fc was captured by GG-7 preadsorbed on the glass beads. Data measured in three cation conditions as well as control data are presented as fluorescence intensity histograms.

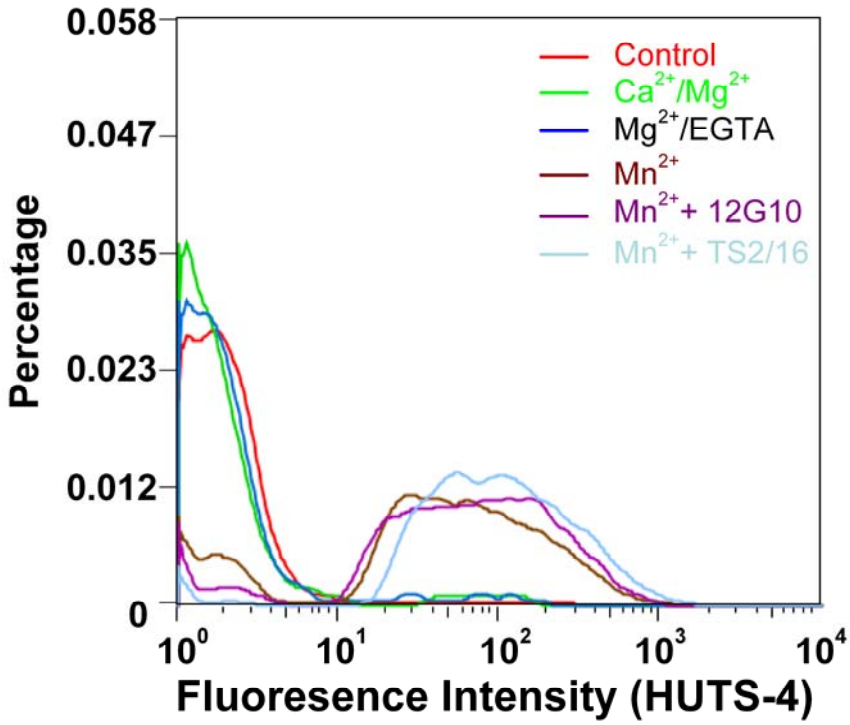

Fig. 5-2 Expression of HUTS-4 epitope by $\alpha_5\beta_1$-Fc in five conditions. Binding of FITC-conjugated anti-β_1 mAb HUTS-4 to $\alpha_5\beta_1$-Fc was analyzed by flow cytometry. $\alpha_5\beta_1$-Fc was captured by GG-7 Fab linked on the glass beads.

Surprisingly, the lifetime-force relationships in all three metal ion conditions have similar trend (Fig. 5-3). As force increased, lifetime first decreased to a minimum, then increased to a maximum, and decreased again, exhibiting a triphasic transition from slip bonds to catch bonds and then to slip bonds again. The first slip bond regime was most clearly observed in Ca^{2+}/Mg^{2+} (Fig. 5-3 A) but became less pronounced in Mg^{2+}/EGTA (Fig. 5-3 B) and Mn^{2+} (Fig. 5-3 C). Of particular interest are the catch bonds, which were observed in all three conditions at forces ranging from 10-30 pN.

To control for potential artifacts of the chimeric integrin that fuses the extracellular portions of the α_5 and β_1 chains with a human IgG Fc (27), the lifetime-force relationship was measured for $FNIII_{7\text{-}10}$/membrane (m) $\alpha_5\beta_1$

interaction in Mg^{2+}/EGTA (chapter 3). Although the lifetimes were shorter, their force dependent curve exhibited the same triphasic pattern (Fig. 5-3 D) qualitatively similar to the $\alpha_5\beta_1$-Fc curves (Fig. 5-3 A-C), confirming that catch bonds existed in the same force range.

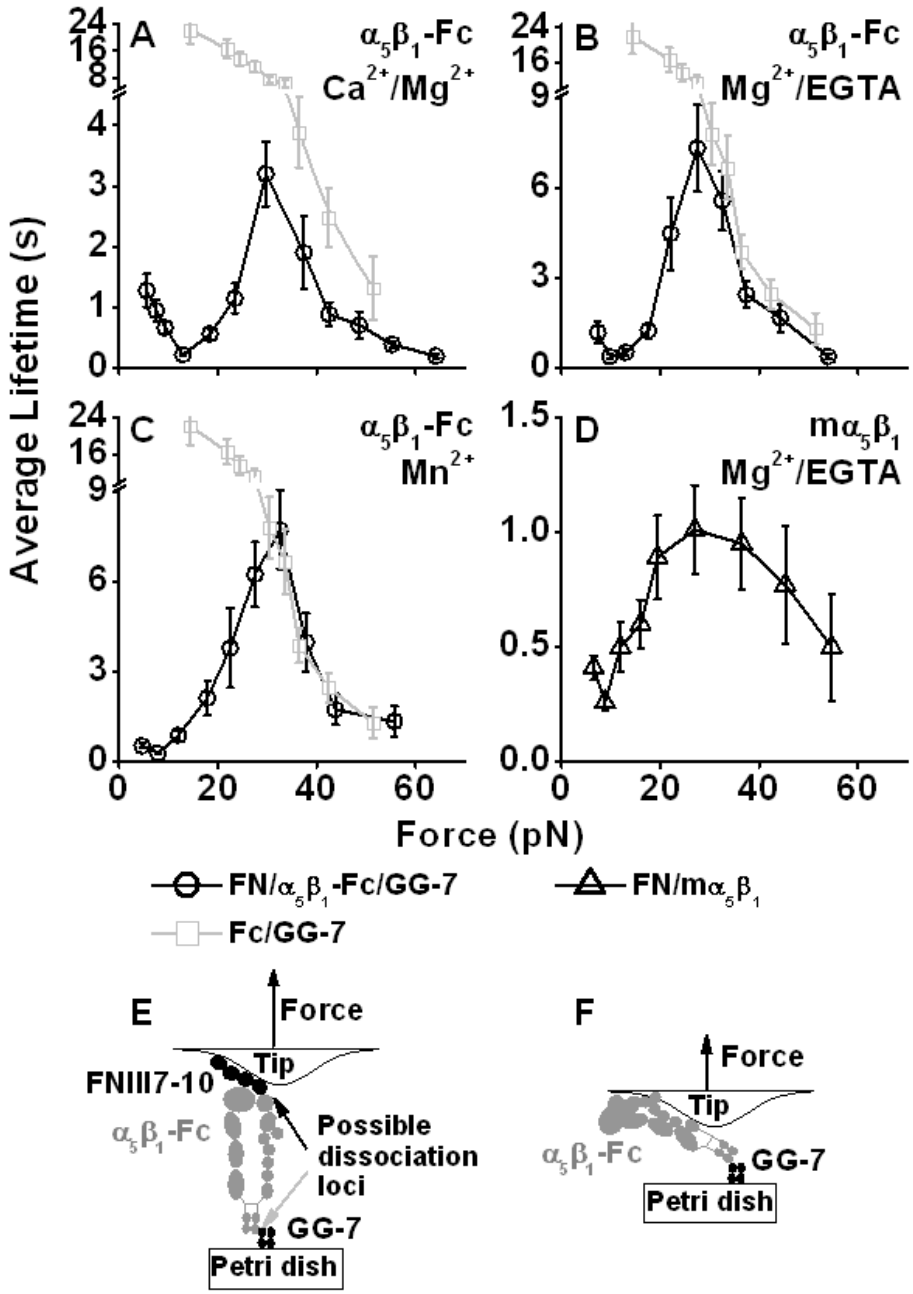

Fig. 5-3. Lifetimes of FN/$\alpha_5\beta_1$ bonds. Plots of lifetime (mean ± s.e.m.) vs. force of $\alpha_5\beta_1$-Fc functionalized Petri dish dissociating from $FNIII_{7\text{-}10}$ coated cantilever tip (black circles) in Ca^{2+}/Mg^{2+} (A), Mg^{2+}/EGTA (B), and Mn^{2+} (C). (D) A qualitatively similar plot (black triangles) of $m\alpha_5\beta_1$ reconstituted into lipid bilayer dissociating from $FNIII_{7\text{-}10}$ coated cantilever tip in Mg^{2+}/EGTA reconfirmed the catch bond observation. Also plotted in A-C is the lifetime (mean ± s.e.m.) vs. force curve of Fc dissociating from GG-7 (gray squares). For (B) and (C), the black circle curve and the gray square curve overlap at forces >30 pN, indicating measured lifetimes at this force range were due to Fc/GG-7 dissociation instead of $FNIII_{7\text{-}10}/\alpha_5\beta_1$-Fc dissociation. (E) Cartoon of the molecular arrangement indicating possible dissociation loci between $FNIII_{7\text{-}10}$ and $\alpha_5\beta_1$-Fc or $\alpha_5\beta_1$-Fc and GG-7. (F) Cartoon of the molecular arrangement for experiments that measured the capturing strength of the Fc/GG-7 interaction.

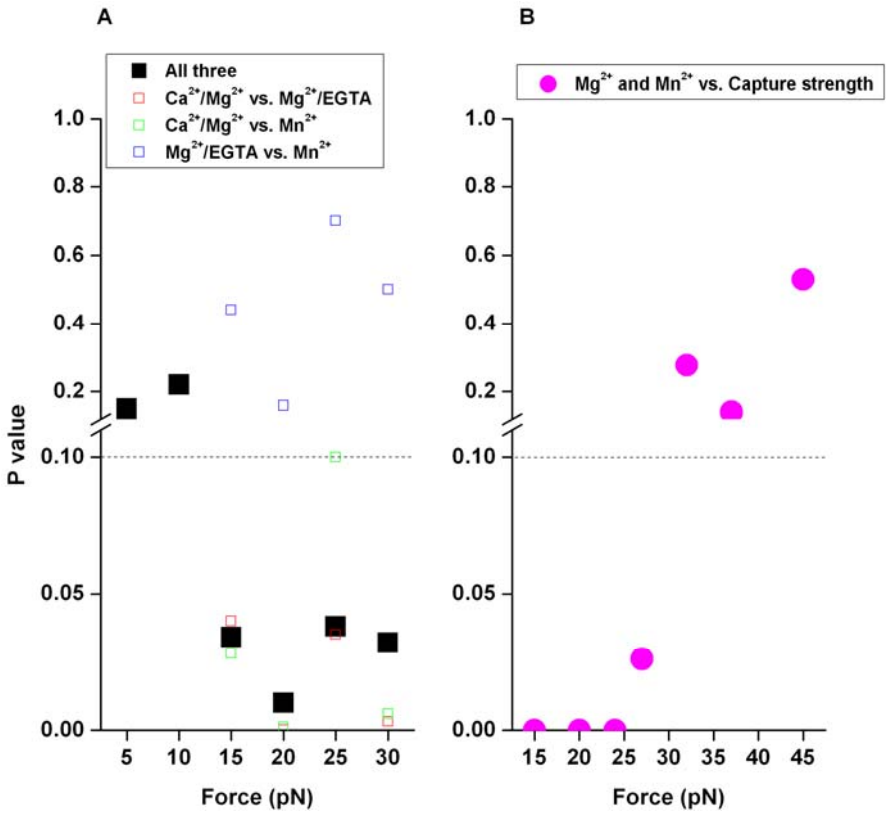

Fig. 5-4 Statistical analysis of force-lifetime relationships of FN/$\alpha_5\beta_1$-Fc/GG-7 interaction. (A) Statistical analysis of force-relationships in the catch bond region among three metal ion conditions for FN/$\alpha_5\beta_1$-Fc/GG-7 interaction. The black squares are P value acquired from ANOVA comparing the values of the three curves at the same force level. Below 10 pN, P values are higher than 0.1, indicating the differences among three curves are not significant. Beyond 15 pN, the differences among the three curves are significant. Student t tests between each pair of curves indicate that in the Ca^{2+}/Mg^{2+} condition, beyond 15 pN, the lifetimes are significantly smaller than the other two conditions, Mg^{2+}/EGTA and Mn^{2+}, which showed no significant differences in the entire catch bond region. (B) Statistical analysis among force-lifetime relationships of FN/$\alpha_5\beta_1$-Fc/GG-7 interaction in Mg^{2+}/EGTA, Mn^{2+}, and Fc/GG-7 interaction. Below 30 pN, the lifetime of the capture strength is significantly higher than the lifetime of FN/$\alpha_5\beta_1$-Fc/GG-7 interaction.

Since $\alpha_5\beta_1$-Fc was captured by preadsorbed GG-7, rupture of the molecular complex might result from dissociation of the FN/$\alpha_5\beta_1$ bond or the Fc/GG-7 bond (Fig. 5-3 E). We neglect potential detachment of $FNIII_{7\text{-}10}$ from the cantilever tip or of GG-7 from the Petri dish because physioadsorption of proteins is generally much stronger than specific protein-protein interactions. To determine the rupture loci, we overlaid the force-dependent lifetimes of directly

adsorbed $\alpha_5\beta_1$-Fc interacting with GG-7 (see Fig. 5-3 F) on each panel of Fig. 5-3 A-C (gray squares). Slip bonds were observed over the entire force range tested. The mean lifetimes at forces <25 pN were much longer than those of $FNIII_{7-10}$ interacting with captured $\alpha_5\beta_1$-Fc, indicating that the observed catch bonds were characteristic of the FN/$\alpha_5\beta_1$ bond rather than the Fc/GG-7 bond. However, at forces >30 pN, the black circle curves in Fig. 5-3 B and C became indistinguishable to the gray square curve, suggesting that the second slip bonds of the former curves result from dissociation of the Fc/GG-7 bond rather than the FN/$\alpha_5\beta_1$ bond. Since the reciprocal mean lifetime of two bonds in series is the sum of reciprocal mean lifetimes of the two bonds, the FN/$\alpha_5\beta_1$ bond lifetimes in Mg^{2+}/EGTA or Mn^{2+} must be substantially longer than the Fc/GG-7 bond lifetimes at forces >30 pN, which were indistinguishable to the lifetimes of the FN/$\alpha_5\beta_1$ and Fc/GG-7 bonds in series. The FN/$\alpha_5\beta_1$ bond in Mg^{2+}/EGTA or Mn^{2+} might continue to behave as catch bonds at forces >30 pN before (and if) it transitioned to slip bonds. In Ca^{2+}/Mg^{2+}, by contrast, transition to slip bonds occurred at ~30 pN as the peak lifetime of the FN/$\alpha_5\beta_1$-Fc/GG-7 serial bonds was significantly shorter than that of the Fc/GG-7 bond (Fig. 5-3 A).

LIFETIME-FORCE RELATIONSHIP OF $FNIII_{7-10}$/tr$\alpha5\beta1$ INTERACTIONS

Despite different populations of bent and extended, or close and open headpieces, catch bonds were observed in all three cation conditions. The lifetimes were shorter in Ca^{2+}/Mg^{2+} (Fig. 5-3 A) than Mg^{2+}/EGTA (Fig. 5-3 B), which were similar to Mn^{2+} (Fig. 5-3 C). This indicates that catch bonds may not

result from a force-induced unbending of the integrin. To obtain more definitive evidence, we repeated the experiments shown in Fig. 5-3 A-C except that $\alpha_5\beta_1$-Fc was replaced by tr$\alpha_5\beta_1$-Fc that contains only a five-domain headpiece of the integrin fused with Fc (27), thereby eliminating the difference between the bent and extended conformations. As expected, catch bonds were still observed, confirming that the integrin legs – and the unbending conformational change – were not required for the FN/$\alpha_5\beta_1$ catch bonds (Fig. 5-4 A-C). Regardless of the cation conditions, the lifetime vs. force curves in the catch bond regime became quite similar (comparing Fig. 5-4 A-C). Interestingly, truncating the integrin leg regions further prolonged lifetimes (Fig. 5-4, comparing black circles and black triangles) and abolished the cation regulation of forced-dissociation of FN/$\alpha_5\beta_1$ bonds. The force where catch bonds might transition to slip bonds could not be determined, for the average lifetimes of the FNIII$_{7\text{-}10}$/tr$\alpha_5\beta_1$-Fc/CG-7 serial bonds coincided with the Fc/GG-7 bond at force >25 pN in all three cation conditions (Fig. 5-4 A-C, comparing black circles and gray squires), indicating that these represented lifetimes of the Fc/GG-7 bond rather than the FNIII$_{7\text{-}10}$/tr$\alpha_5\beta_1$-Fc bond. These results suggest that cations differentially shorten lifetimes of the FN/$\alpha_5\beta_1$ catch bonds and this regulatory mechanism requires the integrin legs.

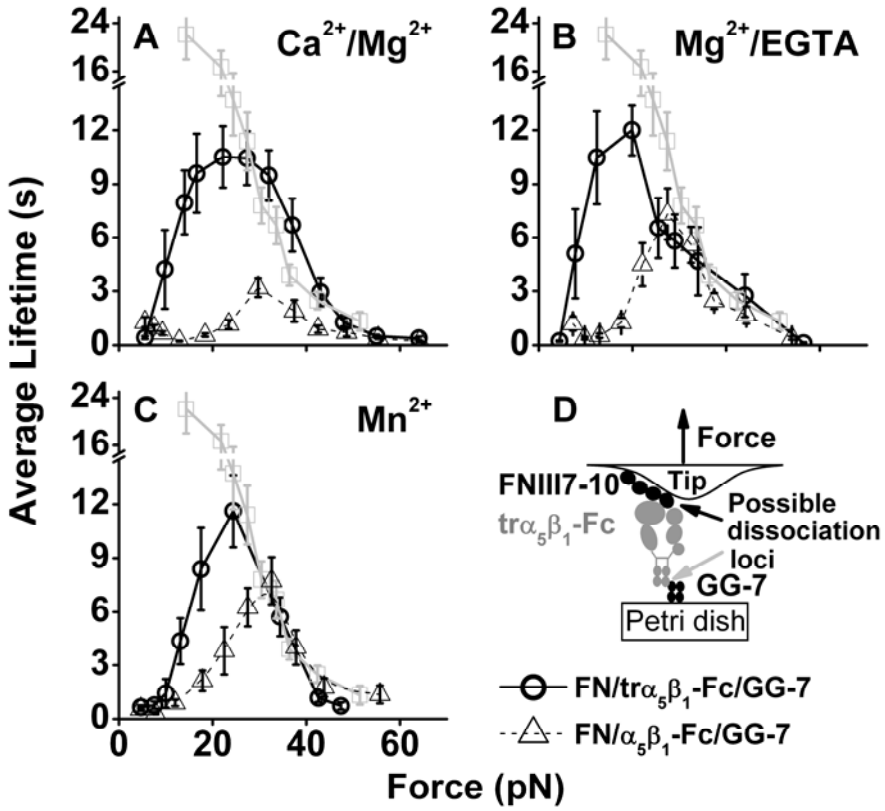

Fig. 5-5. Lifetimes of FN/tr$\alpha_5\beta_1$ bonds. Plots of lifetime (mean ± s.e.m.) vs. force of tr$\alpha_5\beta_1$-Fc functionalized Petri dish dissociating from $FNIII_{7\text{-}10}$ (thick black circles) in Ca^{2+}/Mg^{2+} (A), Mg^{2+}/EGTA (B), and Mn^{2+} (C). (D) Cartoon of the molecular arrangement indicating possible dissociation loci between $FNIII_{7\text{-}10}$ and tr$\alpha_5\beta_1$-Fc or tr$\alpha_5\beta_1$-Fc and GG-7. Overlain in A-C are the lifetime vs. force curves of $\alpha_5\beta_1$-Fc functionalized Petri dish dissociating from $FNIII_{7\text{-}10}$ (thin black triangles) and $\alpha_5\beta_1$-Fc dissociating from GG-7 (gray squares).

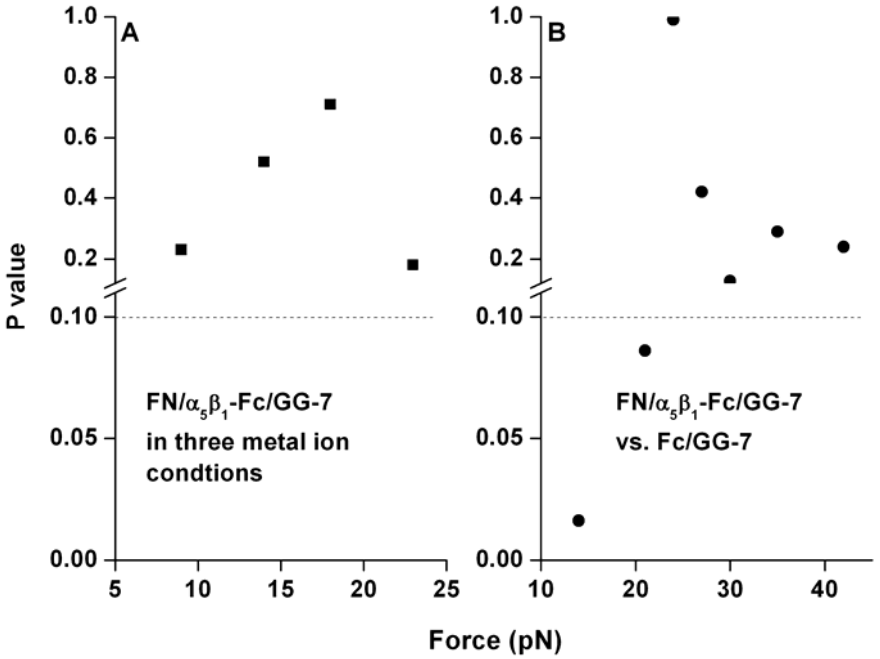

Fig. 5-6 Statistical analysis of force-lifetime relationships of FN/tr$\alpha_5\beta_1$-Fc/GG-7 interaction. (A) Statistical analysis of force-relationships in the catch bond region among three metal ion conditions for FN/tr$\alpha_5\beta_1$-Fc/GG-7 interaction. The black squares are P value acquired from ANOVA comparing the values of the three curves at the same force level. The average lifetimes did not show significant differences in the entire catch bond region. (B) Statistical analysis among force-lifetime relationships of FN/tr$\alpha_5\beta_1$-Fc/GG-7 interaction in the three metal ion conditions and Fc/GG-7 interaction. Below 23 pN, the lifetime of the capture strength is significantly higher than the lifetime of FN/$\alpha_5\beta_1$-Fc/GG-7 interaction.

LIFETIME-FORCE RELATIONSHIP WITH PRESENCE OF ACTIVATING ANTIBODIES

Previous cell adhesion assays have shown that $\alpha_5\beta_1$ is inactive with low affinity for FN in Ca^{2+}/Mg^{2+} but can be activated by Mg^{2+}/EGTA or Mn^{2+} to higher affinity states (2, 5), which was also observed in Fig. 4-2 A. Interestingly, although lifetimes were prolonged at each level of force by activation with Mg^{2+}/EGTA or Mn^{2+}, the triphasic pattern was not affected by the different affinity states, in particular, catch bonds were observed in all three metal ion conditions (Fig. 5-3 A-C). To further examine whether the qualitative characteristics of force-dependent $\alpha_5\beta_1$-FN dissociation could be regulated by integrin activation, we

measured $\alpha_5\beta_1$-FN lifetimes in 2 mM Mn^{2+} in the presence of 10 μg/ml of either mAb 12G10 or TS2/16, which are known to further activate $\alpha_5\beta_1$ to higher affinity states (36-39) as seen in Fig. 2A.

Addition of 12G10 did not change the average lifetime at the lowest force measured (~5 pN) but increased its sensitivity to force in the catch bond regime so lifetime rose more rapidly with increasing force (Fig. 5-5 A). The force at which the average lifetime peaked was left-shifted to ~15 pN beyond which catch bonds transitioned to slip bonds. Thus, 12G10 prolonged $\alpha_5\beta_1$-FN lifetimes in the 7-20 pN force range, consistent with its classification as an activating mAb but shortened $\alpha_5\beta_1$-FN lifetimes in the 20-40 pN force range, contrary to the said classification (Fig. 5-5 A). In addition, the peak average lifetime of 5.6 s at 15 pN in the presence of 12G10 was shorter than the average lifetimes in the absence of 12G10 at forces >28 pN, e.g., 7.7 s at 30 pN, which could have been even longer should the measured lifetimes not be cut short by the Fc-GG-7 dissociation. Therefore, although 12G10 prolonged $\alpha_5\beta_1$-FN lifetime at forces ranging from 7-20 pN, it prevented further lifetime prolongation by higher forces.

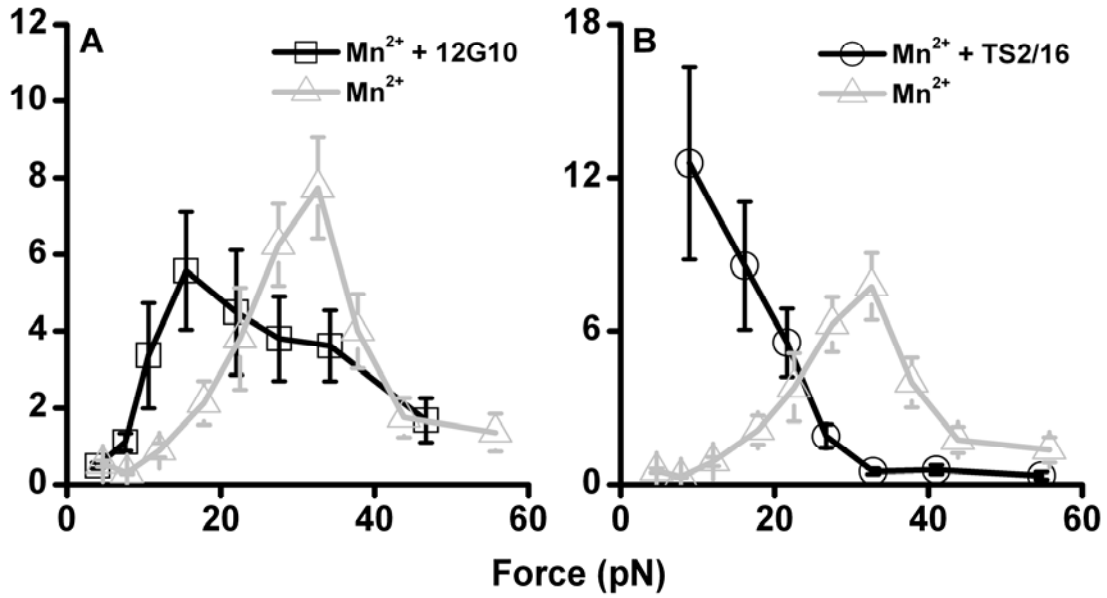

Fig. 5-7. Antibody regulation of catch bonds. Plots of lifetime (mean ± s.e.m.) vs. force of $\alpha_5\beta_1$-Fc dissociation from $FNIII_{7-10}$ in 2 mM Mn^{2+} plus 12G10 (A) or TS2/16 (B). The lifetime vs. force curves of Fig 5-1 C (light gray) was replotted here for comparison.

In sharp contrast, addition of TS2/16 substantially prolonged the average lifetime at the lowest force measured (~7 pN), consistent with the activating role of the mAb (Fig. 5-5 B). However, the average lifetime became much shorter than that in the absence of TS2/16 at forces >25pN, contrary to the said activating role. As a result, the triphasic $\alpha_5\beta_1$-FN slip-catch-slip bonds were changed to monophasic slip bonds by the binding of TS/16 to $\alpha_5\beta_1$, because the average lifetime now monotonically decreased with increasing force in the entire range of forces tested.

Binding pockets of 12G10 and TS2/16 overlap and were mapped to residue 207~218 of β1 subunit (40). This region lies in the α2 helix of β A domain (Fig. 5-6 A) which is close to the α1 helix. Integrin activation appears to involve an inward shift of the α1 helix from the low to high affinity conformation (6, 11, 12), which may be induced by force (26), thereby giving rise to catch bonds.

Binging of TS2/16 may shift the α1 helix to the inward position (41) and indeed caused monophasic slip bonds (Fig. 5-5 B), which has prolong bond lifetimes at low forces. If the α1 helix were already in the fully active conformation, force may only destabilize it, thereby resulting in slip bonds.

However, binding of 12G10 did not eliminate catch bond. Therefore, the mechanism of catch bond requires further study of different conformations induced by the two antibodies.

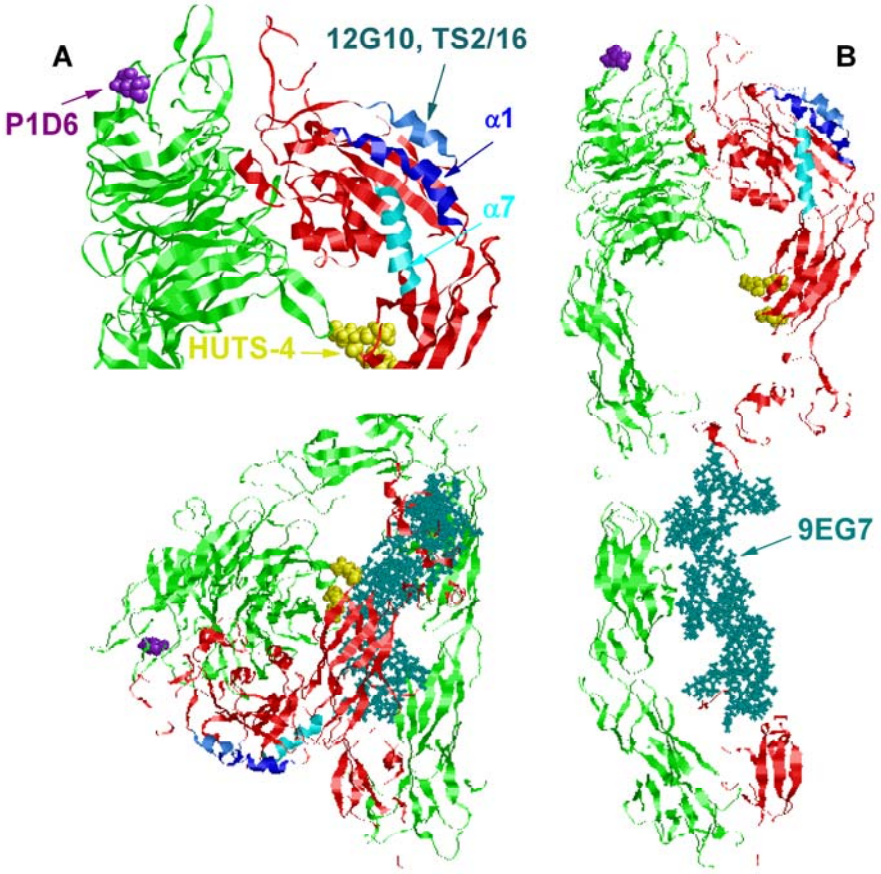

Fig. 5-8 Mapping antibodies' binding epitopes on integrin structure. (A) β-propeller of α subunit (green), A domain and part of hybrid domain of β subunit (red) were shown. Binding epitopes of 12G10 and TS2/16 lie at α2 helix of A domain (skyblue). Binding epitopes of P1D6 are in β propeller (yellow, spacefill). α1 (blue) and α7 (cyan) helices that involve in conformational change in the A domain upon activation were also pointed out. (B) Binding epitopes of 9EG7 as integrin in bent and extended conformations were shown.

Discussion

Catch bonds represent counterintuitive behaviors that have recently been observed in selectin-ligand (29, 30), actin/myosin (42), FimH/mannose (43), and GPIbα/VWF (44) interactions. Based on the integrin structures and their conformational change models, it has been speculated that integrin/ligand interactions may also behave as catch bonds (4, 17, 21-23). However, published work did not observe integrin/ligand catch bonds (45-47). In the previous work, force-ramp experiments were used to measure ramp rate-dependent rupture forces, which were analyzed by dynamic force spectroscopy assuming that dissociation occurs along a single pathway and bond lifetime decreases exponentially with increasing force as modeled by Bell (48). Using AFM force-clamp experiments, we observed a triphasic force dependence of FN/$\alpha_5\beta_1$ bond lifetimes that deviates from the Bell model (Figs. 5-3). In particular, a catch bond regime was observed where lifetimes increased with increasing force.

The affinity of FN/$\alpha_5\beta_1$ binding was low in Ca^{2+}/Mg^{2+} but high in Mg^{2+}/EGTA or Mn^{2+} (33), which was manifested as different adhesion frequencies (Fig. 4-1 A and C). At low force (<10 pN), FN/$\alpha_5\beta_1$ bonds dissociated rapidly (lifetimes <2 s) in all three conditions (Fig. 5-3 A-C), suggesting that Mg^{2+}/EGTA or Mn^{2+} increased the on-rate for association but did not significantly impact the off-rate for dissociation, consistent with the stress-free off-rates of integrin $\alpha_L\beta_2$ dissociating from intercellular adhesion molecule 1 measured in these cations (49). Our flow cytometry data suggest that more $\alpha_5\beta_1$-Fc became

extended in Mg^{2+}/EGTA and Mn^{2+} than in Ca^{2+}/Mg^{2+} condition (Fig. 5-1), consistent with previous flow cytometric (50), crystallographic (6), and electronic microscopic (11) studies. It has been suggested that force applied to a bent integrin may straighten it to an extended integrin, thereby giving rise to catch bonds (4, 17, 21-23). However, catch bonds were observed in the same force regime despite the different cation conditions (Fig. 5-3 A-C), indicating that force-induced unbending is not a required conformational change for $\alpha_5\beta_1$ to form catch bonds with FN. Comparing to the Ca^{2+}/Mg^{2+} condition, the catch bonds were more pronounced (i.e., lifetimes further prolonged) in Mn^{2+} and in Mg^{2+}/EGTA, which were indistinguishable, correlating with the similar 9EG7 epitope expression of $\alpha_5\beta_1$ in these two cation conditions (Fig. 5-1). This suggests that integrin unbending may increase the stability of the FN/$\alpha_5\beta_1$ bond in the catch bond regime.

Moreover, HUTS-4 reported that in Ca^{2+}/Mg^{2+}, Mg^{2+}/EGTA conditions, hybrid domain did not swing out whereas in Mn^{2+}, it did. Hybrid domain swing-out gives integrin higher affinity (2, 11, 14), which was confirmed by the binding frequency data (Fig. 4-1). However, remarkably, lifetime-force relationships were indistinguishable in Mg^{2+}/EGTA and Mn^{2+} conditions. The swing-out of hybrid domain neither enhanced the bond lifetime at low force, nor changed the way force regulated the bond lifetime.

Different structural models have been proposed for the catch bonds between selectins and ligands (51), FimH and mannose (43), and GPIbα and VWF (44). What are the conformational changes required for the catch bonds

between $\alpha_5\beta_1$ and FN? The integrin legs form extensive contacts with the headpiece in a bent but not an extended $\alpha_5\beta_1$. The observation that catch bonds were less pronounced in the bent $\alpha_5\beta_1$ suggests that these contacts may hinder such conformational changes. Similar to the recombinant $\alpha_5\beta_1$-Fc fusion protein, native $\alpha_5\beta_1$ purified from cell membrane and reconstituted into glass-supported bilayers also formed catch bonds with FN in the same force range, although the lifetimes were shorter (Fig. 5-3 D). The longer lifetimes of the FN/$\alpha_5\beta_1$-Fc catch bonds may result, at least partly, from the higher percentage of $\alpha_5\beta_1$-Fc found in extended conformation than m$\alpha_5\beta_1$ in the same cation condition (52). As discussed above, catch bonds were less pronounced (i.e., lifetimes less prolonged) in the bent conformation. Also, m$\alpha_5\beta_1$ could be pulled out of membrane more easily than $\alpha_5\beta_1$-Fc from GG-7, which might as well contribute to the shorter lifetime of FN against m $\alpha_5\beta_1$ observed in the experiments.

The headpiece-only tr$\alpha_5\beta_1$-Fc construct formed even more pronounced catch bonds with FN (Fig. 5-4), suggesting that truncating the legs further reduced the hindrance for such conformational changes. Moreover, the lifetime vs. force curves of the $FNIII_{7\text{-}10}$/tr$\alpha_5\beta_1$-Fc bonds measured in the three cation conditions were indistinguishable, indicating that the integrin legs are required for the cations to regulate catch bonds.

However, since most $\alpha_5\beta_1$-Fc in Mn^{2+} condition were already extended (52), leg hindrance might not be enough to explain the more pronounced catch bond of tr$\alpha_5\beta_1$-Fc/$FNIII_{7\text{-}10}$ interaction. In $\alpha_5\beta_1$-Fc, β1 subunit is longer than α5

subunit (Fig. 5-7 B) and both α5 and β1 subunits coordinate RGD docking. Therefore, when stretched, α5 subunit would undertake more load than β1 subunit did. In tr$\alpha_5\beta_1$-Fc, α and β subunit have similar length (Fig. 5-7 A). Thus, more loads would distribute on the truncated β1 subunit and it requires less force to induce similar degree of conformational change as the whole β1 subunit. This might contribute to the more pronounced catch bond for tr$\alpha_5\beta_1$-Fc/FNIII$_{7\text{-}10}$ interaction in addition to the leg hindrance discussed above.

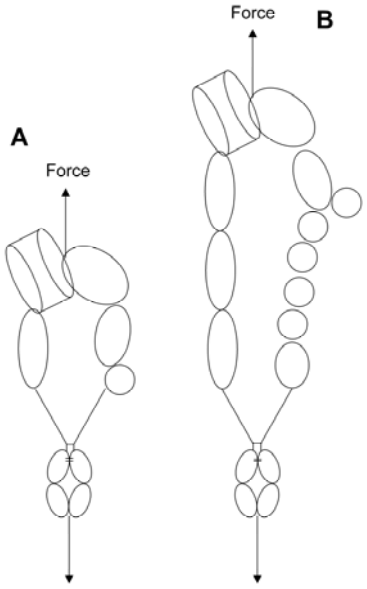

Fig. 5-9 Cartoons of speculated molecule arrangements for tr$\alpha_5\beta_1$ and $\alpha_5\beta_1$. The longer length of β subunit in $\alpha_5\beta_1$ might contribute to the less pronounced catch bond compared to tr$\alpha_5\beta_1$/FN interaction.

Binding of TS2/16 resulted in monophasic slip bonds (Fig. 5-5 D). This is similar to the effects of a single-residue replacement of L-selectin at the ligand binding site and of two single-residue replacements of VWF away from the receptor binding site, which respectively convert the L-selectin/ligand (53) and GPIbα/VWF (44) catch bonds to slip bonds. TS2/16 binds the α2 helix of the βA domain, which is adjacent to the α1 helix (Fig. 5-6) (41). Integrin activation

appears to involve an inward shift of the α1 helix from the low to high affinity conformation (14, 36, 41), which may be induced by force (26), thereby giving rise to catch bonds. Binging of TS2/16 may shift the α1 helix to the inward position (41), which would prolong bond lifetimes at low forces. If the α1 helix were already in the fully active conformation, force may only destabilize it, thereby resulting in slip bonds.

As cell adhesion molecules, integrins function as mechanical connectors. They also transduce signals bidirectionally from inside-out and from outside-in across the cell membrane. Such a dual role makes integrins prime candidates for force sensing molecules in mechanotransduction (54). Catch bonds provide a physical mechanism for force sensing if different bond lifetimes correspond to distinct signals. The potential for force applied via a bound ligand to induce integrin conformational change also expands the concept of outside-in signaling. The ability of integrin/ligand bonds to strengthen with force may be of great importance not only for leukocyte trafficking, which occurs under shear force, but also for the migration of many other cell types, which involves cyclic adhesion and detachment between the cell and the ECM. Catch bonds provide a mechanical mechanism for the cell to regulate adhesion by applying different forces at different times and locations when and where different adhesion strengths are desired.

CHAPTER 6

LIFETIME OF FN/$\alpha_5\beta_1$ AT LOW FORCES WITH A PRE-STRESS

A PRE-STRESS APPLIED VIA A BOUND LIGAND PROLONGS LIFETIMES AT LOW FORCE

FN/$\alpha_5\beta_1$ bonds dissociated rapidly at low forces and increased pulling force prolonged the bond lifetimes. The data presented in previous chapter suggest that the bond may be stabilized by force through conformational changes at the binding pocket. Are such force-induced conformational changes stable if the force is reduced? In other words, will the bond be weakened (with short lifetime) again if the applied force is reduced? To answer such questions, FN/$\alpha_5\beta_1$ bond was pulled to ~30 pN (referred to as a prestress) and then the force was reduced to a lower level (< 10 pN) where the lifetime was measured (Fig. 6-1).

Without a pre-stress, the lifetimes of FN/$\alpha_5\beta_1$-Fc/GG-7 measured at low forces (< 10 pN) were <1 s as have been shown in chapter 5 (Fig. 5-3). With the 30 pN pre-stress, the lifetime of FN/$\alpha_5\beta_1$-Fc/GG-7 bond at the same level of force (~7 pN) became much longer (Fig. 6-2 A). Thus, once stretched, the FN/$\alpha_5\beta_1$-Fc/GG-7 bond remained strong even when the force was reduced. In other words, reducing force could not weaken the FN/$\alpha_5\beta_1$/GG-7 bond once the bond had been stretched. Interestingly, lifetimes of P1D6/$\alpha_5\beta_1$-Fc/GG-7 bonds measured at low forces were identical with or without a pre-stress, suggesting that the putative conformational changes assumed to give rise to catch bonds

could only be induced by applying force via a bound ligand to specific integrin structures (Fig. 6-2 B). The effect of pre-stress was further confirmed by similar experiments on FN/tr$\alpha_5\beta_1$-Fc/GG-7 in Ca^{2+}/Mg^{2+} (Fig. 6-3 A) and FN/m$\alpha_5\beta_1$ in Mg^{2+}/EGTA (Fig. 6-3 B), which indicated that this behavior was not because of artifact of the Fc fusion and it did not require the integrin leg region.

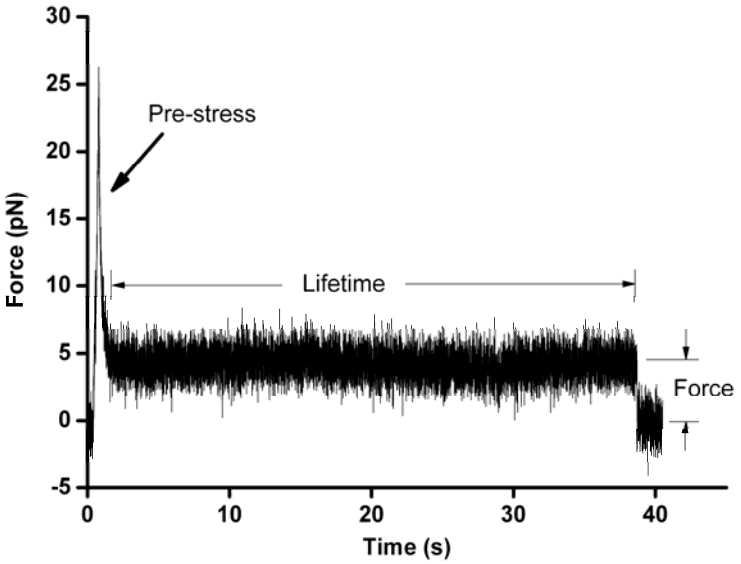

Fig. 6-1 An example of lifetime measurement of FN/$\alpha_5\beta_1$ bond at 5 pN with a 26 pN pre-stress. The pre-stress induced conformational changes that give rise to long lifetimes. The bond lifetime at 5 pN with such pre-stress lasted longer than 30 s, much longer than the one without the pre-stress (chapter 5).

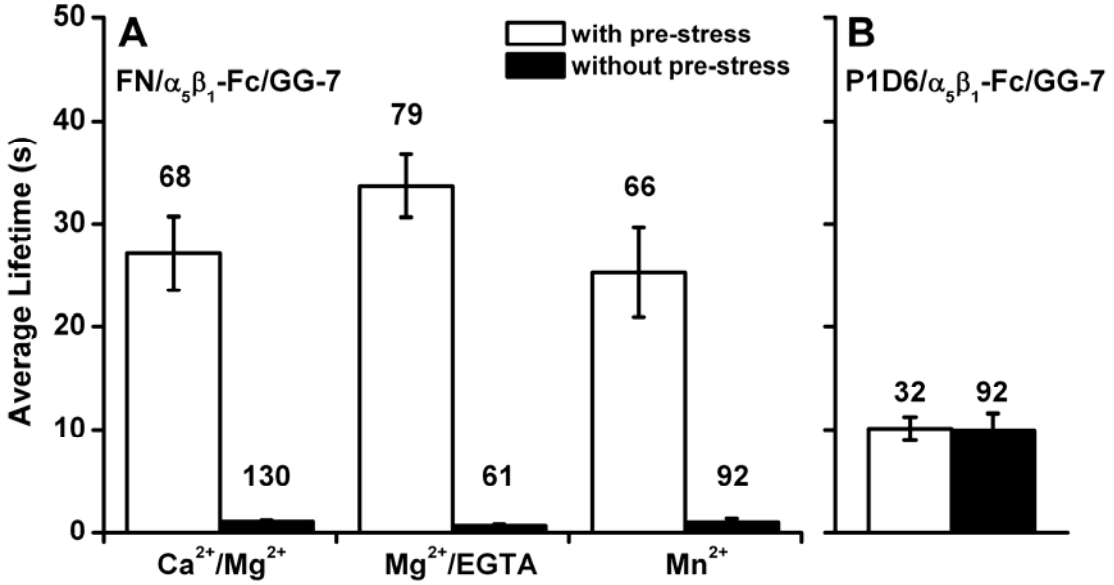

Fig. 6-2 Average lifetimes ± s.e.m at forces <10 pN with (open bars) or without (solid bars) a pre-stress was shown for FN/$\alpha_5\beta_1$-Fc/GG-7 interaction in three metal ion conditions (A) and for P1D6/$\alpha_5\beta_1$-Fc/GG-7 interaction (B). Numbers of measurements were indicated on top of each bar. Clear differences between the open and solid bars were observed for the FN/$\alpha_5\beta_1$-Fc/GG-7 interaction in all three conditions but not for the P1D6/$\alpha_5\beta_1$-Fc/GG-7 interaction.

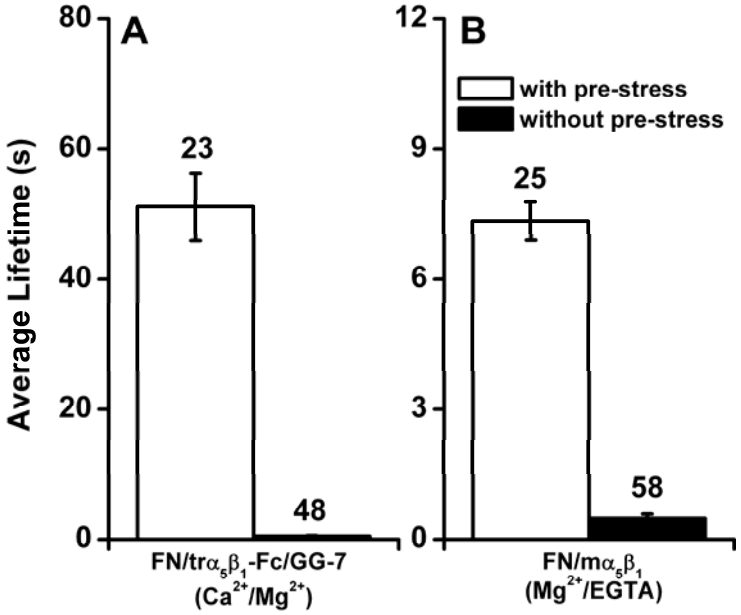

Fig. 6-3 Average lifetime ± s.e.m at forces <10 pN were shown for FN/tr$\alpha_5\beta_1$-Fc/GG-7 interaction in Ca^{2+}/Mg^{2+} (A) and for FN/m$\alpha_5\beta_1$ interaction in Mg^{2+}/EGTA (B) with (open bars) or without a pre-stress (solid bars).

The 30 pN pre-stress appeared to be enough to induce a stable state of long FN/$\alpha_5\beta_1$-Fc bond lifetime that remained stable even after the force was

reduced. What is the minimum force that can induce such a stable state? Does, and if so, how the bond state (at < 10 pN) change according to different levels of pre-stress? To answer the questions, the FN/$\alpha_5\beta_1$-Fc/GG-7 bond lifetimes at ~7 pN were measured after different levels of pre-stress in 2 mM Mg^{2+}/EGTA condition. The average lifetime increased gradually as pre-stress increased and reach a plateau of ~40 seconds at about 30 pN (Fig. 6-4). The plateau average lifetime was compared to the Bell model prediction of $\alpha_5\beta_1$-Fc/GG-7 interaction at 7 pN (Fig. 6-5). Plotted together was the average lifetime of FN/tr$\alpha_5\beta_1$-Fc/GG-7 at 7 pN with a pre-stress (Fig. 6-5). Both values of FN/(tr)$\alpha_5\beta_1$-Fc/GG-7 were close to that of $\alpha_5\beta_1$-Fc/GG-7 interaction, indicating that the dissociation occurred at (tr)$\alpha_5\beta_1$-Fc/GG-7 interface instead of between FN and (tr)$\alpha_5\beta_1$-Fc. Therefore, the lifetime measurements were limited by the dissociation of (tr)$\alpha_5\beta_1$-Fc/GG-7 interaction and the trend of the lifetime vs. pre-stress curve could not be characterized beyond 30 pN where the FN/(tr)$\alpha_5\beta_1$ bond might live even longer than 40 s (Fig. 6-4).

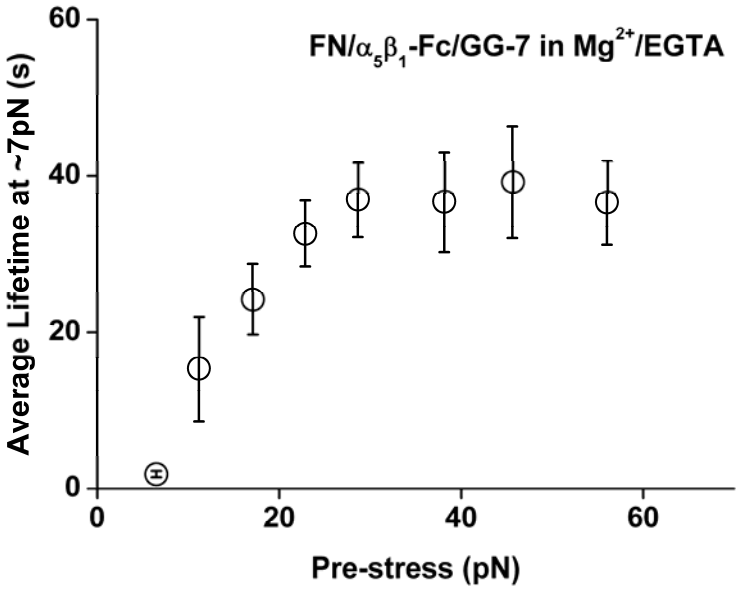

Fig. 6-4 Average lifetime at ~7 pN vs. pre-stress for FN/$\alpha_5\beta_1$-Fc/GG-7 in 2 mM Mg^{2+}/EGTA.

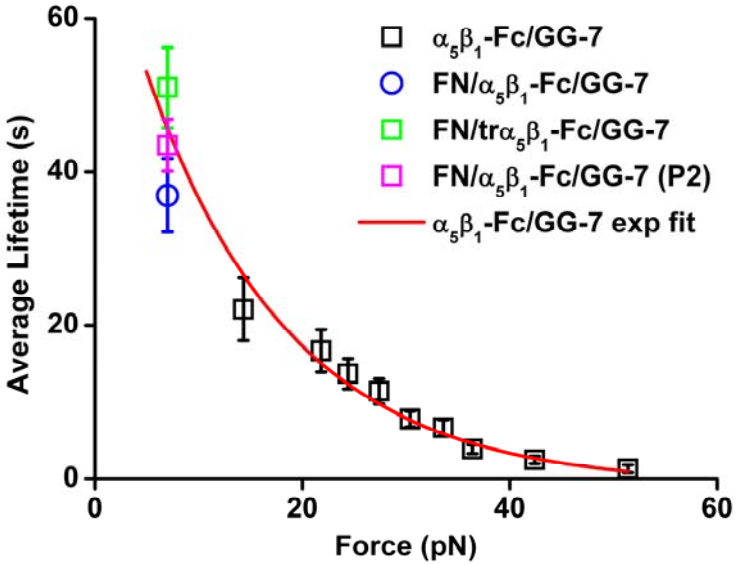

Fig. 6-5 $\alpha_5\beta_1$-Fc/GG-7 lifetime-force relationship was fit with Bell model to predict the average lifetime at 7 pN, which was compared with the average lifetime of FN/$\alpha_5\beta_1$-Fc/GG-7 and FN/tr$\alpha_5\beta_1$-Fc/GG-7 at 7 pN with a 30 pN pre-stress. Lifetime of P2 population was also shown (see below).

To explore how a brief pre-stress prolonged the lifetime at low forces, the linearized lifetime distributions with different pre-stresses were plotted and compared (29) (Fig. 6-6). The lifetime distribution displayed a single exponential decay at low pre-stresses (<8 pN), became multi-exponentially distributed at pre-

stresses ranging from 8- 26 pN, and returned to a single exponential decay at pre-stresses >26 pN (Fig. 6-6). Single exponential distribution originated from single bond state whereas the multi-exponential distribution observed here was assumed to result from a mixture of two bond states:

$$(FN/\alpha_5\beta_1\text{-}Fc)_1/GG\text{-}7 \xrightarrow{k_1} FN + \alpha_5\beta_1\text{-}Fc/GG\text{-}7$$
$$\downarrow k_3$$
$$(FN/\alpha_5\beta_1\text{-}Fc)_1 + GG\text{-}7$$
$$(FN/\alpha_5\beta_1\text{-}Fc)_2/GG\text{-}7 \xrightarrow{k_2} FN + \alpha_5\beta_1\text{-}Fc/GG\text{-}7$$
$$\downarrow k_3$$
$$(FN/\alpha_5\beta_1\text{-}Fc)_2 + GG\text{-}7$$

,

which is described by:

$$P = A\exp[-(k_1+k_3)t]+(1-A)\exp[-(k_2+k_3)t] \qquad \text{(Eq. 6-1)}$$

Lifetime distributions at low (< 8 pN) and high (> 25 pN) pre-stresses were fit by single exponential distribution:

$$P = \exp[-(k+k_3)t]$$

.

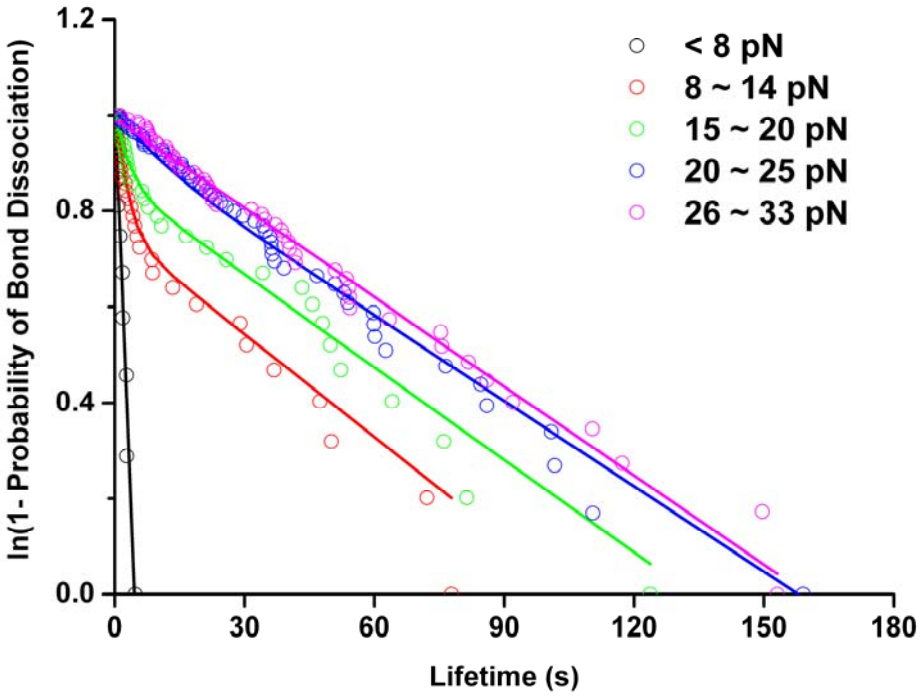

Fig. 6-6 Lifetime distributions in different pre-stress bins. When pre-stresses are lower than 8 pN or higher than 26 pN, the lifetimes are distributed as single exponential. When pre-stresses are between 8 and 26 pN, lifetime distributions can be well fitted by double exponential distributions.

The apparent dissociation rates k_1+k_3, k_2+k_3, and $k+k_3$ were plotted against the pre-stress (Fig. 6-7 A). The dissociation rates can be grouped into two populations. One population (P1) has the high kinetic rates, including the $k+k_3$ at pre-stress < 8 pN and k_1+k_3 at pre-stress between 8 and 26 pN. The second population (P2) has the low dissociation rates, including k_2+k_3 and $k+k_3$ at pre-stress between 8 and 26 pN and beyond 26 pN, respectively. The first population decreased as pre-stress increased whereas the second population stayed constant. Apparently the pre-stress prolonged the lifetime at low forces by inducing a bond state that give rise to very long lifetimes (P2 in Fig. 6-7 A). The efficiency of pre-stress to transit the bond to such state can be described by the percentage of the second population (parameter 1-A in f. 6-1) in the lifetime

distribution. As pre-stress increased, the transition efficiency increased gradually and reach 100 percent at 26 pN.

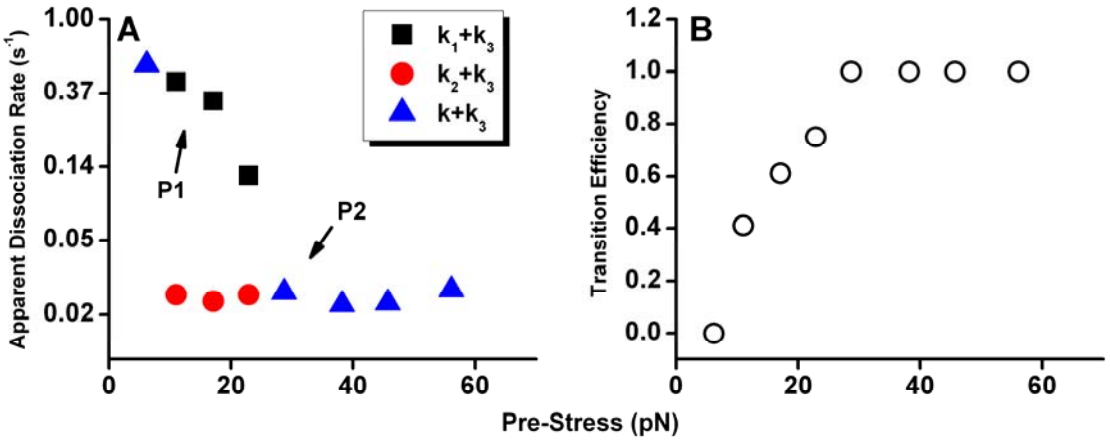

Fig. 6-7 Kinetic rates and transition efficiency. (A) Apparent kinetic rates of lifetime distributions with single exponential decay ($k+k_3$, blue triangles) and double exponential decay (k_1+k_3, black squares; k_2+k_3, red circles). The observed bonds were grouped into two populations, P1 and P2, according to the kinetic rates. P1 has high kinetic rates and decreased as pre-stress increased whereas P2 has low kinetic rates and remained constant. P1 and P2 represented different bond states that gave short and long lifetimes, respectively. (B) The efficiency of the pre-stress to transit bond to the P2 state (with long lifetime) defined as the percentage of lifetimes that lied in P2 state, is plotted vs. pre-stress.

The mean of kinetic rates of P2 was converted to lifetimes ($1/(k_2+k_3)$ or $1/(k+k_3)$ at pre-stress beyond 26 pN) to compare with lifetimes of $\alpha_5\beta_1$-Fc/GG-7 interaction ($1/k_3$) at 7 pN (Fig. 6-5). P2 population of FN/ $\alpha_5\beta_1$-Fc/GG-7 interaction lied very close to the curve of the Bell model fit of the $\alpha_5\beta_1$-Fc/GG-7 lifetime-force relationship, indicating lifetimes measured in P2 were dissociation at $\alpha_5\beta_1$-Fc/GG-7 instead of FN/$\alpha_5\beta_1$-Fc interface, namely, $k+k_3 \approx k_3$. Therefore, the kinetic rates of FN/$\alpha_5\beta_1$-Fc, k, must be much smaller than k_3 and was not measurable with current experimental setup. Moreover, the reason why the kinetic rates in P2 remained constant as pre-stress increased was because the limitation of the $\alpha_5\beta_1$-Fc/GG-7 dissociation. The trend of FN/$\alpha_5\beta_1$-Fc kinetic rates could not be

characterized. On the other hand, the kinetic rates of P1 were much higher than k_3 and reflected dissociations at the FN/$\alpha_5\beta_1$-Fc interface.

GLOBAL CONFORMATION OF INTEGRIN IN RELATION TO LIFETIMES AT LOW FORCE

The pre-stress induced a transition to a state of FN/$\alpha_5\beta_1$ bond that gave very long lifetimes at low forces. Without the pre-stress, the bond was in another state that gave very short lifetimes at the same level of low forces. Did the two states correlate to different global conformations of $\alpha_5\beta_1$-Fc? To answer this question, force-extension curves during the stretching-relaxation cycle were analyzed to examine the global conformation differences of the integrin before and after the application of the pre-stress (Fig. 6-8). The molecular extension difference (ED) identified the global conformational changes, e.g., unbending, induced by the stretching that did not recover during relaxation (Fig. 6-9). In the three metal ion conditions, majority of force-extension curves did not show any extension differences, i.e., global conformational differences, before and after the pre-stress (89%, 72%, and 77% in 1 mM Ca^{2+}/Mg^{2+}, 2 mM Mg^{2+}/EGTA, and 2 mM Mn^{2+}, respectively) (Fig. 6-9).

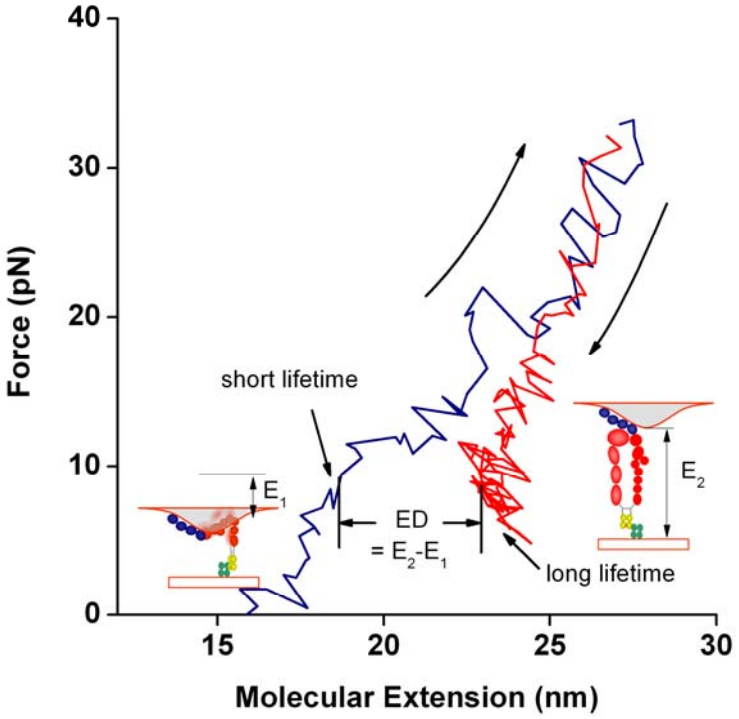

Fig. 6-8 Force vs. molecular extension plot. Molecular extension difference (ED) identified integrin's global conformational change before and after the pre-stress.

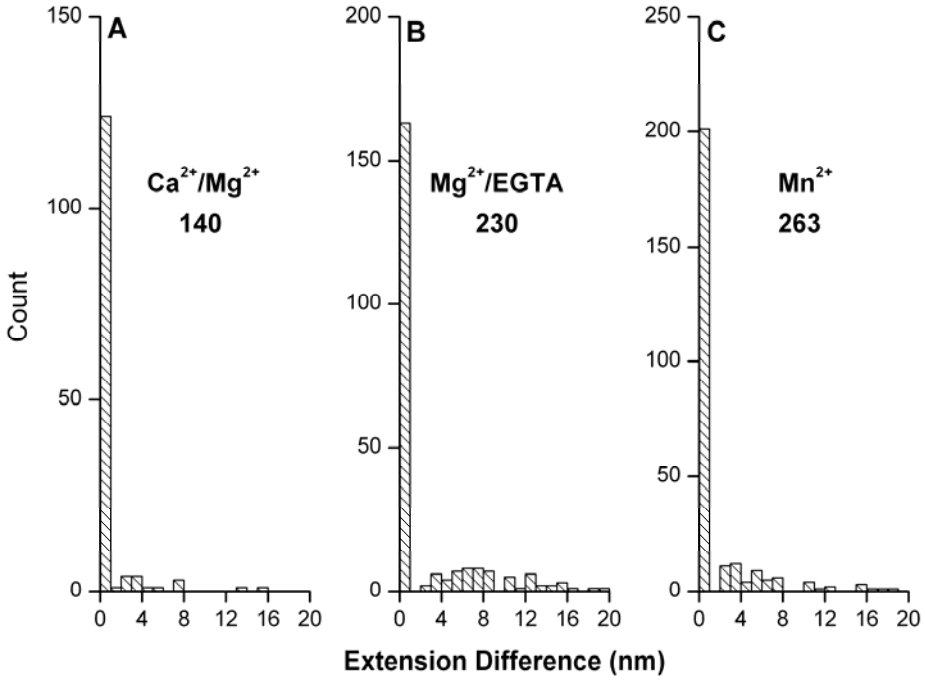

Fig. 6-9 Histograms of extension differences (ED) after one stretching-relaxation cycle for FN/$\alpha_5\beta_1$-Fc/GG-7 in 1 mM Ca^{2+}/Mg^{2+} (A), 2 mM Mg^{2+}/EGTA (B), and 2 mM Mn^{2+} (C).

The results obtained in the Ca^{2+}/Mg^{2+} condition is particularly interesting because a high percentage of integrin was in bent conformation before the stretching (Fig. 5-1). The data suggest that after the stretching-relaxation cycle, the FN/$\alpha_5\beta_1$-Fc/GG-7 could restore the original global conformation as prior to the stretching. Among the force-extension curves that did not have extension differences, two kinds were typical (Fig. 6-10). The first kind did not display any hysteresis (Fig. 6-10 curve 1) during the stretching-relaxation cycle. The second kind did show hysteresis but the extension restored at the end of the relaxation (Fig. 6-10 curves 2, 3). Curve 2 in Fig. 6-10 displayed a sudden decrease of molecular extension and a snap-back restoration of the molecular conformation. Moreover, before and after the snap-back restoration, the curve demonstrated two distinct conformations of the FN/$\alpha_5\beta_1$-Fc/GG-7 complex. Curve 3, however, showed gradual restoration to the original conformation. Because hysteresis can reveal structural differences of the FN/$\alpha_5\beta_1$-Fc/GG-7 complex during the stretching-relaxation cycle, the percentage of curves that show hysteresis and the snap-back restoration was compared in the three metal ion conditions (Fig. 6-11). The percentage of both features decreased as the metal ion condition changed from Ca^{2+}/Mg^{2+} to Mg^{2+}/EGTA and Mn^{2+}. The fact that metal ions were able to regulate these two features, especially the snap-back restoration, provides direct evidence that they are properties of the integrin $\alpha_5\beta_1$-Fc. In addition, similar experiments for FN/trα5β1-Fc/GG-7 did not reveal any snap-back restoration feature (Fig. 6-11). Moreover, the percentage of force-extension curves with the snap-back restoration was highest in Ca^{2+}/Mg^{2+} condition and the

fact that the snap-back restoration occurred close to the end of relaxation strongly suggests that the snap-back restoration was $\alpha_5\beta_1$-Fc switching from the extended conformation to the bent conformation. A molecular dynamic simulation demonstrated a 5-7 nm extension of integrin $\alpha_V\beta_3$ that was stretched from bent to extended conformation (unpublished data from Wei Chen). Indeed, the histogram of molecular extensions restored during the snap-back grip showed a length of 6~7 nm (Fig. 6-12). All together, the above evidences demonstrated that $\alpha_5\beta_1$-Fc was able to restore to the bent conformation after the stretching-relaxation cycle.

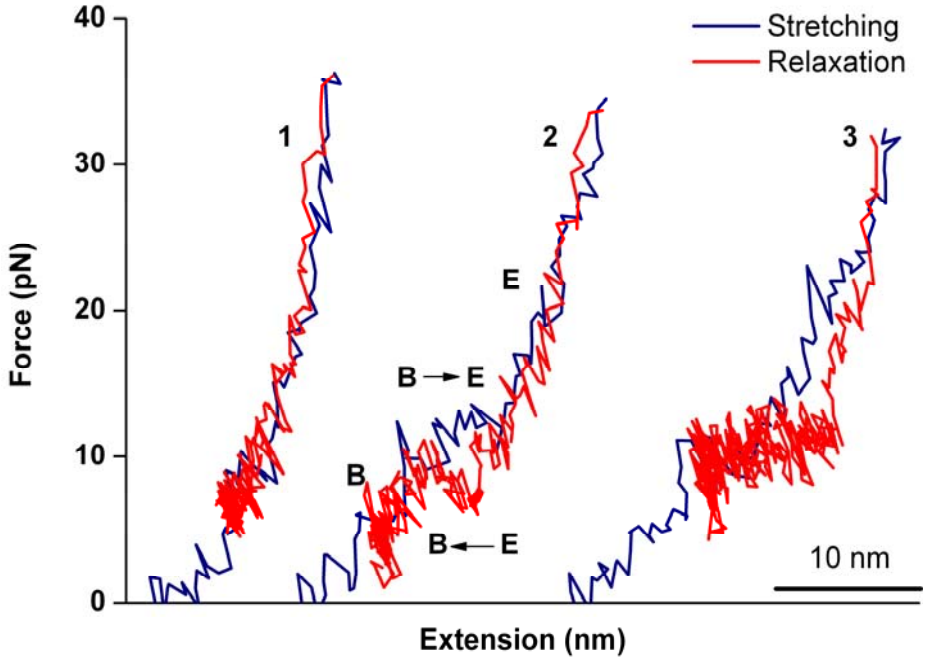

Fig. 6-10 Two typical force-extension curves during the stretching and relaxation cycle that did not show extension differences before and after the pre-stress. (A) without hysteresis and (B) with hysteresis. Curve B clear revealed two stable integrin conformations and the transition between them.

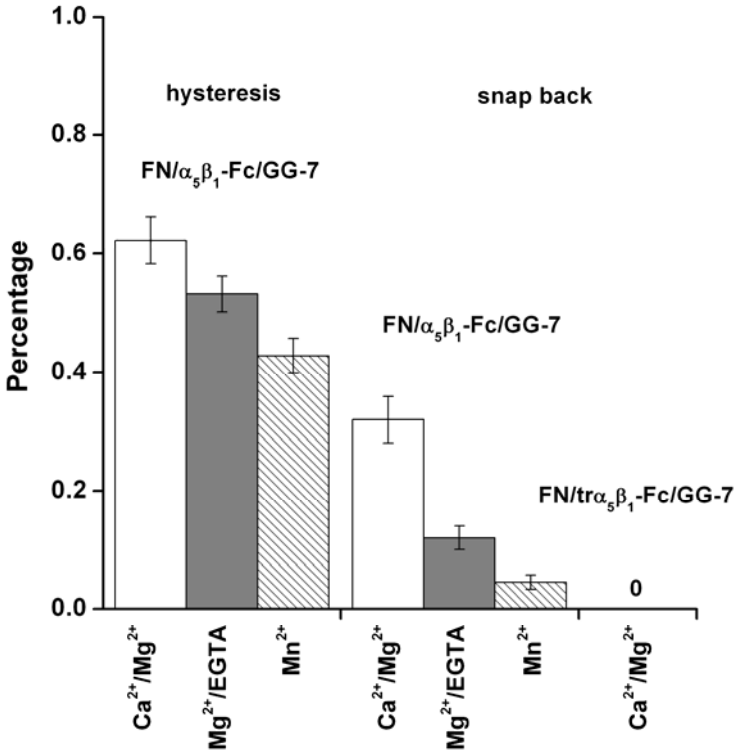

Fig. 6-11 Percentage of force-extension curves that display hysteresis or the snap back grip during the stretching-relaxation cycle for FN/$\alpha_5\beta_1$-Fc/GG-7 and FN/tr$\alpha_5\beta_1$-Fc/GG-7. Error bars are standard error estimated from binomial distribution.

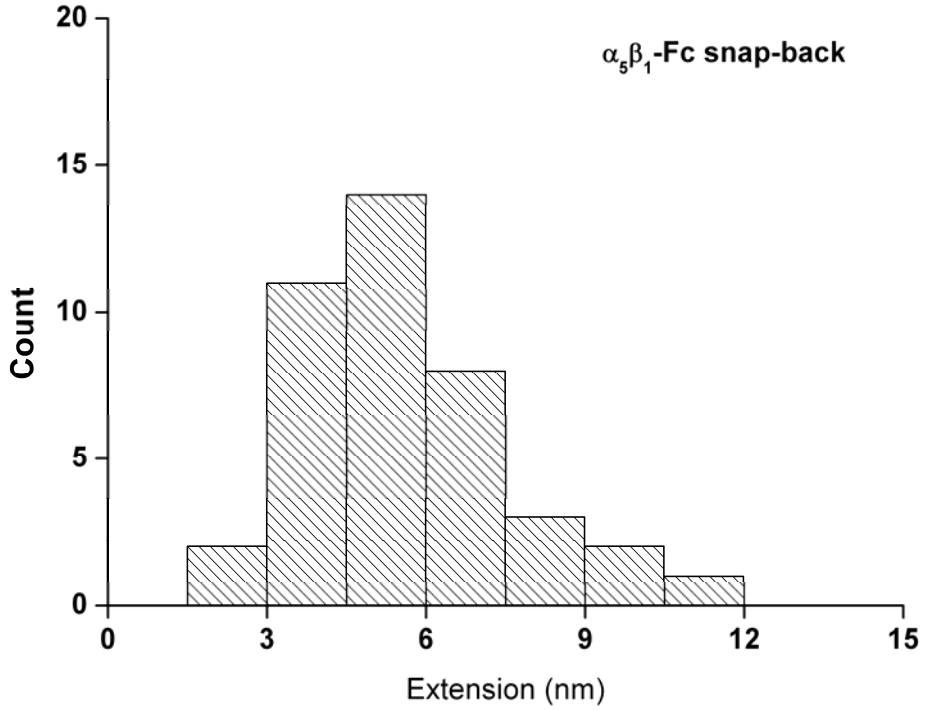

Fig. 6-12 Histogram of molecular extension restored by the snap-back restoration during the relaxation of FN/$\alpha_5\beta_1$-Fc/GG-7 complex.

Discussion

Chapter 5 described that force could induce a FN/$\alpha_5\beta_1$-Fc bond state that gave very long lifetimes, a catch bond phenomenon. In this chapter, we demonstrated that the bond state induced by force stayed stable even after the fore was reduced to a very low level. In other words, lower the force would not weaken FN/$\alpha_5\beta_1$-Fc bond once it had been stretched. This kind of behavior has also been demonstrated in FimH/mannose system (43). In addition, the efficiency of the force to induce such a strong bond state for FN/$\alpha_5\beta_1$-Fc in 2 mM Mg^{2+}/EGTA condition was characterized. The probability of force to induce the strong bond state increased as force increased and when the force reached 26 pN, all bond was transit to the strong state. However, because the lifetimes were cut short by $\alpha_5\beta_1$-Fc dissociating from GG-7, the trend of lifetime beyond 26 pN could not be characterized.

During cell migration, there are multiple mechanisms for cells to regulate tail detachment. Integrin/ligand interactions at the trailing edge were either dispersed in the cell membrane, ripped from the cell membrane and remain attached to the substratum, or form a new aggregate (55). However, majority of the integrin remained fixed to the substrate and detached from the cell as the cell advanced (55). This coincide with the data here that integrin/ligand bond could not be weakened.

Choquet et al. demonstrated in 1997 that force applied to $FNIII_{7\text{-}10}$ coated beads bound on fibroblast cells could reinforce the linkage between the bead and the cell (56). The $FNIII_{7\text{-}10}$ coated beads bound to the fibroblast cells could be

readily moved by forces exerted on the beads applied through optical tweezers. The authors then constrained the beads against the cell movement with laser tweezers for 10 seconds and released them. For beads that went through this process, the linkage between the bead and cell became much stronger and could not be moved again by a similar level of force that was capable of moving beads that did not went through such process. The authors attributed this phenomenon to the strengthening of the interactions between cytoskeleton and integrin cytoplasmic domains by force (56). However, results in this chapter offer another factor in this phenomenon. The initial binding between $FNIII_{7\text{-}10}$ coated beads and the fibroblast cells were weak, since force could move the beads against the cell relatively easily. Force could strength the bond between the FN and integrin, therefore contributes to the stronger linkage between the beads and cell.

Moreover, we observed reversible unbending of $\alpha_5\beta_1$ binding with FN under mechanical force, which proved that integrin bending and unbending is dynamic. Importantly, integrin could restore bent conformation even when engaged with its ligand, providing a mechanism for mechanotransduction.

CHAPTER 7

$\alpha_5\beta_1$ UNFOLDING UNDER FORCE

FORCECLAMP MEASUREMENT REVAELS MULTIPLE STEPS PHENOMENON

Mechanical regulation of the $\alpha_5\beta_1$/FN bond was characterized by measuring lifetime-force relationships using force clamp technique. The initial application of force clamp technique was to study stepwise unfolding of titin (57). During a lifetime measurement, structural changes under force occurred (such as unfolding) and gave molecular extension a sudden increase that resulted in a force drop. The force clamp program attempted to keep the pulling force on the molecule constant and in response to the force drops, it retracted the Petri dish away from the cantilever tip. Thus, the final force curve displayed dropping spikes that were separated by lifetime intervals at constant force and the distance between the Petri dish and the cantilever tip displayed stepwise increase (Fig. 7-1).

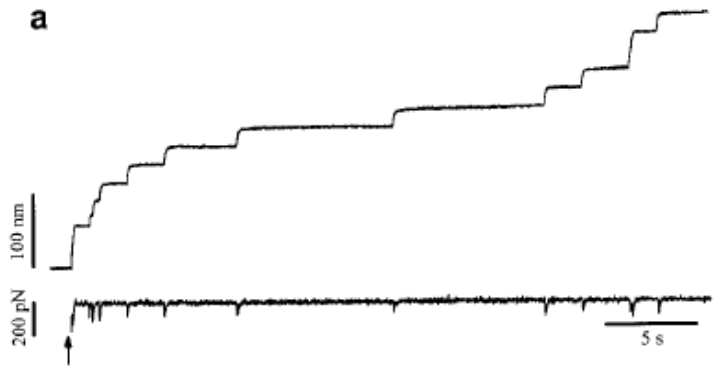

Fig. 7-1 A typical force curve of titin unfolding measured with force-clamp technique (57). The bottom curve showed lifetime kind of measurements at a constant force. The top curve recorded distance changes between the surface and the cantilever tip, which demonstrate stepwise increase corresponding to the force drop in the bottom curve.

During the lifetime measurements of $FNIII_{7-10}/\alpha_5\beta_1$-Fc/GG-7 interaction, similar force curves were observed as the one in Fig. 7-1 (Fig. 7-2). The multiple steps phenomenon can be explained by dissociation of multiple $FN/\alpha_5\beta_1$-Fc bonds or structural changes of the molecules under the pulling force. With ~20% adhesion frequency, a typical value in the experiments, if every force drop in the force curve represent a bond dissociation, assume each bond form independently, the percentages of lifetime events that display double steps and triple are estimated to be 8% and 0.5% among all adhesion events based upon Poisson distribution. However, in reality, the percentage of such lifetime events was much higher than the estimated values. Moreover, as the force under which the lifetimes were measured increases, the histograms of number of steps shifted toward higher number of steps (Fig. 7-3). This strongly suggests against the possibility that the multiple steps were caused by multiple bonds dissociation because if it were so, pulling to different forces would not change the number of bonds formed and thus change the number of steps in the force curves.

Therefore, the multiple steps phenomenon were caused by structural changes occurred in the molecules.

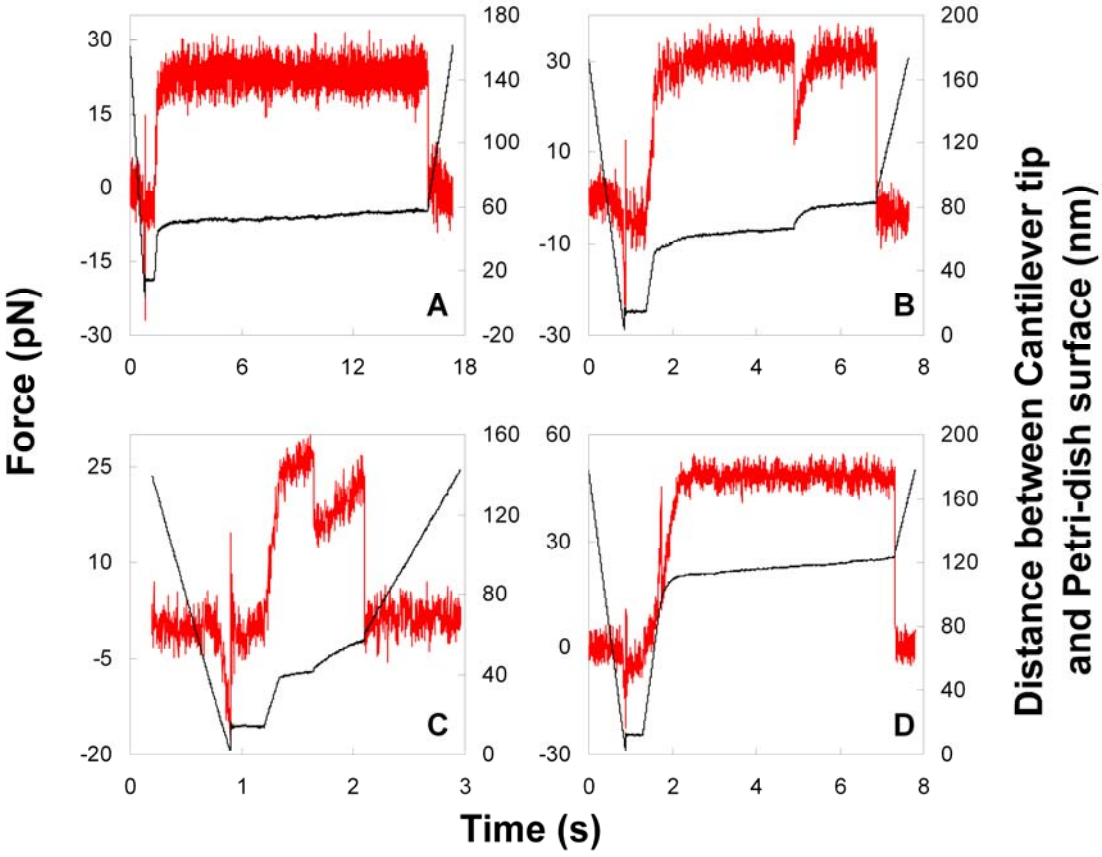

Figure 7-2. Force-clamp experiments demonstrate structural changes of the molecules under force. Four types of force-scan traces were shown with 1 (A) or 2 (B, C, D) breaks The goal was to apply a given level of tensile force on the molecular bond(s) that linked the two surfaces (*red curves, left ordinate*). When the force followed the distance increase or plateau, the molecules gradually deformed from or remained in their stable conformations. Before final separation of the AFM tip from the sample surface, an abrupt force drop (break) suggested either a sudden increase in the length of the molecular linkage (e.g., unfolding of one globular domain in a protein domain series) or dissociation of one of multiple molecular bonds in parallel. The break triggered a feedback control loop to retract the cantilever to resume, or "clamp", the force to this level (if possible), as indicated by the second increasing and second plateau blue line segments in B and C. Complete rupture of the molecular linkage again triggered PZT retraction (rightmost increasing blue line segments), but could not resume force to the preset level. The duration (t_{11}) of the force plateau in A represents lifetime of a molecular bond at a constant force without any prior break. The duration (t_{21}) of the first force plateau in B represents time to sudden length increase (e.g., time-to-unfold). The duration (t_{22}) of the second force plateau in B also represents lifetime of a molecular bond at a constant force, but measured after the first break. The duration of plateau in C is also t_{21}, although the premature dissociation prevented a t_{22} measurement. Likewise, the duration of plateau in D is also t_{22}, although the first break occurred before reaching the desired level. The length increment (l_{21}) at the same force was also measured in B.

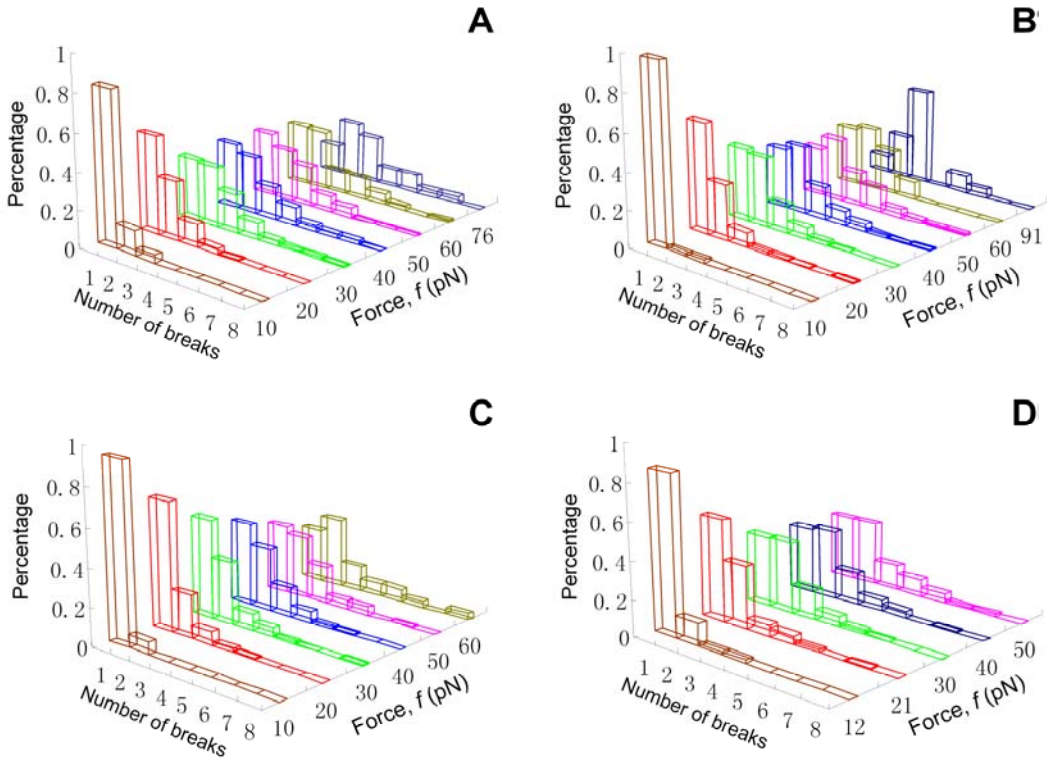

Figure 7-3. Families of histograms of number of breaks observed in the force-clamp experiments. Histograms are shown for FNIII$_{7\text{-}10}$/$\alpha_5\beta_1$-Fc/GG-7 interaction in 1 mM Ca^{2+}/Mg^{2+} (A), 2 mM Mg^{2+}/EGTA (B), 2 mM Mn^{2+} (C), and P1D6/$\alpha_5\beta_1$-Fc/GG-7 interaction (D) in respective ranges of forces. For all four conditions, the histograms right-shift toward higher number of breaks as force increases, suggesting that the breaks represent unfolding of individual domains in a protein with multiple domains in series rather than dissociation of individual bonds in a bond cluster with multiple bonds in parallel.

THE MULTIPLE STEPS PHENOMENON IS CAUSED BY $\alpha_5\beta_1$ STRUCTURAL CHANGES

Where did the structural changes observed in the force clamp experiments originated? In the AFM experiments, FNIII$_{7\text{-}10}$/$\alpha_5\beta_1$-Fc/GG-7, P1D6/$\alpha_5\beta_1$-Fc/GG-7, and FNIII$_{7\text{-}10}$/HFN7.1/anti-mouse Fc complexes were pulled. Mechanical unfolding of FN type III module has been studied and the module could unfold at force as little as ~75 pN (58). However, significant amount of structural change events of FNIII$_{7\text{-}10}$/$\alpha_5\beta_1$-Fc/GG-7 complex were observed even at force of 20 pN

(Fig. 7-3, 7-4). In addition, P1D6/$\alpha_5\beta_1$-Fc/GG-7 complex showed similar number of steps histograms as $FNIII_{7\text{-}10}$/$\alpha_5\beta_1$-Fc/GG-7 complex (Fig. 7-4). Moreover, $FNIII_{7\text{-}10}$/HFN7.1/anti-mouse Fc complex did not show significant amount of multi-breaks adhesion events at similar force range (Fig. 7-4). Therefore, the data indicated that the structural changes occurred in the force clamp experiments were not originated from $FNIII_{7\text{-}10}$. Furthermore, no studies have shown that antibodies could unfold or undertake other structural changes at force lower than 60 pN and previous lifetime measurements of antigen/antibody interactions have not shown multiple steps in the force curves (29, 30) (Fig. 7-4). Therefore, we suggest that the structural changes observed in the force clamp experiments are originated from $\alpha_5\beta_1$-Fc.

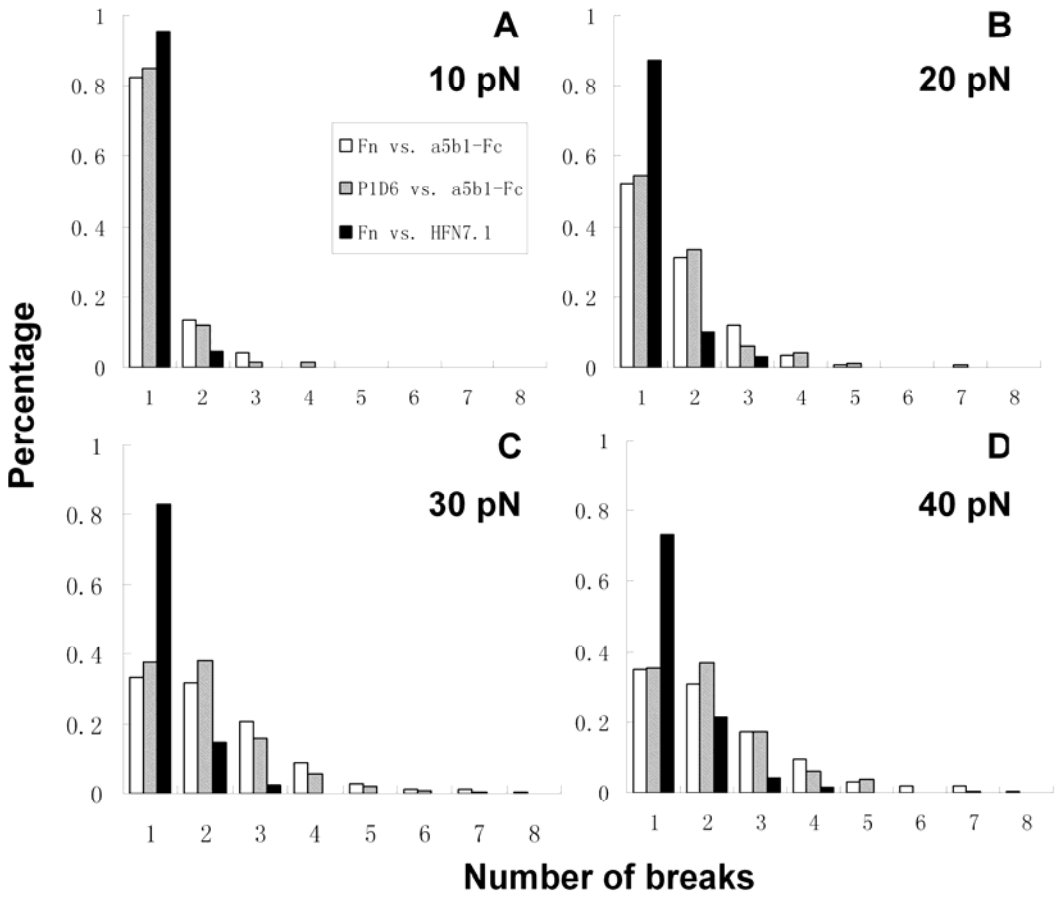

Figure 7-4. Histograms of number of breaks for FN/$\alpha_5\beta_1$-Fc/GG-7, P1D6/$\alpha_5\beta_1$-Fc/GG-7 and FNII7-10/HFN7.1/anti-mouse Fc interactions in a range of forces, ~10 (A), ~20 (B), ~30 (C), and ~40 (D) pN. The histograms of $FNIII_{7-10}$/$\alpha_5\beta_1$/GG-7 and P1D6/$\alpha_5\beta_1$/GG-7 interactions are similar but different from those of the $FNIII_{7-10}$/HFN7.1/anti-mouse Fc interaction, which shows much less number of peaks. This demonstrates that the multi-break phenomenon is originated from integrin $\alpha_5\beta_1$ instead of the ligand $FNIII_{7-10}$.

$\alpha_5\beta_1$ UNFOLDING DOES NOT AFFECT OVERALL TREND OF LIFETIME-FORCE RELATIONSHIPS

The lifetime-force relationships shown in chapter 5 were lifetime measurements with only one step when the bond dissociated (Fig. 7-2 A). The events with more than one step were excluded. Therefore, it is necessary to examine if excluding the multiple steps events would change the trend of lifetime-force relationships of the one-step lifetime events. When single step lifetime

events were excluded, the ones with two steps dominate the rest of the events (Fig. 7-3, 7-4). The lifetimes of the second step in two-step force clamp measurements, t_{22} (Fig. 7-2 B, D), were plotted against force to compare with lifetime-force relationships of t_{11} (Fig. 7-2 A, Fig. 5-3) (Fig. 7-5). For all five situations, the lifetime-force relationships were very similar for t_{11} and t_{22} (Fig. 7-5). This indicates that the structural changes of integrin did not affect the feature of binding pocket of the bonds.

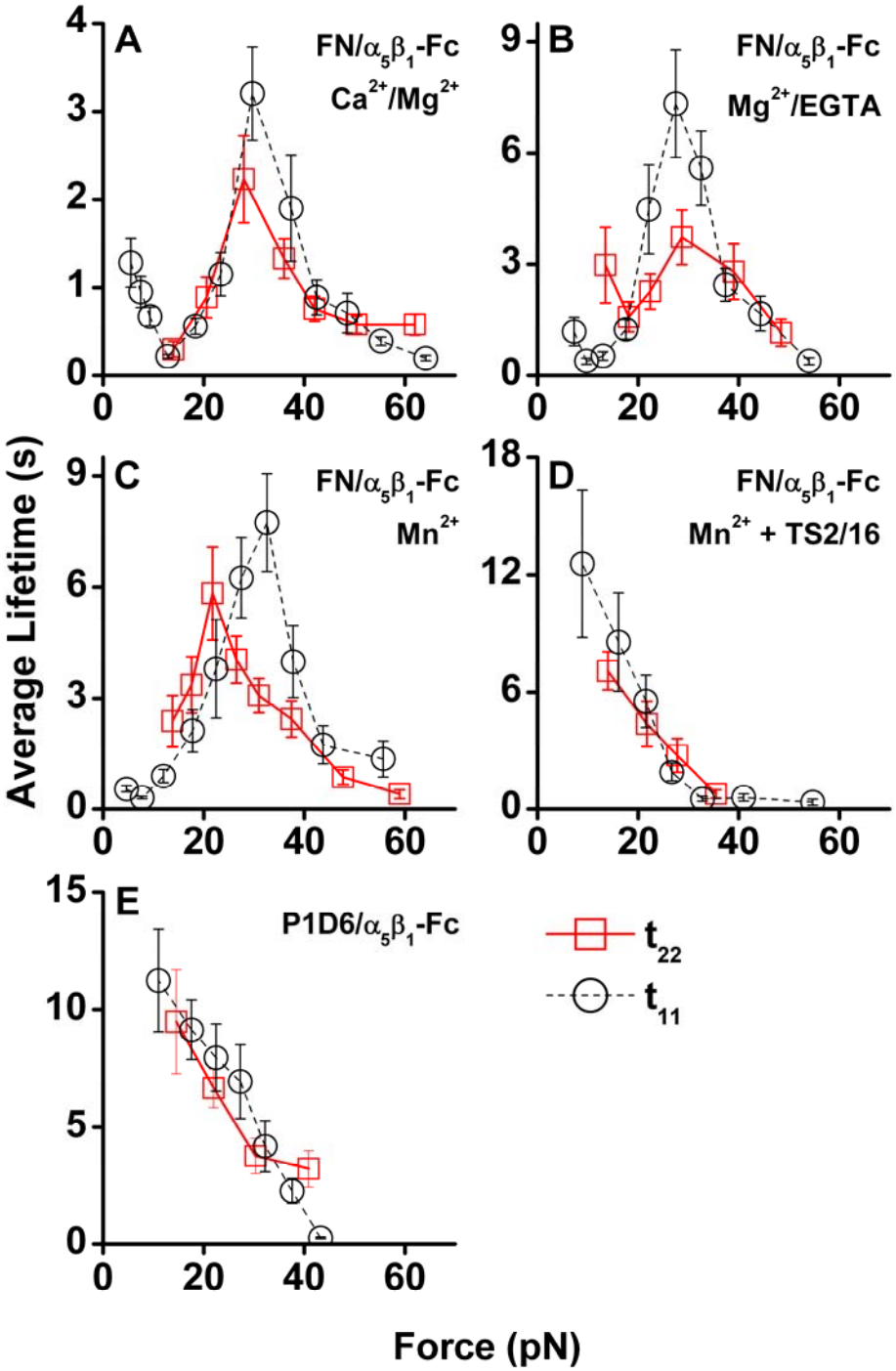

Fig. 7-5 Plots of average bond lifetime $<t_{22}>$ ± s.e.m. against force (red square) in comparison of $<t_{11}>$ ± s.e.m. for $FNIII_{7-10}$ vs. $\alpha_5\beta_1$-Fc in 1 mM Ca^{2+}/Mg^{2+} (A), 2 mM Mg^{2+}/EGTA (B), 2 mM Mn^{2+} (C), and 2 mM Mn2+ plus 10 μg/ml TS2/16, as well as for anti-$\alpha_5\beta_1$ mAb (P1D6) vs. $\alpha_5\beta_1$-Fc (E).

Properties of the structural changes in $\alpha_5\beta_1$

It is also interesting to investigate the features of the structural changes under the pulling force. In this case, the t_{21} reflects the lifetime for the structural changes to occur and its relationships with force were plotted in Fig. 7-6. First of all, the t_{21} revealed monotonically decreasing of lifetimes as force increased, a typical slip bond, in sharp contrast to the catch bonds observed for t_{11} and t_{22}. This is consistent with previous lifetime measurements that demonstrated protein unfolding as slip bonds kind of behavior (59). Second, for $FNIII_{7\text{-}10}/\alpha_5\beta_1$-Fc interaction, t_{21} varies, especially at the low forces (< 20 pN). In 2 mM Mn^{2+} plus TS2/16 condition, t_{21} is significantly longer than the other conditions (compare D with A, B, C). This is because lifetimes at low force in that condition were much longer (Fig. 5-3 B), which enabled structural changes of $\alpha_5\beta_1$ occurred at low force to be observed before the $FNIII_{7\text{-}10}/\alpha_5\beta_1$-Fc bond dissociated. For P1D6/ $\alpha_5\beta_1$-Fc interaction, t_{21} vs. force curve deviated from others, probably because the pulling position was different from $FNIII_{7\text{-}10}$ upon $\alpha_5\beta_1$-Fc.

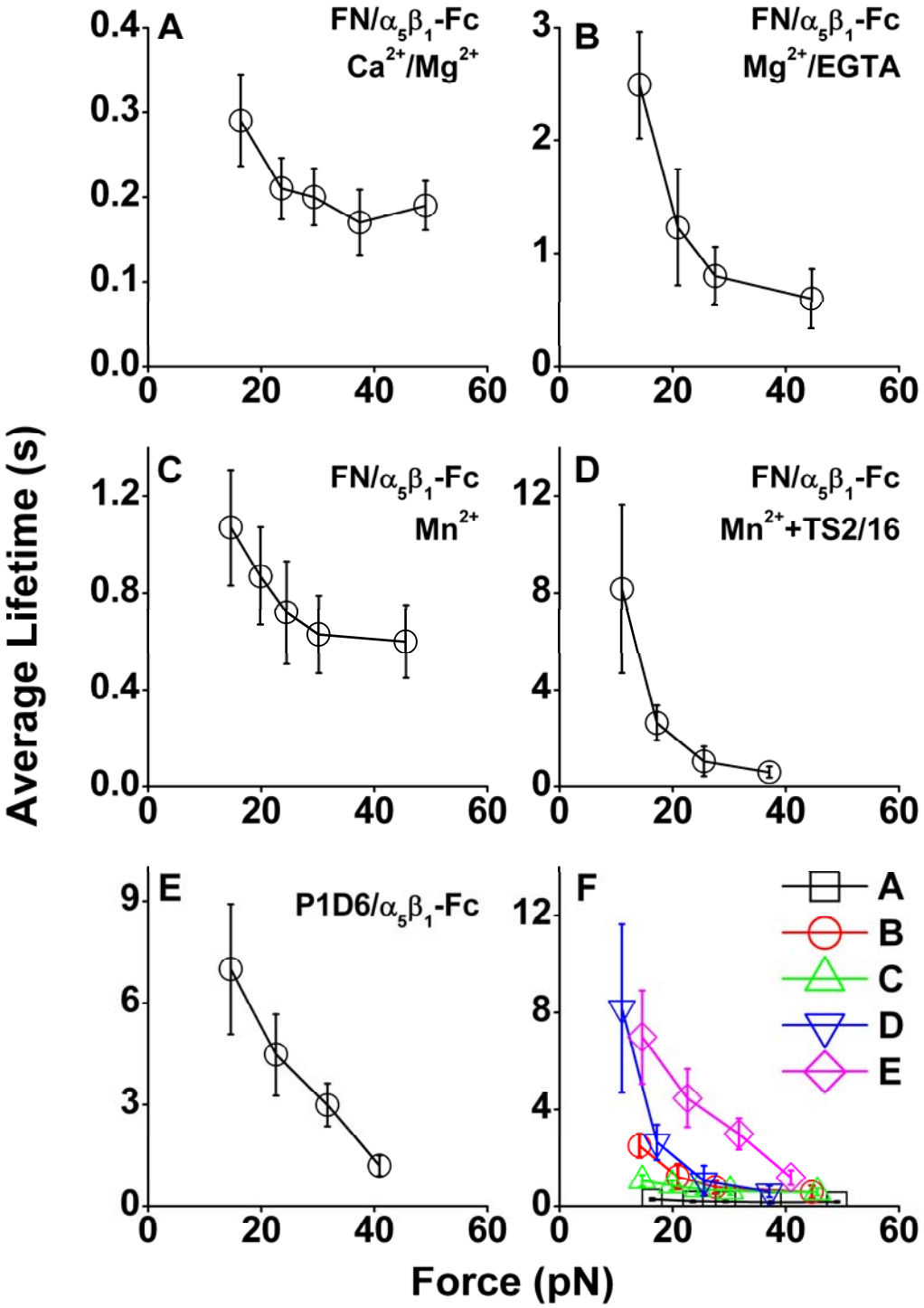

Figure 7-6. Plots of average time-to-first break $<t_{21}>$ ± s.e.m. against force for $FNIII_{7-10}$ vs. $\alpha_5\beta_1$-Fc in 1 mM Ca^{2+}/Mg^{2+} (A), 2 mM Mg^{2+}/EGTA (B), 2 mM Mn^{2+} (C), and 2mM Mn^{2+} plus 10 μg/ml TS2/16, as well as for anti-$\alpha_5\beta_1$ mAb (P1D6) vs. $\alpha_5\beta_1$-Fc (E). All the curves were replotted in (F) for comparison. The short $<t_{21}>$ at force < 20 pN for FN vs. $\alpha_5\beta_1$-Fc in 1 mM Ca^{2+}/Mg^{2+}, 2mM Mg^{2+}/EGTA and 2mM Mn^{2+} (A - C) are probably caused by the short $<t_{11}>$ lifetimes at such force, i.e., if the first break did not occur soon enough the FN/$\alpha_5\beta_1$-Fc bond could have dissociated, which prevents long $<t_{21}>$ to be observed.

Another feature of the structural changes is the corresponding length changes in the molecule. To measure the length changes, force-time curves (Fig. 7-7 A) were transferred to force-extension curves (Fig. 7-7 B), in which the lengths changes can be measured. The histograms of all the length changes were plotted for FN/$\alpha_5\beta_1$-Fc/GG-7 in 1 mM Ca^{2+}/Mg^{2+}, 2 mM Mn^{2+} conditions and FN/tr$\alpha_5\beta_1$-Fc/GG-7 in 1 mM Ca^{2+}/Mg^{2+} condition. All histograms display complicated patterns and at least three peaks were clear in each one. However, the histograms of FN/$\alpha_5\beta_1$-Fc/GG-7 and FN/tr$\alpha_5\beta_1$-Fc/GG-7 are overall similar, indicating that majority of the structural changes occurred in the headpiece.

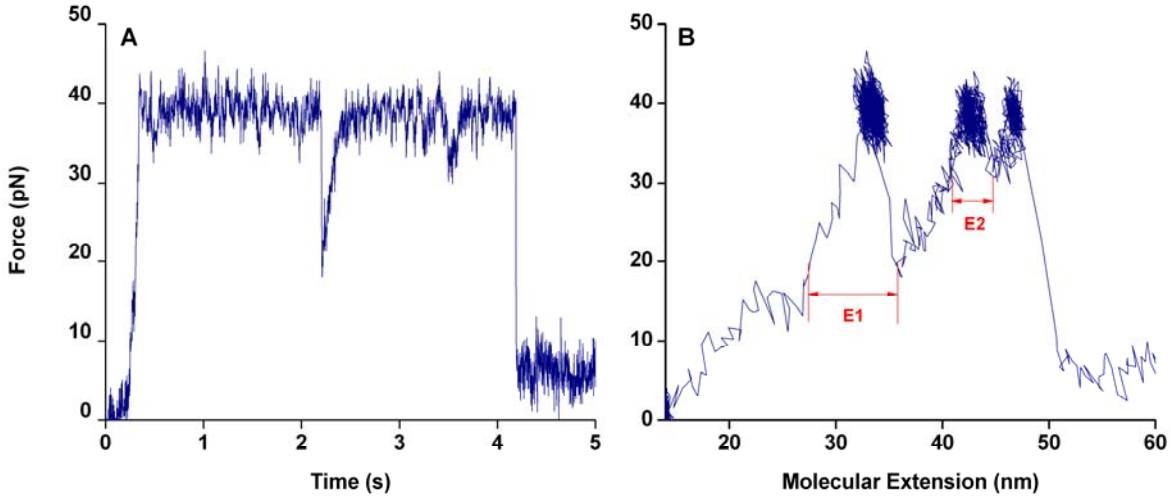

Fig. 7-7 Length changing measurement in one lifetime event using forceclamp technique. During the lifetime event, three sudden force drops were observed. The first two drops represented structural changes of $\alpha_5\beta_1$ and the third one was dissociation of either FN from $\alpha_5\beta_1$-Fc or $\alpha_5\beta_1$-Fc from GG-7. The regular force-time curve (A) used to measure lifetime was transferred to force-extension curve (B) in order to measure the length changes caused by the molecular structural changes. Corresponding to the two force drops were two length changes, E1 and E2.

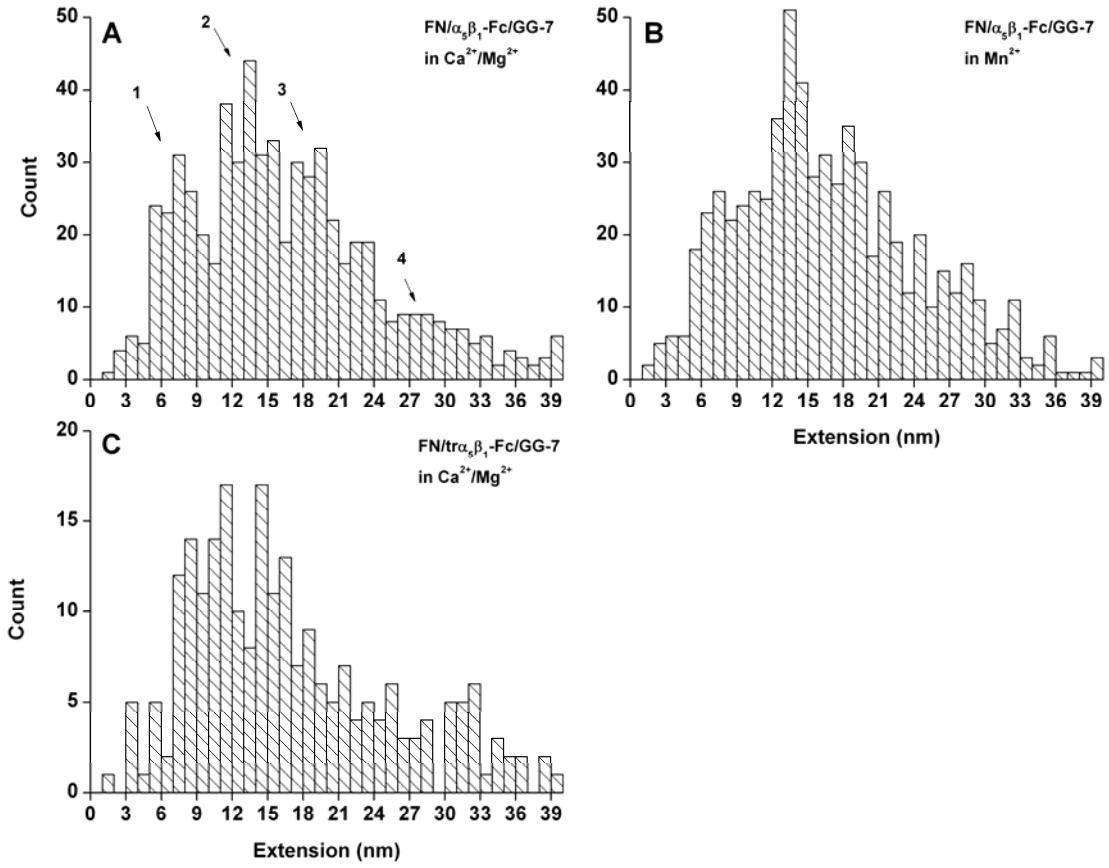

Fig. 7-8 Histograms of molecular extension caused by structural changes of $\alpha_5\beta_1$-Fc in Ca^{2+}/Mg^{2+} (A), Mn^{2+} (B) conditions and tr$\alpha_5\beta_1$ in Ca^{2+}/Mg^{2+} condition (C). All histograms demonstrate several molecular extension located at ~ 8 nm, 14 nm, 19~20 nm, 28~30 nm.

Discussion

During the lifetime measurements of FNIII$_{7\text{-}10}$/$\alpha_5\beta_1$-Fc/GG-7, FNIII$_{7\text{-}10}$/tr$\alpha_5\beta_1$-Fc/GG-7 and P1D6/$\alpha_5\beta_1$-Fc/GG-7 interactions, multiple force drops were observed. These force drops could be caused by multiple bonds dissociation or structural changes occurred in the molecules. By comparing the histograms of number of breaks at different force levels, and between different molecular systems, we proved that the force drops were caused by structural changes occurred in integrin $\alpha_5\beta_1$. The structural changes did not change the trend of lifetime-force relationship of FN/$\alpha_5\beta_1$/GG-7 bond. Moreover, the lifetime for the

structural changes to occur and molecular length changes caused by them were characterized.

The similarity between the histograms of $FNIII_{7\text{-}10}/\alpha_5\beta_1$-Fc/GG-7 and $FNIII_{7\text{-}10}/tr\alpha_5\beta_1$-Fc/GG-7 systems suggests that majority of the structural changes occurred at the headpiece which include β propeller, thigh domain of α5 subunit and A (I-like), hybrid, and PSI domains of β1 subunit. However, which domain or domains unfolded? The thigh domain and hybrid domain are Ig-like domains and unfolding forces of such domains are higher than 100 pN (60). In this study, the force range was between 5 and 60 pN. Therefore, the unfolding of thigh and hybrid domain was less likely. Moreover, PSI domain in the whole integrin did not undertake forces and it has four disulfide bonds, so the odds for it to unfold were also small. What left are the β-propeller domain in the α subunit and the A (I-like) domain in the β subunit. In fact, β-propeller is a big domain and only three disulfide bonds were identified (Fig. 7-10); In addition, A domains of Von Willebrand factor, which adopt similar folding pattern as I-like domain (Rossmann fold), have been shown to be easy to unfold (61). Thus, the β-propeller and I-like domains are the suspected domains to unfold in the lifetime experiments. To provide definitive evidences to identify which domains unfolded, better-designed experiments are needed, such as using mAbs that bind different domains of integrin or test isolated integrin domains.

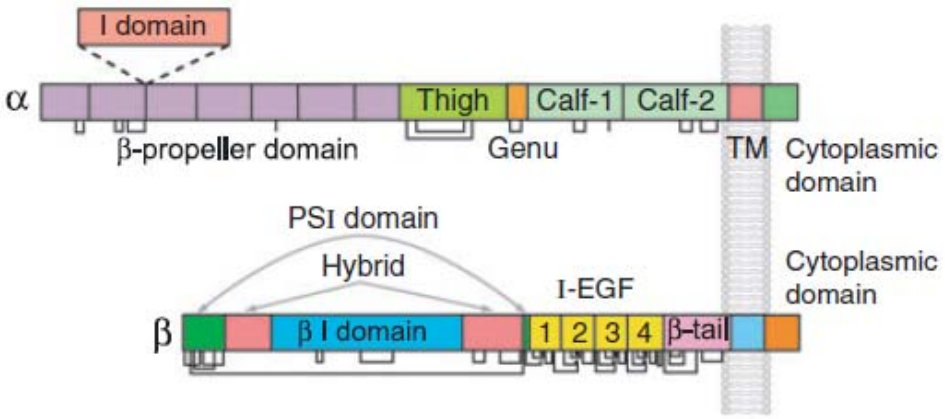

Fig. 7-9 Integrin architecture. Organization of domains within the primary structure of $\alpha_L\beta_2$ (4). The disulfide bonds were connected by gray lines. In the b subunit, except A (I-like) domain, the domains are smaller (4 EGF domains, β-tail domain) and with multiple disulfide bonds. In the α subunit, domains are bigger and with less disulfide bonds.

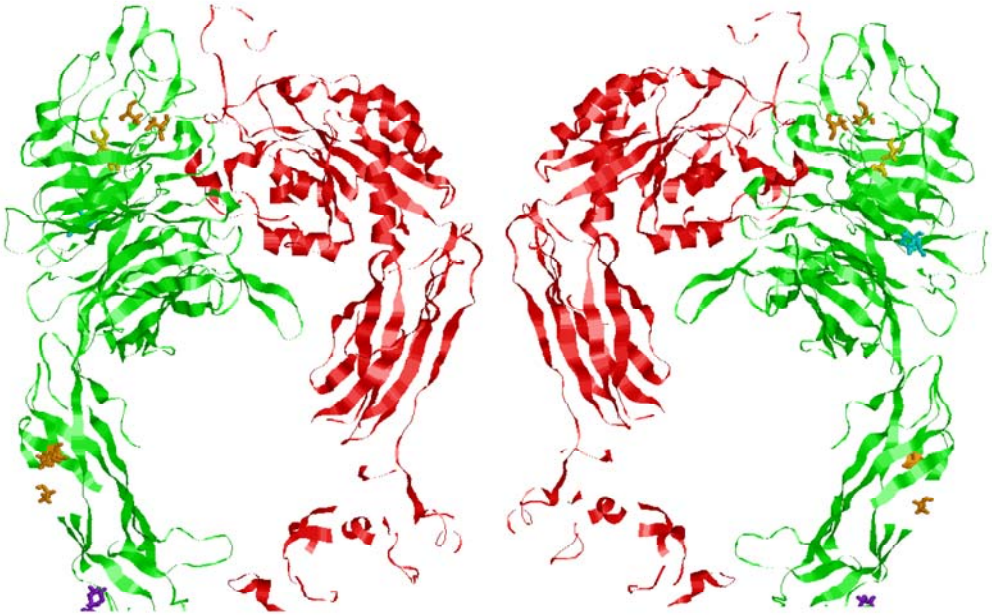

Fig. 7-10 Mirror view of cysteine residues that form disulfide bonds in β propeller and thigh domains of α5 subunit. Whole headpiece of integrin is displayed as ribbons. α subunit is green and β subunit is red. Cysteine residues that form disulfide bonds are shown with same color.

Another important question is the physiological relevance of integrin unfolding at such small forces. Previous studies demonstrated that during cell

migration, majority of the integrin at the trailing edge detached from the cell as the cell advanced (55). Therefore, the cell may cleave the integrin/ligand complex to allow tail detachment. The unfolding of integrin will expose some sequences that could be cleaved by certain enzymes. Of course, more evidences are needed to shed light on this point.

CHAPTER 8

FUTURE RECOMMENDATIONS

Integrins provides transmembrane mechanical links to transmit forces from extracellular contacts to intracellular structures (e.g., the cytoskeleton) and signals for a wide variety of cellular processes. Previous chapters demonstrated how force regulates dissociation of FN/$\alpha_5\beta_1$ bond in relationship with $\alpha_5\beta_1$'s affinity and conformation states.

Catch bond behavior was observed for FN/ $\alpha_5\beta_1$ bond in three metal ion conditions (1 mM Ca^{2+}/Mg^{2+}, 2 mM Mg^{2+}/EGTA, and 2 mM Mn^{2+}). The first major question is the physiological relevance of the catch bond. Especially in the Mn^{2+} condition that not only extends integrin but open the headpiece that gives integrin a high association rate to its ligand, the lifetime at low force (< 10 pN) is still short (< 2 s). It makes sense that integrin/ligand bond needs to hold very long at high force (shown by the lifetime at ~ 30 pN) to help form firm adhesion, but why short lifetimes at low forces? Can integrin use this mechanism to differentiate soluble fibronectin from fibronectin in the ECM? Does cell use this mechanism to avoid unwanted integrin/ligand interaction at certain places by not applying pulling force at it? Chapter 5 showed that TS2/16 eliminated catch bond and changed FN/$\alpha_5\beta_1$ interaction to a slip bond. Therefore, physiological relevance of the catch bond might be studied by examine the effect of TS2/16 on cell behaviors, such as migration, spreading, etc.

How similar is the integrin activated by Mn^{2+} compared to the integrin on the cell that is activated by inside-out signaling? Does the integrin on the cell

activated by inside-out signaling still display catch bond? Experiments carried out on living cells are suitable to examine this question.

Is the catch bond feature universal for all integrin/ligand interactions? Wei (Jack) Chen, a member of Dr. Cheng Zhu's lab, has preformed preliminary experiments demonstrating the catch bond between $\alpha_L\beta_2$ and ICAM-1. This could potentially explain why firm adhesion promoted by lymph node chemokines was only observed under shear forces but not in a shear-free environment (20). It will be of interest to examine the force-relationships of other integrins interacting with their ligands, such as $\alpha_V\beta_3$ and $\alpha_{IIb}\beta_3$, whose biological functions have been extensively studied.

The second major question is the structural mechanism responsible for the catch bond. The ultimate structural changes that account for the catch bond has to lie at the binding pocket of the receptor/ligand bond. A structural conformation at the binding pocket that gives short lifetimes is changed by force to other conformations that give long lifetimes. Integrins switched from bent to extend conformation did not induce such structural changes at the binding pocket. And in fact, bent conformation suppressed ability of force to induce such structural changes. In addition, hybrid domain swing out did not change the lifetime-force relationship, suggesting that such motion was also not enough to induce the structural changes at the binding pocket that gives rise to long lifetimes.

The structural mechanism of integrin I domain activation has been well studied. Because of the homology between the I and the A (I-like) domains,

comparison of the two will be helpful. In the activated I domain, one or two turns of downward movement of the α7 helix resulted in intermediate and high affinity states, respectively (62-64). In contrast, in the crystal structure of the activated A (I-like) domain, the α7 helix moved downward just one turn (5.3 Å), similar to the intermediate state of the I domain. Therefore, the conformation of A (I-like) domain observed in β3 open headpiece (14) could be in an intermediate state that result in high association rate but short lifetimes. Force could pulled down the α7 helix in the A (I-like) domain further more to induce a similar conformation as the fully activated I domain and prolong lifetimes. To test this hypothesis, lifetime-force relationships should be measured when α7 helix of A (I-like) domain is fixed in certain positions by introducing disulfide bonds in a similar fashion to the studies on I domain (62).

Another possibility for catch bond mechanism is the contribution of synergy site binding between the FNIII9 domain in FN and β propeller domain in the α5 subunit of the integrin. The synergy site binding has been suggested to contribute to the binding strength of FN/$\alpha_5\beta_1$ interaction in the presence of TS2/16 (65). Interestingly, FN/$\alpha_5\beta_1$-Fc catch bond was eliminated with presence of TS2/16. Therefore, it will be of great interest to examine the lifetime-force relationships of FN/$\alpha_5\beta_1$ bond with mutations in the synergy site.

Chapter 6 demonstrated that the strong bond state induced by force that result in long lifetimes remained stable after the force is reduced. In another way, reducing the force cannot weaken FN/$\alpha_5\beta_1$ bond once been stretched. What mechanism (if there is any) does cell use to weaken the integrin/ligand

interaction? Previous studies demonstrated multiple mechanisms for cells to regulate tail detachment. Integrin/ligand interactions were either dispersed in the cell membrane, ripped from the cell membrane and remain attached to the substratum, or form a new aggregate (55). However, majority of the integrin remained fixed to the substrate and detached from the cell as the cell advanced (55). Therefore, the cell may just cleave the integrin/ligand complex instead of having a mechanism to weaken the bond. However, the hypothesis needs to be examined carefully on what cleaves integrin, how and where integrin is cleaved.

Furthermore, the lifetime measured was limited by the $\alpha_5\beta_1$-Fc/GG-7 dissociation. Therefore, protocols that enable measurement of integrin/ligand dissociation should be developed.

In addition to the lifetime measurements, a dynamic transition between integrin bent and extend conformation was observed. The transitions were observed under mechanical force and the processes were not in equilibrium. To better characterize the transition, equilibrium processes (with slow loading rate) should be examined under different conditions, such as different metal ions, activating or inhibiting antibodies, ligands, etc.

We also observed integrin unfolding under relative small force range (10 ~ 60 pN). Which domains unfolded and are there physiological relevance? Using antibodies that bind different locations of $\alpha_5\beta_1$ will help locate the unfolding domains. Integrin unfolding might expose some sequences at where integrin could be cleaved.

Integrin/ligand interaction was studied using atomic force microscopy mostly between a single pair of receptor and ligand. However, integrins do not work alone. Integrins cluster at focal complex, focal adhesion site, etc. Therefore, how integrin work in cluster is also an important topic for the future.

APPENDIX A

FORCE CLAMP LABVIEW PROGRAM

Front panel:

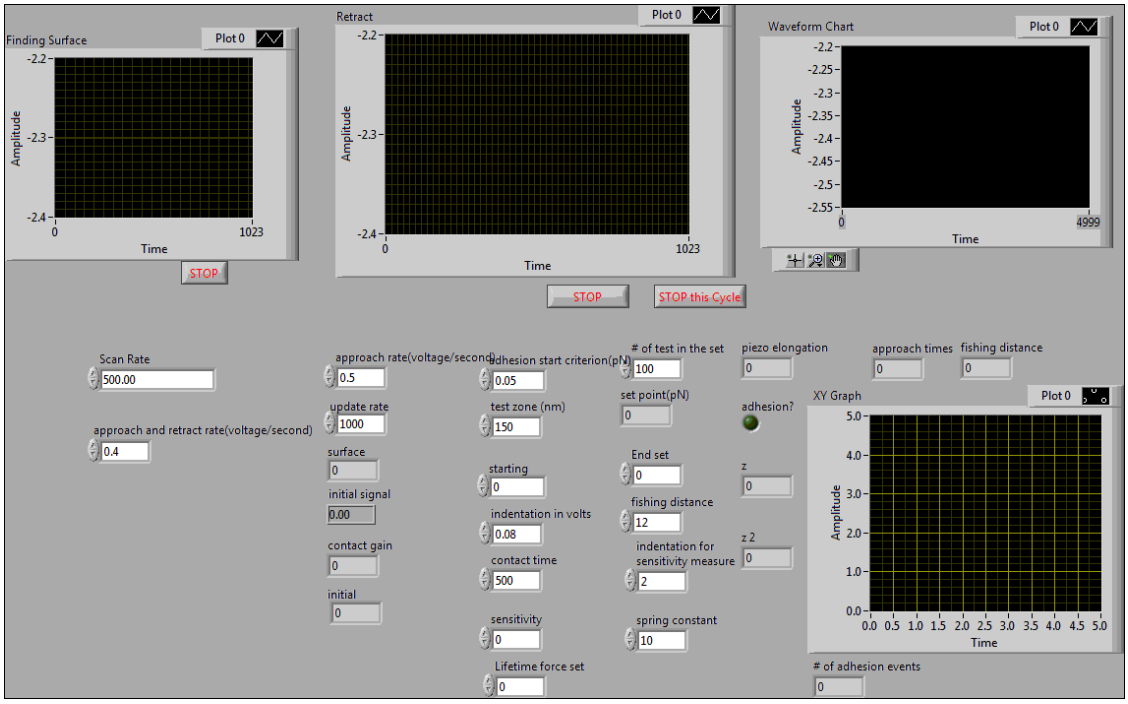

State diagram:

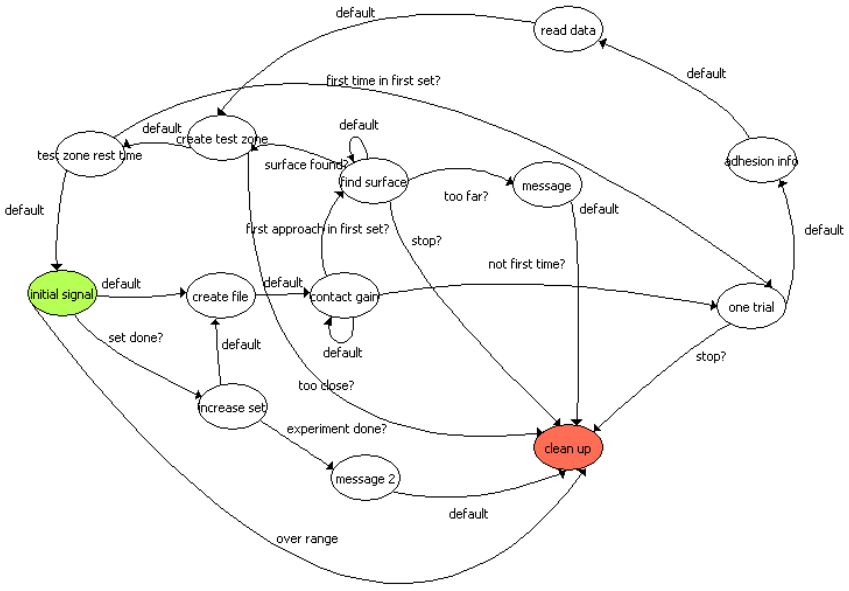

Block Diagram:

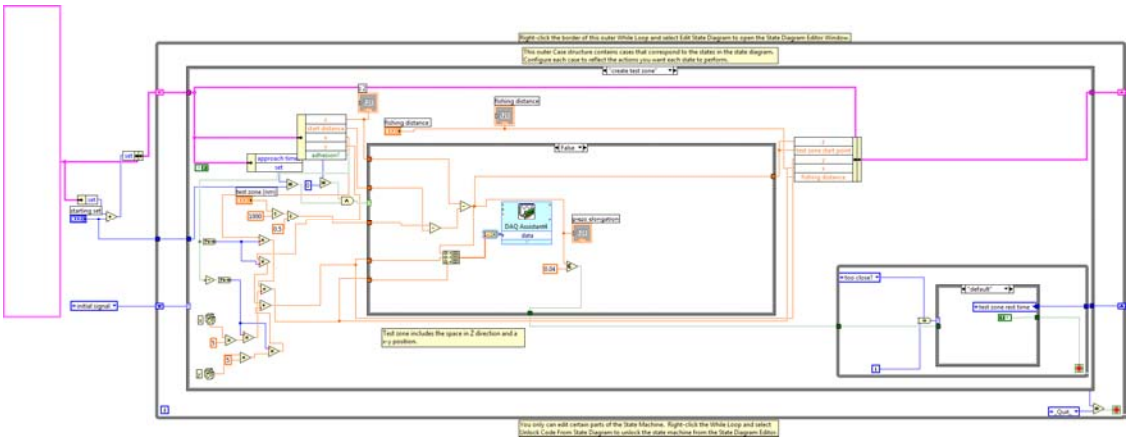

REFERENCES

1. Takagi J, Springer TA (2002) Integrin activation and structural rearrangement. *Immunological Reviews* 186:141-163

2. Junichi Takagi KS, Timothy A. Springer, and Thomas Walz (2003) Structure of integrin $\alpha 5\beta 1$ in complex with fibronectin. *EMBO Journal* 22:4607-4615

3. Hynes RO (2002) Integrins: bidirectional, allosteric signaling machines. *Cell* 110:673-687

4. Luo BH, Carman CV, Springer TA (2007) Structural basis of integrin regulation and signaling. *Annu Rev Immunol* 25:619-647

5. Campbell ID (2008) Studies of focal adhesion assembly. *Biochemical Society Transactions* 036:263-266

6. Xiong JP, Stehle T, Diefenbach B, Zhang R, Dunker R*, et al.* (2001) Crystal structure of the extracellular segment of integrin $\alpha V\beta 3$. *Science* 294:339-345

7. Xiong J-P, Stehle T, Zhang R, Joachinliak A, Frech M*, et al.* (2002) Crystal Structure of the Extracellular Segment of Integrin $\alpha_V\beta_3$ in Complex with an Arg-Gly-Asp Ligand. *Science* 296:151

8. Carrell NA, Fitzgerald LA, Steiner B, Erickson HP, Phillips DR (1985) Structure of human platelet membrane glycoproteins IIb and IIIa as determined by electron microscopy. *J. Biol. Chem.* 260:1743-1749

9. Weisel J, Nagaswami C, Vilaire G, Bennett J (1992) Examination of the platelet membrane glycoprotein IIb-IIIa complex and its interaction with fibrinogen and other ligands by electron microscopy. *J. Biol. Chem.* 267:16637-16643

10. Wippler J, Kouns W, Schlaeger E, Kuhn H, Hadvary P*, et al.* (1994) The integrin alpha IIb-beta 3, platelet glycoprotein IIb-IIIa, can form a functionally active heterodimer complex without the cysteine-rich repeats of the beta 3 subunit. *J. Biol. Chem.* 269:8754-8761

11. Takagi J, Petre BM, Walz T, Springer TA (2002) Global conformational rearrangements in Integrin extracellular domains in outside-In and inside-out signaling. *Cell* 110:599-611

12. Parise L, Helgerson S, Steiner B, Nannizzi L, Phillips D (1987) Synthetic peptides derived from fibrinogen and fibronectin change the conformation of purified platelet glycoprotein IIb-IIIa. *J. Biol. Chem.* 262:12597-12602

13. Beglova N, Blacklow SC, Takagi J, Springer TA (2002) Cysteine-rich module structure reveals a fulcrum for integrin rearrangement upon activation. *Nature Structural Biology* 9:282

14. Xiao T, Takagi J, Coller BS, Wang JH, Springer TA (2004) Structural basis for allostery in integrins and binding to fibrinogen-mimetic therapeutics. *Nature* 432:59-67

15. Ratnikov BI, Partridge AW, Ginsberg MH (2005) Integrin activation by talin. *Journal Of Thrombosis And Haemostasis: JTH* 3:1783-1790

16. Wegener KL, Partridge AW, Han J, Pickford AR, Liddington RC*, et al.* (2007) Structural Basis of Integrin Activation by Talin. *Cell* 128:171-182

17. Chigaev A, Buranda T, Dwyer DC, Prossnitz ER, Sklar LA (2003) FRET detection of cellular α4-integrin conformational activation. *Biophys J* 85:3951-3962

18. Chen CS, Tan J, Tien J (2004) Mechanotransduction at cell-matrix and cell-cell contacts. *Annu Rev Biomed Eng* 6:275-302

19. Balaban NQ, Schwarz US, Riveline D, Goichberg P, Tzur G*, et al.* (2001) Force and focal adhesion assembly: a close relationship studied using elastic micropatterned substrates. *Nat Cell Biol* 3:466-472

20. Woolf E, Grigorova I, Sagiv A, Grabovsky V, Feigelson S-W*, et al.* (2007) Lymph node chemokines promote sustained T lymphocyte motility without triggering stable integrin adhesiveness in the absence of shear forces. *Nat Immunol* 8:1076-1085

21. Zhu C, Lou JZ, McEver RP (2005) Catch bonds: physical models, structural bases, biological function and rheological relevance. *Biorheology* 42:443-462

22. McEver RP, Zhu C (2007) A catch to integrin activation. *Nat Immunol* 8:1035-1037

23. Alon R, Dustin ML (2007) Force as a facilitator of integrin conformational changes during leukocyte arrest on blood vessels and antigen-presenting cells. *Immunity* 26:17-27

24. Astrof NS, Salas A, Shimaoka M, Chen J, Springer TA (2006) Importance of force linkage in mechanochemistry of adhesion receptors. *Biochemistry* 45:15020-15028

25. Jin M, Andricioaei I, Springer TA (2004) Conversion between three conformational states of integrin I domains with a C-terminal pull spring studied with molecular dynamics. *Structure* 12:2137-2147

26. Puklin-Faucher E, Gao M, Schulten K, Vogel V (2006) How the headpiece hinge angle is opened: new insights into the dynamics of integrin activation. *J Cell Biol* 175:349-360

27. Coe APF, Askari JA, Kline AD, Robinson MK, Kirby H*, et al.* (2001) Generation of a minimal $\alpha_5\beta_1$ integrin-Fc fragment. *J Biol Chem* 276:35854-35866

28. Petrie TA, Capadona JR, Reyes CD, Garcia AJ (2006) Integrin specificity and enhanced cellular activities associated with surfaces presenting a recombinant fibronectin fragment compared to RGD supports. *Biomaterials* 27:5459-5470

29. Marshall BT, Long M, Piper JW, Yago T, McEver RP*, et al.* (2003) Direct observation of catch bonds involving cell-adhesion molecules. *Nature* 423:190-193

30. Sarangapani KK, Yago T, Klopocki AG, Lawrence MB, Fieger CB*, et al.* (2004) Low force decelerates L-selectin dissociation from P-selectin glycoprotein ligand-1 and endoglycan. *J Biol Chem* 279:2291-2298

31. Hutter JL, Bechhoefer J (1993) Calibration of atomic-force microscope tips. *Rev Sci Instrum* 64:1868-1873

32. Muller B, Zerwes HG, Tangemann K, Peter J, Engel J (1993) Two-step binding mechanism of fibrinogen to αIIbβ3 integrin reconstituted into planar lipid bilayers. *J Biol Chem* 268:6800-6808

33. Mould PA, Akiyama SK, Humphries MJ (1995) Regulation of integrin α5β1-fibronectin interactions by divalent cations. *J Biol Chem* 270:26270-26277

34. Huang J, Chen J, Chesla SE, Yago T, Mehta P*, et al.* (2004) Quantifying the effects of molecular orientation and length on two-dimensional receptor-ligand binding kinetics. *J Biol Chem* 279:44915-44923

35. Bazzoni G, Shih D-T, Buck CA, Hemler ME (1995) Monoclonal Antibody 9EG7 Defines a Novel beta(1) Integrin Epitope Induced by Soluble Ligand and Manganese, but Inhibited by Calcium. *J. Biol. Chem.* 270:25570-25577

36. Mould AP, Barton SJ, Askari JA, McEwan PA, Buckley PA*, et al.* (2003) Conformational changes in the integrin beta A domain provide a mechanism for signal transduction via hybrid domain movement. *J Biol Chem* 278:17028-17035

37. Mould AP, Garratt AN, McLaughlin WP, Takada Y, Humphries MJ (1998) Regulation of integrin function: evidence that bivalent-cation-induced conformational changes lead to the unmasking of ligand-binding sites within integrin α5β1. *Biochem J* 331:821-828

38. Mould A-P, Garratt A-N, Askari J-A, Akiyama S-K, Humphries M-J (1995) Identification of a novel anti-integrin monoclonal antibody that recognises a ligand-induced binding site epitope on the β1 subunit. *FEBS letter* 363:118-112

39. Garcia A-J, Takagi J, Boettiger D (1998) Two-stage Activation for alpha 5beta 1 Integrin Binding to Surface-adsorbed Fibronectin. *J. Biol. Chem.* 273:34710-34715

40. Takada Y, Puzon W (1993) Identification of a regulatory region of integrin beta 1 subunit using activating and inhibiting antibodies. *J. Biol. Chem.* 268:17597-17601

41. Mould AP, Askari JA, Barton S, Kline AD, McEwan PA*, et al.* (2002) Integrin activation involves a conformational change in the α1 helix of the β subunit A-domain. *J. Biol. Chem.* 277:19800-19805

42. Guo B, Guilford WH (2006) Mechanics of actomyosin bonds in different nucleotide states are tuned to muscle contraction. *Proc Natl Acad Sci USA* 103:9844-9849

43. Yakovenko O, Sharma S, Forero M, Tchesnokova V, Aprikian P*, et al.* (2008) FimH forms catch bonds that are enhanced by mechanical force due to allosteric regulation. *J Biol Chem* 283:11596-11605

44. Yago T, Lou J, Wu T, Yang J, Miner JJ*, et al.* (2008) Platelet glycoprotein Ibα forms catch bonds with human WT vWF but not with type 2B von Willebrand disease vWF. *J Clin Invest* 118:3195-3207

45. Zhang X, Wojcikiewicz E, Moy VT (2002) Force spectroscopy of the leukocyte function-associated antigen-1/Intercellular adhesion molecule-1 interaction. *Biophys J* 83:2270-2279

46. Zhang X, Craig SE, Kirby H, Humphries MJ, Moy VT (2004) Molecular basis for the dynamic strength of the integrin $\alpha_4\beta_1$/VCAM-1 interaction. *Biophys J* 87:3470-3478

47. Li F, Redick SD, Erickson HP, Moy VT (2003) Force measurements of the α5β1 integrin-fibronectin interaction. *Biophys J* 84:1252-1262

48. Bell GI (1978) Models for the specific adhesion of cells to cells. *Science* 200:618-627

49. Zhang F, Marcus WD, Goyal N-H, Selvaraj P, Springer TA*, et al.* (2005) Two-dimensional kinetics regulation of $\alpha_L\beta_2$-ICAM-1 interaction by conformational changes of the αL-inserted domain. *J Biol Chem.* 280:42207-42218

50. Humphries MJ (2000) Integrin structure. *Biochem Soc Trans* 28:311-339

51. Lou J, Zhu C (2007) A structure-based sliding-rebinding mechanism for catch bonds. *Biophys J* 92:1471-1485

52. Mould AP, Travis MA, Barton SJ, Hamilton JA, Askari JA*, et al.* (2005) Evidence that monoclonal antibodies directed against the integrin β subunit plexin/semaphorin/integrin domain stimulate function by inducing receptor extension. *J Biol Chem* 280:4238-4246

53. Klopocki AG, Yago T, Mehta P, Yang J, Wu T*, et al.* (2008) Replacing a lectin domain residue in L-selectin enhances binding to P-selectin glycoprotein ligand-1 but not to 6-sulfo-sialyl Lewis x. *J Biol Chem* 283:11493-11500

54. Schwartz MA, DeSimone DW (2008) Cell adhesion receptors in mechanotransduction. *Curr Opin Cell Biol* 20:551-556

55. Palecek SP, Schmidt CE, Lauffenburger DA, Horwitz AF (1996) Integrin dynamics on the tail region of migrating fibroblasts. *J Cell Sci* 109:941-952

56. Choquet D, Felsenfeld DP, Sheetz MP (1997) Extracellular matrix rigidity causes strengthening of integrin-cytoskeleton linkages. *Cell* 88:39-48

57. Oberhauser AF, Hansma PK, Carrion Vazquez M, Fernandez JM (2001) Stepwise unfolding of titin under force-clamp atomic force microscopy. *Proc Natl Acad Sci USA* 98:468-472

58. Li L, Huang HH, Badilla CL, Fernandez JM (2005) Mechanical unfolding intermediates observed by single-molecule force spectroscopy in a fibronectin type III module. *J Mol Biol* 345:817-826

59. Brujic J, Hermans RI, Garcia-Manyes S, Walther KA, Fernandez JM (2007) Dwell-time distribution analysis of polyprotein unfolding using force-clamp spectroscopy. *Biophys J* 92:2896-2903

60. Rief M, Gautel M, Oesterhelt F, Fernandez JM, Gaub HE (1997) Reversible unfolding of individual titin immunoglobulin domains by AFM. *Science* 276:1109-1112

61. Auton M, Cruz MA, Moake J (2007) Conformational stability and domain unfolding of the Von Willebrand factor A domains. *J Mol Biol* 366:986-1000

62. Shimaoka M, Lu C, Palframan RT, von Andrian UH, McCormack A*, et al.* (2001) Reversibly locking a protein fold in an active conformation with a disulfide bond: integrin alphaL I domains with high affinity and antagonist activity in vivo. *Proc Natl Acad Sci U S A* 98:6009-6014

63. Lee JO, Rieu P, Arnaout MA, Liddington R (1995) Crystal structure of the A domain from the alpha subunit of integrin CR3 (CD11b/CD18). *Cell* 80:631-638

64. Lee JO, Bankston LA, Arnaout MA, Liddington RC (1995) Two conformations of the integrin A-domain (I-domain): a pathway for activation? *Structure* 3:1333-1340

65. Garcia AJ, Schwarzbauer JE, Boettiger D (2002) Distinct Activation States of $\alpha_5\beta_1$ Integrin Show Differential Binding to RGD and Synergy Domains of Fibronectin. *Biochemistry* 41:9063-9069